

https://dspace.org/

Investigation of nozzle contour in the CSIR supersonic wind tunnel

Vallabh, Bhavya

2016

http://hdl.handle.net/10539/20999

Vallabh, Bhavya (2016) Investigation of nozzle contours in the CSIR supersonic wind tunnel, University of Witwatersrand, Johannesburg, <http://wiredspace.wits.ac.za/handle/10539/20999>

Downloaded from a DSpace repository. https://dspace.org/

Investigation of Nozzle Contours in the CSIR Supersonic Wind Tunnel

Bhavya Vallabh

A research report submitted to the Faculty of Engineering and the Built Environment, University of the Witwatersrand, Johannesburg, in partial fulfilment of the requirements for the degree of Master of Science in Engineering

Johannesburg 2016

ABSTRACT

The nozzle contour profiles of the CSIR's supersonic wind tunnel (high speed wind tunnel) were designed to produce smooth, uniform and shock-free flow in the operating section of the facility. The existing profiles produce weak waves in the test section region which induces flow gradients and flow angularities in the air flow, effectively degrading the air flow quality, which in turn perturbs the wind tunnel data. The wind tunnel geometry and tunnel constraints were employed in accordance with the method of characteristics technique to design the supersonic nozzle profiles. The Sivells' nozzle design method was deemed the most feasible which calculates the profile downstream of the inflection point. The throat block profile was amalgamated with this profile to yield a profile from the throat to the test section. A boundary layer correction was applied to the profiles to account for viscous effects which cause a Mach number reduction from the desired test section Mach number. An automatic computation was used for the profile design and a computational method analysed the Mach distribution, flow angularity and density gradient (to determine the occurrence of shocks and expansions) of the profiles implemented in the tunnel, for the full Mach number range of the HSWT. The methods used, achieved uniform and shock-free flow such that the Mach number and flow angularity were within the acceptable quality limits of the HSWT.

DECLARATION

I declare that this research report is my own unaided work, except where otherwise acknowledged. It is being submitted in partial fulfilment of the requirements for the degree of Master of Science in Engineering to the University of the Witwatersrand, Johannesburg. It has not been submitted before for any degree or examination to any other University.

_____

Bhavya Vallabh

23 May 2016

CONTENTS

ABSTRACT I

DECLARATION II

CONTENTS III

LIST OF FIGURES V

LIST OF TABLES VII

1. INTRODUCTION 1

1.1 Background and Motivation 1

1.2 Objectives 2

2. LITERATURE REVIEW 3

2.1 The CSIR's HSWT (Supersonic Wind Tunnel) 3

2.2 The Method of Characteristics 5

2.3 Supersonic Nozzle Design 8

2.4 Sivells' Nozzle Design Method 14

2.5 Nozzle Boundary Layer Treatment 17

3. DESIGN OF A SUPERSONIC NOZZLE 19

3.1 Facility Constraints 19

3.2 Analytical Technique Adapted from Sivells' Nozzle Design Method 22

3.3 MATLAB Code 26

3.4 Plate Stress 29

4. NUMERICAL FLOW INVESTIGATION 30

4.1 Computational Method 30

4.2 Discretisation Technique 31

4.3 Turbulence Modelling 33

4.4 Boundary Layer Thickness Correction using CFD 33

5. RESULTS AND DISCUSSION 36

5.1 Existing HSWT Nozzle Profiles 36

5.2 Initial Methods Considered for New Profiles 39

5.3 Final Method for New Profiles 40

5.4 Computational Results of the Uncorrected Profiles 43

5.5 Boundary Layer Thickness Correction 46

5.6 Plate Stress 50

5.7 Profile Uniqueness 51

5.8 Comparison of Profiles 54

6. CONCLUSIONS 57

7. RECOMMENDATIONS 58

8. REFERENCES 59

APPENDIX A: HSWT NOZZLE DESIGN CODE 61

A.1 Main_Program.m 61

A.2 ProfileFilename.m 62

A.3 Throat_R.m 63

A.4 SourceFlow.m 66

A.5 WallFunction.m 68

A.6 ContourCalc.m 76

APPENDIX B: BOUNDARY LAYER CORRECTION CODE 78

APPENDIX C: PLATE STRESS CODE 79

LIST OF FIGURES

Figure 1.1: CSIR's supersonic wind tunnel facility (HSWT) 1
Figure 1.2: Weak waves can be seen in the HSWT test section at Mach 2.5 produced by the HSWT's nozzle 2
Figure 2.1: Schematic of the supersonic blow down tunnel at the CSIR [2] 4
Figure 2.2: Flexible nozzle and jack assembly of the HSWT [2] 4
Figure 2.3: Expansion fan caused by supersonic airflow around a corner [6] 5
Figure 2.4: Grid points and characteristic lines for a characteristic mesh in a flow field [10] 6
Figure 2.5: Left ($C+$) and right ($C-$) running characteristic lines in a flow field [10] 6
Figure 2.6: Calculation of internal points in a characteristic grid [10] 7
Figure 2.7: Calculation of wall points in a characteristic grid [10] 8
Figure 2.8: Incident wave reflected from a plane surface [8] 9
Figure 2.9: Incident wave cancels by turning the wall [8] 9
Figure 2.10: Schematic of a supersonic nozzle designed by the method of characteristics [5] 9
Figure 2.11: Schematic of the upper portion of a supersonic nozzle design using symmetry [5] 10
Figure 2.12: A graphical aid necessary to complete a MOC calculation 11
Figure 2.13: Gradients required to calculate the contour coondinates 13
Figure 2.14: Curvature of a nozzle profile [12] 14
Figure 2.15: Characteristic diagram for a continuous curvature nozzle as described by Sivells [12] 15
Figure 2.16: Numbering system in the characteristic mesh for Sivells' nozzle design method 17
Figure 2.17: Sketch of boundary layer on a flat plate surface with parallel flow [15] 18
Figure 3.1: Components of the convergent-divergent (Laval) nozzle in the HSWT 19
Figure 3.2: Reflections in the expansion region of the nozzle 20
Figure 3.3: Schematic of single throat block geometry for the HSWT nozzle 20
Figure 3.4: Throat block rotation for various angles 21
Figure 3.5: Various throat block rotations for a Mach 3.0 set point 21
Figure 3.6: Geometric constraints of the flexible plate highlighting the fixed test section dimensions 22
Figure 3.7: Schematic of the source flow transformation required for Sivells' nozzle design method 24
Figure 3.8: Characteristic mesh resolution for $r = 3$ and $k = 4$ 25
Figure 3.9: Schematic of characteristic mesh for a resolution, $r = 3$ utilizing Sivells' nozzle design method 26
Figure 3.10: Main program used to generate the nozzle contours by the method of characteristics 27
Figure 4.1: Three-dimensional quarter geometry required as an input for the CFD with specified boundary conditions 31
Figure 4.2: Unstructured volumetric mesh highlighting the boundary layer meshing technique implemented 32
Figure 4.3: Results of the mesh independence study for a profile with a nozzle exit Mach number of $Me = 3.0$ 32
Figure 4.4: Average Wall y-plus values with varying cell size for a nozzle exit Mach number of $Me = 3.0$ 33

Figure 5.1: Existing inviscid, theoretical nozzle profile to produce an exit Mach number of $Me = 3.0$ 37
Figure 5.2: Predicted centreline Mach number distribution of the theoretical nozzle profile designed for $Me = 3.0$ 38
Figure 5.3: Mach number contours on the symmetry plane of the existing theoretical profile designed for $Me = 3.0$ 38
Figure 5.4: Density gradient $kgm3/m$ contours on the symmetry plane of the existing theoretical profile designed for $Me = 3.0$ 38
Figure 5.5: Predicted test section flow angularity distribution produced by the existing theoretical profile designed for $Me = 3.0$ 39
Figure 5.6: Incorporating the throat block into the finite expansion MOC induces reflections in the expansion section 40
Figure 5.7: Source points for the characteristic net, inflection point and throat block profile for $Me = 3.0$ 41
Figure 5.8: Expansion section (throat block), straightening section of wall contour and fixed test section region for $Me = 3.0$ 42
Figure 5.9: Wall slope of the straightening section curve generated for $Me = 3.0$ 42
Figure 5.10: Nozzle contour profiles in increments of $\Delta Me = 0.5$ with the fixed throat and test section regions 43
Figure 5.11: Uncorrected inviscid Mach number contours produced by the new nozzle design method for $Me = 3.0$ 44
Figure 5.12: Uncorrected viscous Mach number contours produced by the new nozzle design method for $Me = 3.0$ 44
Figure 5.13: Uncorrected inviscid density gradient $kgm3/m$ contours produced by the new nozzle design method for $Me = 3.0$ 44
Figure 5.14: Uncorrected viscous density gradient $kgm3/m$ contours produced by the new nozzle design method for $Me = 3.0$ 44
Figure 5.15: Inviscid and viscous centreline Mach distribution using the new nozzle design method for $Me = 3.0$ 45
Figure 5.16: Viscous flow angularity in the test section region using the new nozzle design method for $Me = 3.0$ 46
Figure 5.17: Comparison of uncorrected and corrected nozzle profiles for $Me = 3.0$ 47
Figure 5.18: Corrected inviscid Mach number contours produced by the new nozzle design method for $Me(corrected) = 3.0$ 48
Figure 5.19: Corrected inviscid density gradient $kgm3/m$ contours produced by the new nozzle design method for $Me(corrected) = 3.0$ 48
Figure 5.20: Corrected viscous Mach number contours produced by the new nozzle design method for $Me(corrected) = 3.0$ 48
Figure 5.21: Corrected viscous density gradient $kgm3/m$contours produced by the new nozzle design method for $Me(corrected) = 3.0$ 48
Figure 5.22: Inviscid and viscous centreline Mach distribution using the new nozzle design method for $Me(corrected) = 3.0$ 49

Figure 5.23: Viscous flow angularity in the test section region using the new nozzle design method for $Me(corrected) = 3.0$ 49
Figure 5.24: Velocity contours truncated above 99% of the freestream velocity 50
Figure 5.25: Maximum plate stress for various Mach numbers for corrected profiles calculated for the HSWT 50
Figure 5.26: Nozzle profiles designed to produce a corrected test section Mach number of 1.3 at different inflection point angles 51
Figure 5.27: Corrected viscous Mach number contours produced by the "original" profile for $Me(corrected) = 1.3$ 52
Figure 5.28: Corrected viscous density gradient $kgm3/m$contours produced by the "original" profile for $Me(corrected) = 1.3$ 52
Figure 5.29: Corrected viscous Mach number contours produced by the "modified inflection point" profile for $Me(corrected) = 1.3$ 52
Figure 5.30: Corrected viscous density gradient $kgm3/m$contours produced by the "modified inflection point" profile for $Me(corrected) = 1.3$ 52
Figure 5.31: "Original" and "modified inflection point" centreline Mach distribution using the current nozzle design method for $Me(corrected) = 1.3$ 53
Figure 5.32: Viscous flow angularity in the test section region using the "original" profile for $Me(corrected) = 1.3$ 53
Figure 5.33: Viscous flow angularity in the test section region using the "modified inflection point" profile for $Me(corrected) = 1.3$ 54
Figure 5.34: Profiles for the boundary layer corrected nozzle profiles existing and newly calculated for $Me = 3.0$ 54
Figure 5.35: Viscous centreline Mach distribution for the boundary layer corrected nozzle profiles original and newly calculated for $Me = 3.0$ 55
Figure 5.36: Nozzle profiles modelled with the throat at the origin 56
Figure 5.37: Nozzle profiles modelled with the test section fixed as is the case in the HSWT 56

LIST OF TABLES

Table 3.1: Detailed explanations of the MATLAB functions 27

1. INTRODUCTION

1.1 Background and Motivation

In order to achieve supersonic freestream flow in the test section of a wind tunnel, the flow must be accelerated from stagnation conditions through a convergent-divergent (Laval) nozzle. The area ratio between the nozzle throat and the test section, as well as the pressure ratio between the settling chamber and the test section exit, drives the test section Mach number and the static properties in the test section, respectively. The shape of the nozzle directly affects the flow quality; particularly the Mach number distribution and flow angularity in the test section. For a uniform Mach number distribution, mandatory for wind tunnels, unique shapes for the divergent section of the Laval nozzle are required for a particular test section Mach number. The current nozzle contour shapes in the High Speed (Supersonic) Wind Tunnel (HSWT), as seen in Figure 1.1, of the Aeronautic Systems Competency (ASC) within the Council for Scientific and Industrial Research (CSIR), are used to resolve the test section Mach number [1]. These profiles were calculated using the method of characteristics. The flexible nozzle consists of two plates which make up the top and bottom tunnel walls, shaped and positioned by 8 movable jacks (one main jack and 7 sub-jacks) per plate.



Figure 1.1: CSIR's supersonic wind tunnel facility (HSWT)

The current contours are not accurate because the input contours result in a lower test section Mach number than the desired set point Mach number. There are discrepancies between the theoretically calculated shape and the actual implemented shape, due to the tunnel nozzle shaping mechanism i.e. a finite number of discrete jacking points used to shape the flexible plate. In addition, the inaccurate nozzle contours, at some settings, manifest weak waves as shown in Figure

1.2 (Mach 2.5 nozzle setting). Furthermore, the current shapes do not account for the boundary layer growth along the plate, which is one of the direct causes for the lower test section Mach number than desired. For these reasons, new supersonic nozzle contour profiles need to be calculated for the HSWT, that not only produce shock and expansion free flow in the test section of the wind tunnel, but are corrected for viscous effects as well.

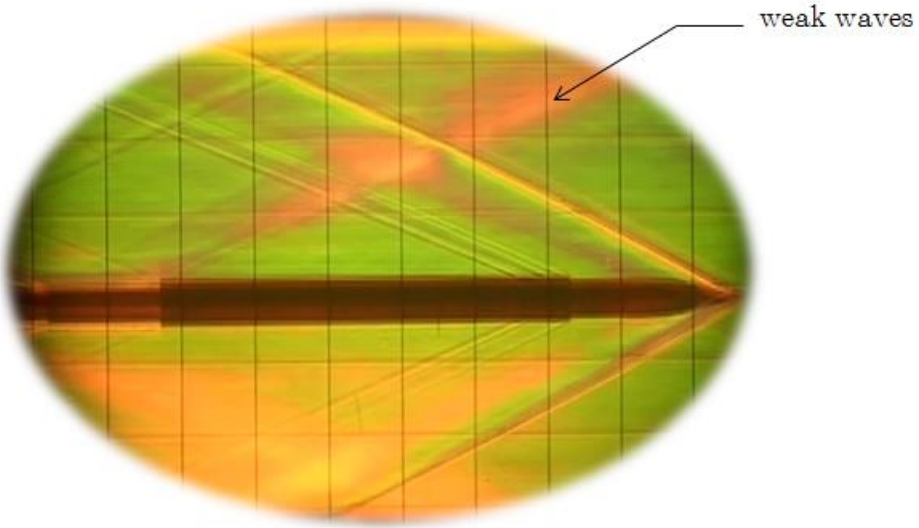

Figure 1.2: Weak waves can be seen in the HSWT test section at Mach 2.5 produced by the HSWT's nozzle

1.2 Objectives

The broad objectives of this study are to:

- Develop a two-dimensional method to predict shock and expansion free nozzle shapes for the divergent section of the supersonic nozzle of the HSWT.
- Include the adaption of the method to model the nozzle profiles with the flexible plate and the fixed diverging tunnel test section.
- Use computational fluid dynamics to determine whether the calculated profiles produce uniform flow in the test section.
- Use viscous simulations to determine the effect of boundary layer growth along the tunnel walls (including the bounding sides walls).
- Develop a method to correct for the decrease in Mach number due to the boundary layer development along the walls of the wind tunnel.

2. LITERATURE REVIEW

2.1 The CSIR's HSWT (Supersonic Wind Tunnel)

The CSIR's trisonic wind tunnel facility was commissioned in 1969. This intermittent blow-down tunnel, illustrated in Figure 2.1, uses a flexible nozzle to achieve freestream Mach numbers ranging from 0.6 to 4.5. Air is pressurised by the charging air compressor and passed through filters and an air dryer, which removes liquid, dust and impurities from the air. Dry air is essential for the operation of the of the HSWT otherwise condensation of water vapour in the air would lead to non-uniformity in the air flow, as well as the formation of undesirable ice particles, due to the sub-zero temperatures achieved at supersonic speeds. The pressurised air is hereafter stored in 4 large high pressure supply vessels with a total volume of approximately 350m^3. An automatic throttle valve discharges the compressed air into the tunnel and a quick acting control valve regulates the stagnation pressure in the settling chamber [2]. Air flows through a wire screen in the settling chamber, which reduces the turbulence in the air stream. The nearly stagnant air in the stagnation chamber is accelerated in the converging nozzle section to a Mach number of unity at the nozzle throat. Uniform accelerating air then passes through the diverging section of the nozzle, which is designed to meet the required supersonic Mach number. Reynolds number variations can be resolved by altering the total pressure. Following the 450mm x 450 mm test section area, a convergent – divergent diffuser decelerates the flow to near sonic conditions at the second throat. The flow decreases to subsonic speeds at the divergent section of the diffuser and the air exhausts back to the atmosphere. The test section area consists of two high quality glass windows on either side of the wind tunnel to permit viewing of the model, which is positioned on the support system downstream of the test section. A National Instruments control system fully automates the tunnel control and test execution. A typical wind tunnel blow lasts 10 - 30 seconds, subject to the test conditions, where the model is moved to pitch and roll attitudes specific to the test. The tunnel is operated remotely from the control room where the support system is programmed to perform attitude changes of the model during a run. Aerodynamic force and moment data, as well as measurement of the freestream and stagnation conditions are typical test capabilities in the HSWT. A colour schlieren system provides optical flow visualisation [3].

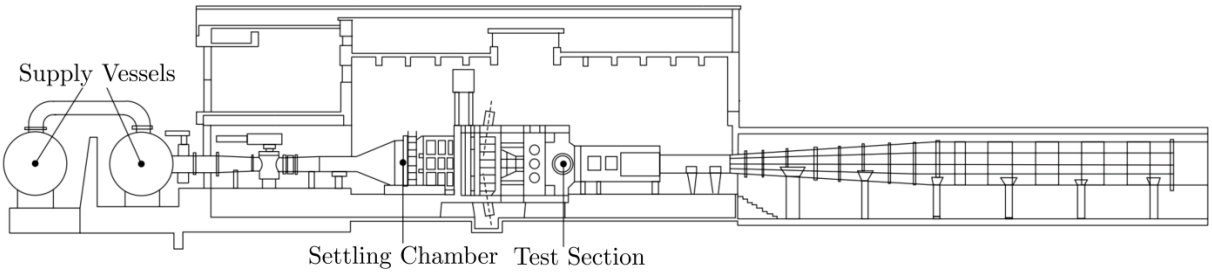

Figure 2.1: Schematic of the supersonic blow down tunnel at the CSIR [2]

2.1.1 The Flexible Nozzle

Two main hydraulic jacks on either side of the wind tunnel (upper and lower) control the nozzle throat blocks that accurately position the minimal nozzle throat area by means of hydraulic control, as displayed in Figure 2.2. The contour design of the divergent portion of the supersonic nozzle is the primary objective the current research, to yield uniform, parallel and shock-free flow in the test section over the entire Mach number testing range of the HSWT. The exit Mach number is determined by the ratio of the sectional area at the test section and the nozzle throat area. Symmetrical nozzle profiles (about the test section centre line) are positioned by altering the throat block and the high strength steel flexible plate in combination. Each plate is positioned by seven equally spaced hydraulic jacks, which are controlled by servo-valves that are signalled by fine resolution digital encoders. The jacks are able to move to a set of positions within the wind tunnel's mechanical and electrical limitations [2]. It is imperative to design the contour profile for the flexible plate in conjunction with the fixed throat block curve. The end of the throat block (or the start of the flexible plate) is the inflection point, which eliminates an abrupt change in curvature in the flexible plate and prevents unnecessary strain onto the plate. In addition the flexible plates allow for "Mach sweeps" to be completed during operation. Downstream of the nozzle the pin-jointed test section region diverges marginally to account for the boundary layer growth within the test section.

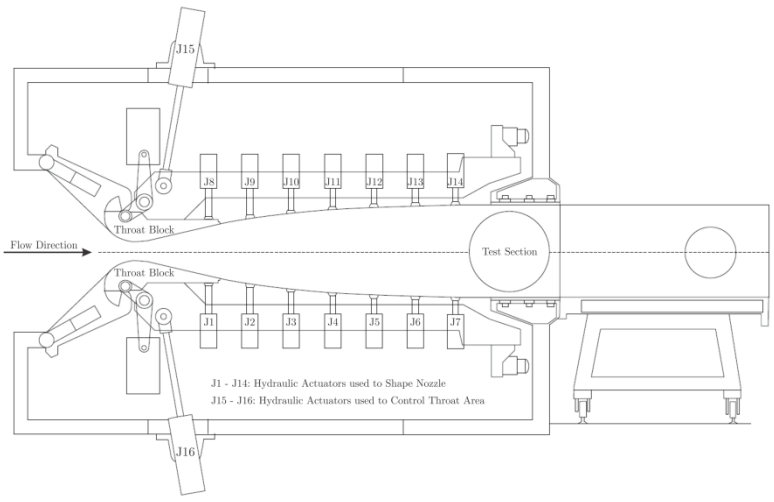

Figure 2.2: Flexible nozzle and jack assembly of the HSWT [2]

2.2 The Method of Characteristics

The Method of Characteristics (MOC) is a numerical technique used to define the properties of supersonic flows in the presence of varying boundaries such as in a wind tunnel or in the presence of some aerodynamic configuration in a supersonic airstream [4]. This method is based on the mathematical theory of characteristics (lines or curves in two-dimensional flow and surfaces in three-dimensional flow) associated with the solution of certain non-linear differential equations of the velocity potential for two dimensional compressible flow theory, as is the case for two-dimensional, steady, isentropic, irrotational flow [5]. The method of characteristics is the most frequently utilized method for designing the contours (shape) of a two-dimensional supersonic converging-diverging nozzle for smooth, uniform and shock free flow, which is of primary interest in this study.

In order to describe the method of characteristics, first consider a region where the flow is turned away from itself, where the air can expand to supersonic speeds, as is the case for the diverging section (aft of the sonic throat) of a supersonic wind tunnel. It is assumed that expansion occurs across a centred fan originating from an abrupt corner as displayed in Figure 2.3 [6].

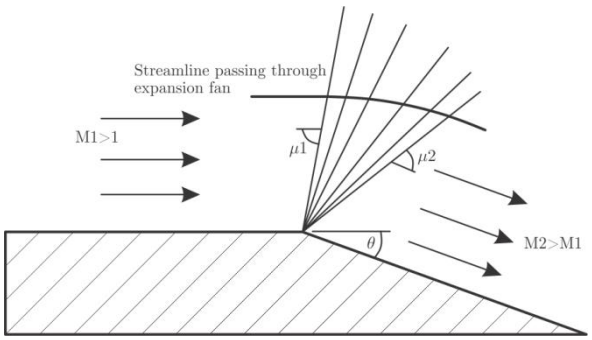

Figure 2.3: Expansion fan caused by supersonic airflow around a corner [6]

These infinitesimal expansion waves (typically known as a Prandtl-Meyer expansion fan) turn the airflow to follow the contour of the wall. The properties through and behind a Prandtl-Meyer expansion fan are dictated by the differential relation in Equation 2.1 where the dependence of the flow angle (θ) on the Mach number (M) and the velocity (V) is evident. When integrated across a wave, the Prandtl-Meyer function results in Equation 2.2, where the Prandtl-Meyer angle (ν) is determined by the ratio of specific heat (γ) of the fluid and the Mach number of interest [7].

$$d\theta = \pm\sqrt{M^2 - 1}\frac{dV}{V} \tag{2.1}$$

$$\nu(M) = \sqrt{\frac{\gamma+1}{\gamma-1}}tan^{-1}\sqrt{\frac{\gamma-1}{\gamma+1}(M^2-1)} - tan^{-1}\sqrt{M^2-1} \tag{2.2}$$

Characteristics are fictitious lines in supersonic flow oriented in specific directions along which pressure waves are propagated (also known as Mach lines) [8]-[9]. The method of characteristics calculates the flow properties at distinct points throughout the flow field represented in a continuous flow field by a series of grid points computed by the intersection of these characteristic lines, as displayed in Figure 2.4. These characteristics are designed to cancel the waves as the flow becomes parallel to the wall leading to uniform flow. The flow field properties (direction and speed) are hence calculated at the distinct grid points throughout the flow field [10].

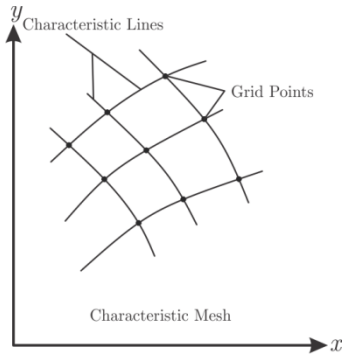

Figure 2.4: Grid points and characteristic lines for a characteristic mesh in a flow field [10]

The characteristic mesh consists of an infinite number of left and right running characteristic lines that interweave the flow field. These lines are designated as the C^+(making a positive angle with the flow direction) and C^- (making a negative angle with the flow direction) characteristics respectively as portrayed in Figure 2.5. For practical calculations, a finite number of lines are employed to make up the characteristic net. The characteristic lines are curved, due to the local Mach angle (μ) being a function of x and y and the local streamline direction (θ) varying throughout the flow.

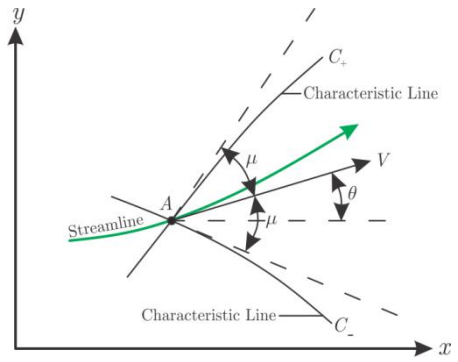

Figure 2.5: Left (C^+) and right (C^-) running characteristic lines in a flow field [10]

The two characteristic lines (C^+ and C^-) run through a common point, A in Figure 2.5, each having slopes in opposite directions. These characteristic slopes, $\left(\frac{dy}{dy}\right)_{char}$ are defined as:

$$\left(\frac{dy}{dx}\right)_{char} = tan(\theta \pm \mu) \tag{2.3}$$

Integration of Equation 2.1 provides the compatibility relations along the characteristic lines where the positive root describes the C^+ characteristic and the negative root describes the C^-characteristic. K^+ and K^- refer to constants along a given characteristic line and should not be mistaken for the C^+ and C^- characteristic lines respectively.

$$\theta + \nu(M) = constant = K^- \quad \text{(along the } C^- \text{ characteristic)} \tag{2.4}$$

$$\theta - \nu(M) = constant = K^+ \quad \text{(along the } C^+ \text{ characteristic)} \tag{2.5}$$

A practical explanation highlighting the two types of points included in a grid namely, internal points and wall points, that is essential for the method of characteristics calculation is discussed in Figure 2.6. An assumption is made that the flow properties and locations of points 1 and 2 are known.

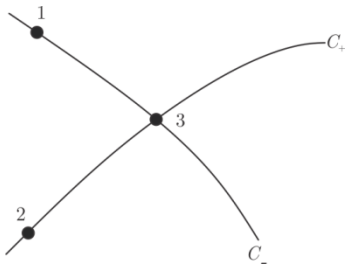

Figure 2.6: Calculation of internal points in a characteristic grid [10]

The method of characteristics allows the computation of the properties at point 3, defined as the intersection point of the characteristic lines originating from points 1 and 2. These curves are the C^+ (point 2 to point 3) and C^- (point 1 to point 3) characteristics. As previously mentioned, the K^+ and K^- are constants along the characteristic line, hence$(K^-)_1 = (K^-)_3 = \theta_1 + \nu_1$, and similarly for point 2. Solving the two algebraic equations we obtain Equations 2.6 and 2.7, which enables the computation of point 3. Consequently, from the Prandtl-Meyer angle, the Mach number can be computed using well established gas dynamics methods.

$$\theta_3 = \frac{1}{2}[(K^-)_1 + (K^+)_2] \tag{2.6}$$

$$\nu_3 = \frac{1}{2}[(K^-)_1 - (K^+)_2] \tag{2.7}$$

In the case of a point falling on the wall contour, as presented in Figure 2.7, where the flow properties and position at point 4 is known, the C- characteristic line intersects the wall at point 3. The slope of the wall (θ_3) is known which allows the wall point to be obtained using the theory that the K^+ and K^- are constant along the C^+ and C^- characteristic lines. From the given information, the Prandlt-Meyer angle can be directly computed [10].

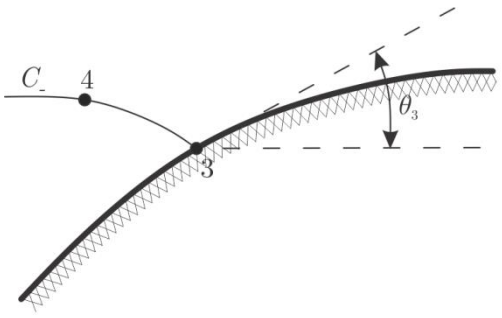

Figure 2.7: Calculation of wall points in a characteristic grid [10]

In summary, the method of characteristic calculation is commenced when the flow properties along an initial data line is known. Subsequently a characteristic mesh is used to aid in the computation of all the characteristic points downstream of the initial line. As the number of characteristic lines increase, so do the number of data points, which increases the complexity, along with the accuracy of the numerical technique. An exact solution can only be computed if an infinite number of characteristic lines are utilized.

2.3 Supersonic Nozzle Design

Aforementioned, an application of the method of characteristics is the design of the contour of supersonic nozzles. This general method uses the method of characteristics equations coupled with illustrations to determine the nozzle profiles. Of particular importance is the design of supersonic nozzles of rectangular cross section, which can be found in most supersonic wind tunnels, to ensure that the flow exiting the nozzle in the test section area is uniform, parallel and free of shock waves, as the presence of waves prevents uniform flow. Wind tunnel nozzles are generally long with slow expansion whilst rocket nozzles expand rapidly to produce short nozzles that minimize weight [5]. The application of this, so called minimum length method for wind tunnels will be further discussed due to its relevance in a vast number of practical applications. Moreover, it is one of the simpler methods, so it is useful to grasp and apply the general MOC technique.

If a weak wave of turning angle $\Delta\alpha$ is incident upon a plane surface, as displayed in Figure 2.8, a reflected wave of turning angle $\Delta\alpha$ must be present to satisfy the boundary conditions at the wall [8].

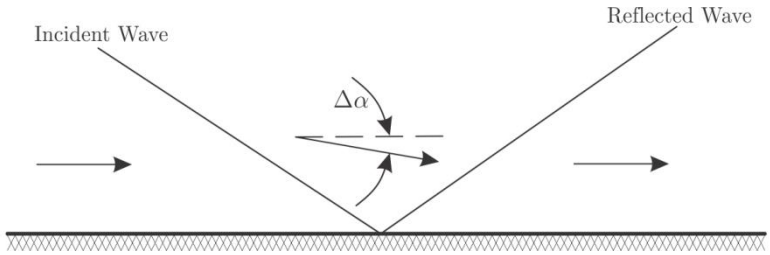

Figure 2.8: Incident wave reflected from a plane surface [8]

In order to cancel the incident wave, the wall needs to turn the exact $\Delta\alpha$ angle at the point of impingement of the incident wave. Thus Figure 2.9 illustrates that there is no reflected wave since the boundary condition at the wall is satisfied without it. The flow is thus parallel to the wall and the incident wave is essentially cancelled [8].

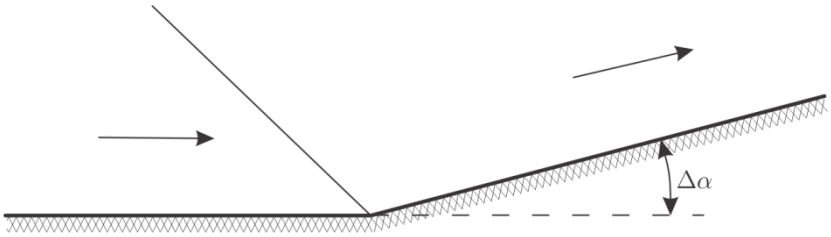

Figure 2.9: Incident wave cancels by turning the wall [8]

For the case of a converging-diverging supersonic wind tunnel nozzle, displayed in the schematic in Figure 2.10, the subsonic flow in the convergent portion of the nozzle is accelerated to sonic conditions at the nozzle throat region. A sonic "line" exists which is marginally curved but for most applications is assumed to be straight. Downstream of the sonic line, the nozzle diverges in the expansion section and converges in the straightening section of the nozzle, to meet the test section region.

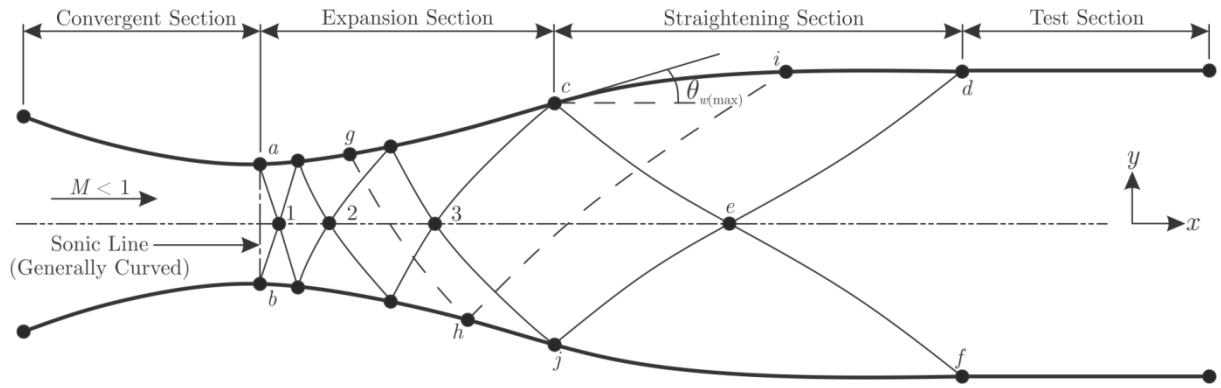

Figure 2.10: Schematic of a supersonic nozzle designed by the method of characteristics [5]

If the upper half of the nozzle is considered, then the angle of the nozzle wall with respect to the horizontal direction, θ_w, initially increases in the region referred to as the expansion section, where expansion waves are generated and propagate across the flow downstream as they reflect from the opposite wall of the nozzle. This region consists of both left and right running characteristic lines, which is defined as a non-simple region where the characteristics are curved lines. The shape of the expansion section is usually arbitrary and varies to accommodate the required nozzle length. An inflection point exists on the nozzle contour aft of the expansion section, where the maximum allowable wall angle is achieved. Downstream of the inflection point, the nozzle wall angle decreases until the wall becomes parallel to the direction of flow at the exit of the nozzle. This region is referred to as the straightening section which is designed to cancel the expansion waves originating in the expansion section. The straightening section of the upper half of the nozzle covers the characteristics of only left running characteristics and is described as a simple region where the characteristic lines are straight. Figure 2.10 illustrates the manner in which the expansion wave at g, originating in the expansion section is reflected at h, on the opposite side of the nozzle wall and cancels at i, in the straightening section of the profile. Downstream of points d, e and f, lies the test section wall where the flow is uniform and parallel at the desired Mach number [5].

The nozzle is symmetric about the x-axis, as defined in Figure 2.10, and to minimize the calculations only the section above the centreline is frequently considered. Hence the waves generated from the top wall will act is if they were reflected from the centreline as represented in Figure 2.11. We thus represent the centreline as an ideal reflecting surface.

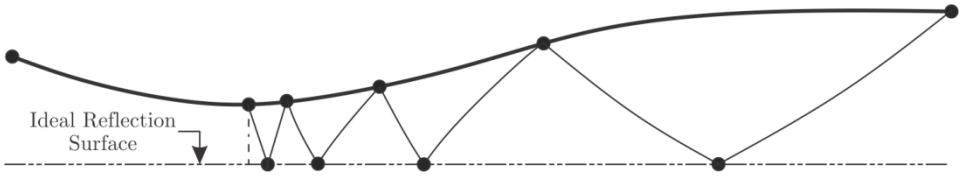

Figure 2.11: Schematic of the upper portion of a supersonic nozzle design using symmetry [5]

Computations of the method can employ either the point-to-point method or the region-to-region method. The former calculates the flow properties at all the points in the flow field, with the points determined by the intersection of the characteristic lines, whilst the latter calculates the flow properties in the regions bounded by the characteristic lines. The point-to-point method is the more appropriate method for this study, since it will produce the wall contour directly. Additional approximations are required to derive the wall contour when the region-to-region method is used.

In addition, numerous characteristic techniques exist for the design of supersonic nozzles, namely the minimum length method, the finite expansion method and the constant gradient method. The minimum length method, typically used in rocket nozzles, are short, thus the expansion section collapses to a point where the expansion takes place through a centred Prandtl-Meyer expansion

wave emanating from a sharp corner at the throat (inflection point) with an angle $\theta_{w,max}$. This maximum expansion angle of the wall is equal to one half of the Prandtl-Meyer function for the design exit Mach number, as portrayed in Equation 2.8 [5].

$$\theta_{w,max} = \frac{\nu_m}{2} \tag{2.8}$$

The finite expansion method usually has an expansion section that is frequently taken as a circular arc of a large radius usually larger than the nozzle throat height. Cases exist where the expansion section is modelled as an arbitrary curve where expansion waves originate from this curve. The expansion angle of these nozzles is typically less than $\theta_{w,max}$. The constant gradient method incorporates a straight expansion section to allow the profile to lengthen to meet the prescribed geometric boundary conditions. This method is unfavourable for a flexible plate nozzle as it would add unnecessary strain to the plate [5]. Once the shape of the expansion section is chosen the nozzle length and expansion angle are determined by the specified exit Mach number. Downstream of the inflection point the wall angle, θ_w, decreases until it becomes parallel to the test section walls at the nozzle exit.

A graphical aid of the upper half of the minimum length nozzle is illustrated in Figure 2.12 which will be referenced to relate points with respect to each other and to compute the coordinates of the boundary surface. Four expansion waves of type I characteristics have been sketched where the fluid particles are continuously accelerated as they pass through the waves. The expansion waves intersect the centreline at points 1, 6, 10 and 13, and are reflected as type II characteristics impinging on the nozzle wall at points 5, 9, 12 and 14 respectively. These reflected waves are in actuality the type II waves arising from the lower wall, which thus turns the flow back towards the horizontal.

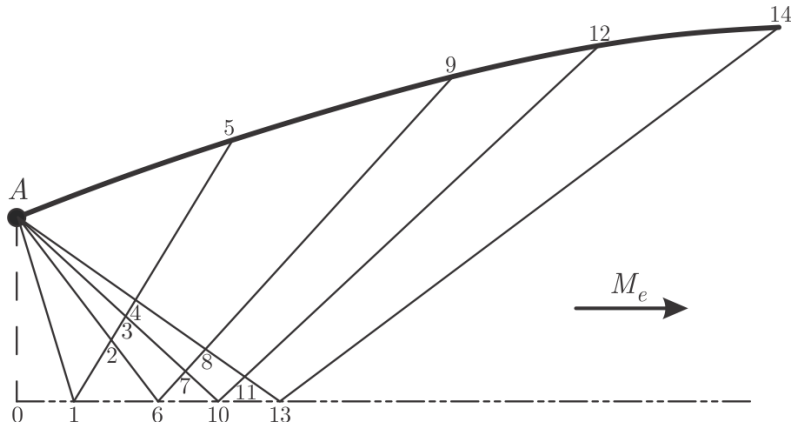

Figure 2.12: A graphical aid necessary to complete a MOC calculation

The inflection point is denoted as point A, with the characteristics numbered consecutively from the first characteristic line on the centreline as point 1 till it impinges on the contour wall at point 5. It then starts at point 6 on the centreline with the second characteristic line till point 9 at the wall, and so forth until the last characteristic line with point 14 on the contour. Verification of the number of points is completed with the Equation 2.9, where n is the number of characteristic lines.

$$number\ of\ points = \frac{n(n+3)}{2} \tag{2.9}$$

Given an exit Mach number, M_e, the Prandtl-Meyer angle is calculated and the maximum expansion angle is found from Equation 2.8. The first expansion wave is taken to be non-zero with a small turn in flow angle, θ_i(assumed to be very small) to allow a disturbance to propagate the information downstream of the nozzle to allow computation. Along the first characteristic line, $K^+ = 0$. The theta values for each point on a characteristic line are calculated from Equation 2.10.

$$\Delta\theta = \frac{\theta_{w,max}}{n} \tag{2.10}$$

Recalling Equation 2.5, the first characteristic line is therefore, $\theta = \nu(M)$. The characteristic line K^- can be therefore computed using Equation 2.4 with all the remaining values computed for the nodes lying on the first characteristic line. Furthermore, the values of K^+, K^-, θ, and ν for the contour is equal to the K^+, K^-, θ, and ν of the previous node. From the contour node, the next node goes back to the centreline, with θ starting at 0 and increasing by $\Delta\theta$. The K^- lines are hence calculated by using the fact that the nodes lie along the same characteristic line i.e. $(K^-)_6 = (K^-)_2$. Thus the Prandtl-Meyer function can be calculated using:

$$\nu(M) = K - \theta \tag{2.11}$$

The K^+ characteristic is hence determined from Equation 2.5. The process is hereafter repeated for each point in the characteristic grid where the values of the K^+, K^-, θ, and ν are calculated for every point. Computations then proceed to calculate the Mach number using the inverse Prandtl-Meyer function while the Mach angle (μ) is evaluated using Equation 2.12 [7].

$$\mu = sin^{-1}\left(\frac{1}{M}\right) \tag{2.12}$$

In the interest of finding the x and y coordinates of the nozzle profile, the gradients referred to as m^- and m^+ in Figure 2.13 must first be calculated, where Point A and B refer to the C^- and C^+ characteristic respectively which intersect at point P, the point of interest.

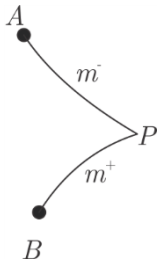

Figure 2.13: Gradients required to calculate the contour coondinates

The gradients ((m^-) negative gradient and (m^+) positive gradient) are calculated using Equations 2.13 to 2.16 utilizing the required equation for the specified nodal point. These equations average the values of $(\theta \pm \mu)$ for the point itself and the corresponding upstream point to produce a more accurate result [9].

$$m^- = tan(\theta_P) \qquad \text{(contour points)} \tag{2.13}$$

$$m^- = tan\left[\frac{(\theta - \mu)_A + (\theta - \mu)_P}{2}\right] \qquad \text{(internal and centreline points)} \tag{2.14}$$

$$m^+ = tan(\theta_P) = 0 \qquad \text{(centreline points)} \tag{2.15}$$

$$m^+ = tan\left[\frac{(\theta + \mu)_B + (\theta + \mu)_P}{2}\right] \qquad \text{(internal and contour points)} \tag{2.16}$$

Consequently, the x and y values for each point in the characteristic mesh is required in order to determine the contour points of the nozzle profile. Equation 2.17 and 2.18 demonstrate the necessary equations.

$$x = \frac{y_A - y_B + m^+ x_B - m^- x_A}{m_2 - m_1} \tag{2.17}$$

$$y = y_b + m_2(x_p - x_b) \tag{2.18}$$

The characteristic mesh developed in this explanatory example is very coarse, for simplicity. Naturally a far finer grid must be used to ensure a smoother and better approximated resultant contour. A computer code similar to the one developed by J. C. Sivells [11] is the most feasible tool for a refined mesh, since calculations of the Mach number extracted from the Prandtl-Meyer function becomes tedious when manually computed. The example described in this section outlines the basic steps necessary to produce a supersonic nozzle contour using the method of characteristics. However, to meet the geometric constraints of the HSWT and produce acceptable flow quality in

the test section of the wind tunnel, a more elaborate characteristic nozzle design method is required, as described subsequently.

2.4 Sivells' Nozzle Design Method

Numerous supersonic wind tunnels incorporate flexible plate nozzles to allow for multiple Mach number ranges to be tested. The flexible plates, frequently supported at discrete points, require continuous curvature such that the theoretical aerodynamic nozzle shape matches the elastic curve of the plate when shaped. James C. Sivells' nozzle design method encompasses the design of two-dimensional supersonic nozzles and maintains continuous curvature of the nozzle thereby ensuring that the flow is parallel, uniform and shock free in the test section region, while meeting dimensional constraints imposed by the facility in question [12].

Foelsch indicated that the straightening section of a nozzle profile can be computed analytically by assuming that the flow is radial at the inflection point of the nozzle. As a result the flow is assumed to originate from a single source point upstream of the inflection point [13]. Ordinarily, the expansion section is chosen arbitrarily or determined analytically, although this does not ensure radial flow at the inflection point.

Presently in the design of supersonic nozzles using the method of characteristics, the characteristics have equal strength where the expansion waves are created in the expansion section and cancelled in the straightening section. The curvatures of the expansion and straightening regions have a finite positive and negative value (for the upper contour), respectively as the angle varies along these sections. The curvature is discontinuous at the inflection point and the test section region since a pure reflection causes the curvature to be zero as seen in Figure 2.14. Riise and Puckett's supersonic nozzle design method ensures that the curvature of the contour is continuous by including a transition region following the expansion region where the characteristics are partially cancelled and partially reflected to ensure that the second (and third) derivatives of the contour are continuous [14].

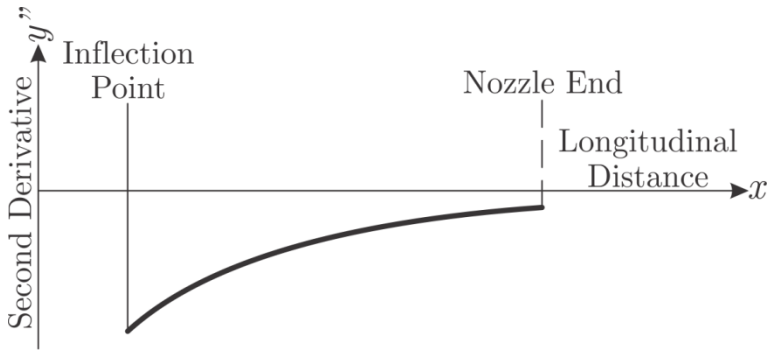

Figure 2.14: Curvature of a nozzle profile [12]

The Sivells' method incorporates the source flow computations from the Foelsch method with the design of a continuous curvature supersonic nozzle from Riise and Puckett to provide the equations to determine the characteristic angles required to satisfy the nozzle length, nozzle height as well as maintain continuous curvature between the expansion and straightening regions. Figure 2.15 assumes that the flow is radial where the arc AO, of a circle around the apparent source, is an equipotential line along which the Mach number is constant. Point A refers to the inflection point, with Point U the nozzle exit having zero curvature. The points P and T are defined as the characteristic points lying at the start of the straightening section [12].

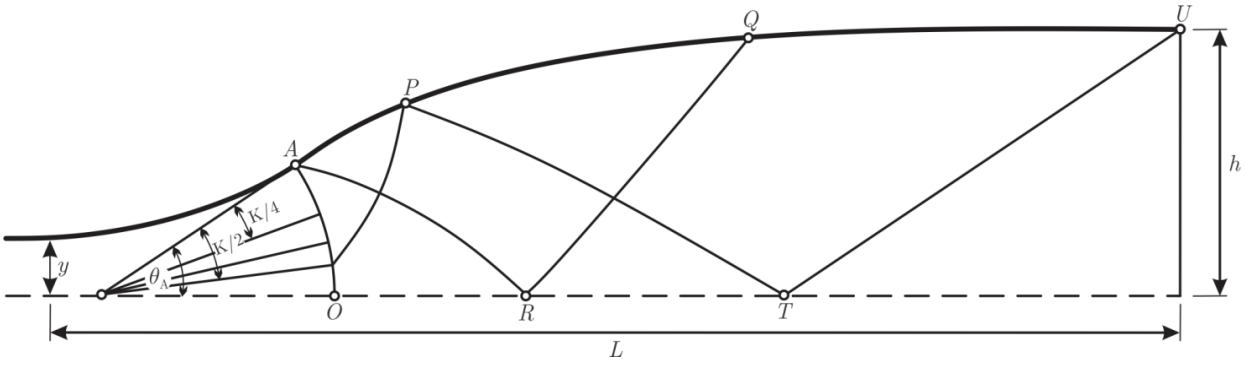

Figure 2.15: Characteristic diagram for a continuous curvature nozzle as described by Sivells [12]

The characteristic point P intersects the arc AO upstream, where the flow inclination crossing the arc is θ_{1P}, while the inflection point (A) angle is θ_A. The parameter K (constant value) is an angle defined by the inflection point angle which is used to define the rate of change of curvature of the nozzle profile as represented in Equations 2.19 to 2.20, which are used to interrelate θ_{1P}, θ_P, θ_A and K, where θ_P refers to the angle at point P.

$$\theta_A - \theta_{1P} = \frac{K}{2} \tag{2.19}$$

$$\theta_A - \theta_P = \frac{K}{8} \tag{2.20}$$

Sivells defines the Prandtl-Meyer angle of the characteristic point P, ν_P (Equations 2.21 and 2.22) in terms of the Prandtl-Meyer angle of the test section, ν_T, defined by the exit Mach number, and the wall angle at the characteristic point, θ_P. Furthermore, the wall angle can be expressed in terms of the inflection point angle, θ_A and the parameter K, where the parameter K ranges from zero to a maximum value of $4\theta_A$. For practical purposes this value should be greater than $2\theta_A$ [12].

$$\nu_P = \nu_T - \theta_P \tag{2.21}$$

$$\nu_P = \nu_T - \theta_A + \frac{K}{8} \tag{2.22}$$

Similarly the Prandtl-Meyer angle at the inflection point, ν_A is defined in Equations 2.23 and 2.24, with the flow inclination represented by the θ_{1P} value.

$$\nu_A = \nu_P - (\theta_P - \theta_{1P}) \tag{2.23}$$

$$\nu_A = \nu_T - \theta_A - \frac{K}{4} \tag{2.24}$$

The Prandtl-Meyer angles at the contour (wall), ν_w, are described in terms of the Prandtl-Meyer angle at A (ν_A), the wall angle (θ_w) and the flow inclination of any fluid that crosses the arc AO (θ_1) from the inflection point A to the characteristic point P. For the characteristic point P to the end of the nozzle at point U, the Prandtl-Meyer angles at the contour, ν_w, are equivalent to the Prandtl-Meyer angle at the test section, ν_T, minus the wall angle (θ_w), as defined in Equations 2.25 to 2.26 respectively. The wall angles are computed via the method of characteristics for supersonic nozzle design [12].

$$\nu_w = \nu_A + \theta_w - \theta_1 \qquad \text{(from Point } A \text{ to Point } P\text{)} \tag{2.25}$$

$$\nu_w = \nu_T - \theta_w \qquad \text{(from Point } P \text{ to Point } U\text{)} \tag{2.26}$$

Referring back to Figure 2.15, the arc AO is divided into r equal parts, where the angle $\frac{K}{2}$ contains k of these r parts so that:

$$\frac{k}{r} = 1 - \frac{\theta_{1P}}{\theta_A} = \frac{K}{2.\theta_A} \tag{2.27}$$

The characteristic mesh is hence created by initiating the characteristic lines on the arc AO at the midpoint of each of these r parts, termed as Points w, x, y and z, as portrayed in Figure 2.16. Moreover, the points on the nozzle contour are numbered consecutively from 1 to $(2r + k)$, with the first point located aft of the inflection point (Point 1). Exercising Sivells' definitions, the inflection point corresponds to a point number of $\frac{1}{2}$ and not zero as is typically used in the method of characteristics. Correspondingly, if one assumes that $\theta_{1P} = 0.25\theta_A$, then from Equation 2.19, $K = 1.5\theta_A$. Incorporating these values into Equation 2.27, results in $k = 0.75r$. Let us assume that $r = 4$, hence $k = 3$ and points P, Q and U have values of $\left(k + \frac{1}{2}\right), \left(2r + \frac{1}{2}\right)$ and $\left(2r + k + \frac{1}{2}\right)$ which calculate to values of 3.5, 8.5 and 11.5 respectively [12].

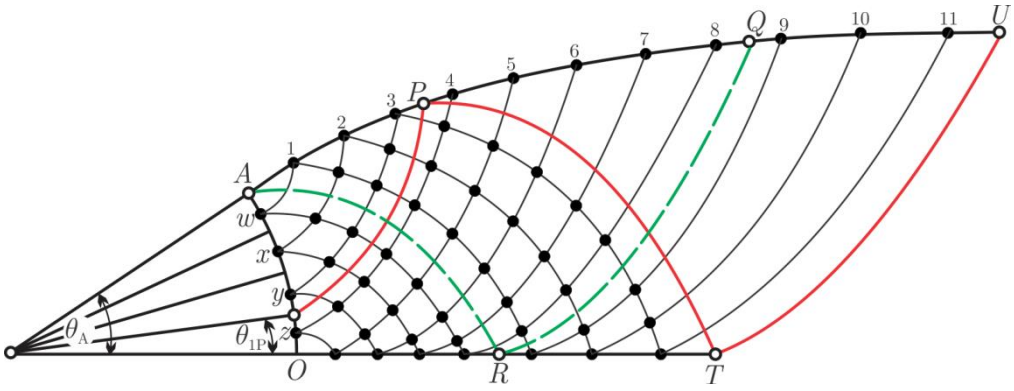

Figure 2.16: Numbering system in the characteristic mesh for Sivells' nozzle design method

If m denotes the point number, equations are specified for the wall angles where k, m and r are integers, as follows.

$$\frac{\theta_w}{\theta_A} = 1 - \left[\frac{(2m-1)^2}{16rk}\right] \qquad \text{(from Point 1 to Point } k\text{)} \tag{2.28}$$

$$\frac{\theta_w}{\theta_A} = 1 - \left[\frac{2m-1-k}{4r}\right] \qquad \text{(from Point } k+1 \text{ to Point } 2r\text{)} \tag{2.29}$$

$$\frac{\theta_w}{\theta_A} = \frac{(4r+2k+1-2m)^2}{16rk} \qquad \text{(from Point } 2r+1 \text{ to Point } 2r+k\text{)} \tag{2.30}$$

Subsequently, all the remaining angles downstream of the inflection point, lying in the characteristic mesh, but not on the contour, are evaluated, at each characteristic point, using the traditional method of characteristics procedure. In summary, using the method of characteristics with the constraints and criteria defined by Sivells, practical nozzle shapes with continuous curvature, specifically suited to the HSWT can be obtained.

2.5 Nozzle Boundary Layer Treatment

The flow of a fluid over any surface results in the introduction of friction forces between the air and the surface. This is due to the viscous nature of the fluid where a loss in velocity and momentum of the fluid stream results as the surface is approached until it reaches zero velocity at the surface. The boundary layer refers to the region where the loss in velocity and momentum occurs [4]. This very thin layer occurs near the surface where the velocity is substantially smaller than at a distance away from the surface. Figure 2.17 highlights the velocity distribution on a surface, with the dimensions normal to the plate, exaggerated for effect, and the velocity distribution uniform upstream of the surface. The boundary layer thickness, δ, increases downstream of the plate as more of the fluid becomes affected by the viscous interaction of the fluid and the surface [15].

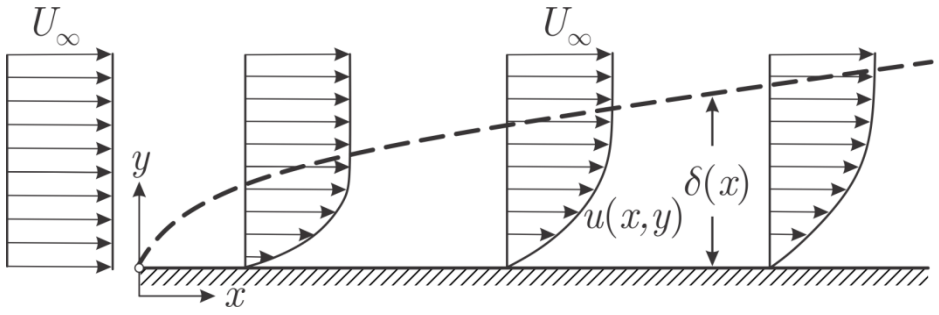

Figure 2.17: Sketch of boundary layer on a flat plate surface with parallel flow [15]

Boundary layers can be classified as either laminar or turbulent depending on the structure and conditions under which they are created. A laminar boundary layer occurs where the flow moves in streams, with each stream sliding past the adjacent layer uniformly and smoothly. In contrast, a turbulent boundary layer is evident by the mixing of fluid streams, formed at high Reynolds numbers. An exchange of mass, momentum and energy occur, but this is larger for the turbulent case [4].

Due to the high Reynolds number in supersonic facilities, the boundary layer is usually turbulent [4]. As the flow is accelerated in the nozzle, the boundary layer is negligibly thin at the throat and starts to become thicker downstream of the throat, as the Mach number increases. The thickest layer occurs within the test section region, which is the region of utmost importance for developing uniform flow [4]. Investigations indicated that the boundary layer for various supersonic nozzles is approximately linear from the inflection point to the end of the nozzle in the test section region [12].Therefore various supersonic wind tunnels have a diverging test section region of constant angle to compensate for the boundary layer growth [16]. Another method that is commonly used for boundary layer correction is to apply a displacement correction factor to the nozzle contour, by adjusting the area ratio for a specific Mach number, to account for the boundary layer. Certain, larger supersonic tunnels have slotted walls, which also helps to reduce the interference caused by the presence of the walls.

3. DESIGN OF A SUPERSONIC NOZZLE

3.1 Facility Constraints

The CSIR's HSWT nozzle incorporates a fixed converging section, a solid throat block (that is free to translate and rotate about a pivot point), a flexible steel plate and a fixed diverging test section region, all of which are interdependent, as represented in Figure 3.1. These work in synergy to control the Mach number and flow quality in the operational section of the wind tunnel. Typically in wind tunnels of this nature, the inflection point occurs where the throat block and the flexible plate meet which ensures that the stress in the plate is minimised by enabling a smooth profile in the flexible plate i.e. the curvature in the plate is continuous and has the same direction over the length of the plate, although the magnitude may vary.

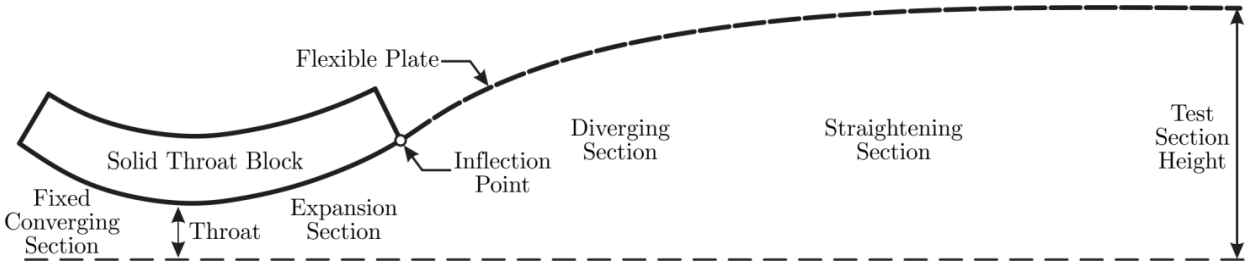

Figure 3.1: Components of the convergent-divergent (Laval) nozzle in the HSWT

The standard procedure for designing a supersonic nozzle using the method of characteristics must be adapted to accommodate the HSWT nozzle constraints i.e. the solid throat block, the length of the flexible plate, the test section height and the fixed diverging test section region. This is necessary as the traditional method of characteristics produces profiles that are considerably short in length with steep wall angles. It is desirable to design profiles for the wind tunnel that are sufficiently long in order to minimize the wall angle thereby ensuring smooth curvature over the plate, as well as to utilize as many jacks as possible to shape the flexible plate. Furthermore, the designed nozzle profiles should keep the Mach number distribution to within 0.5% of the desired Mach number in the test section – a quality assurance criterion stipulated by the facility. As expected, the minimum error occurs at the lowest Mach number and vice versa.

The use of a solid throat block imposes severe limitations in designing for continuous curvature of the flexible plate nozzle. Considering these constraints, the throat block is inherently the expansion region of the nozzle. Applying the traditional method of characteristics with the expansion waves emanating in the expansion region causes multiple reflections in the expansion region of the profile

which increases complexity of the calculations but does not aid in lengthening the profile [17], as portrayed in Figure 3.2.

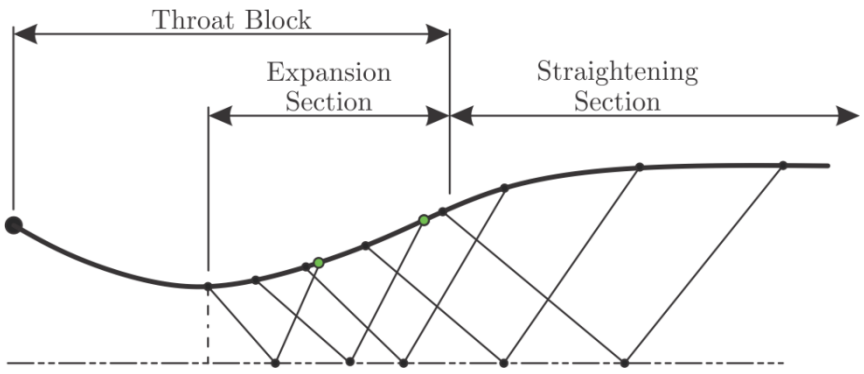

Figure 3.2: Reflections in the expansion region of the nozzle

3.1.1 Throat Block and Test Section Geometry

The main jacks of the HSWT allows the symmetric throat blocks (as diagrammatically represented in Figure 3.3) to both translate and rotate about its pivot point. As a result, multiple solutions for the wall contour shape exist for a single Mach number.

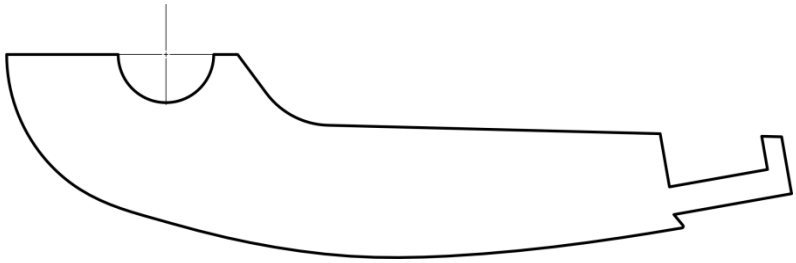

Figure 3.3: Schematic of single throat block geometry for the HSWT nozzle

Figure 3.4 displays the initial throat block geometry (0 degrees) with selected throat rotations whereas Figure 3.5 presents the throat coordinates as they would be translated to meet the required throat dimensions for a Mach 3.0 case. It should be noted that Figure 3.5 merely displays the geometry from the throat of the nozzle whereby the geometry upstream of the throat is removed by computing the gradient change. Additionally, the rotation causes a shift in the inflection point position which allows multiple solutions for one Mach number set point.

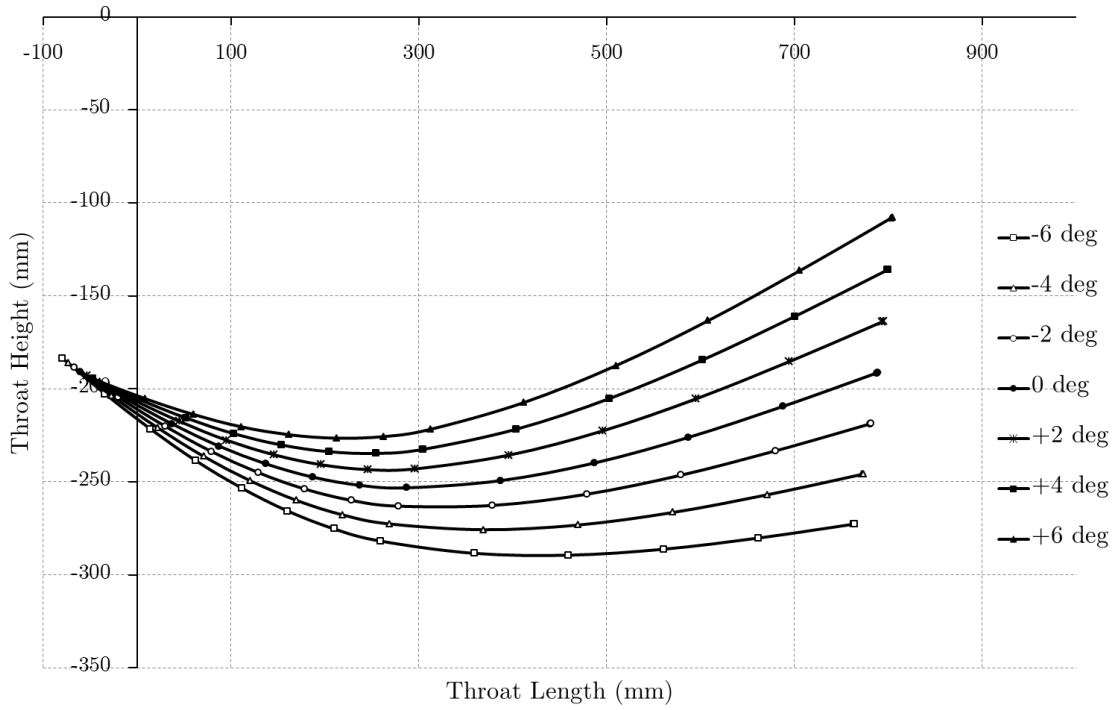

Figure 3.4: Throat block rotation for various angles

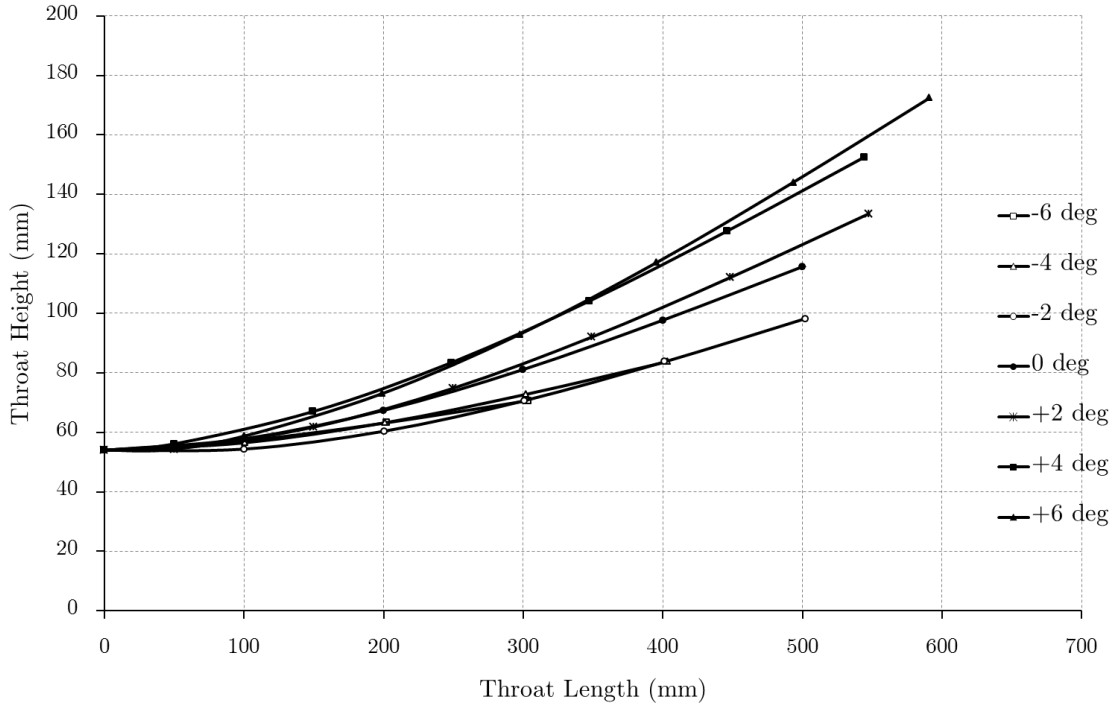

Figure 3.5: Various throat block rotations for a Mach 3.0 set point

Another constraint for this nozzle design is the fixed test section. The flexible plate of the nozzle is allowed to pivot by pin connections at three positions, which allow the flexible plate to bend locally, but restrain its vertical translation. These dimensions are portrayed in Figure 3.6. The nozzle profiles will thus be generated for a terminal height of h = 227.74 mm, which increases to 229.675 mm along the fixed test section region. The HSWT was designed in this manner to attempt to

correct for the freestream displacement induced by the viscous boundary layer effects, which grows along all four walls of the nozzle and instigates a drop in Mach number i.e. the boundary layer alters the effective area ratio between the throat and the nozzle exit. The flexible plate length is 2950 mm with the fixed, pinned region spanning 719.5 mm. The lengths of the profiles, from the inflection point to the test section, for the various Mach numbers must be modelled to be as close to 2230.5 mm as possible. The control points that shape the plate are discretely positioned along the plate and it is desirable to use as many of these control points as possible to allow finer control over the nozzle contour.

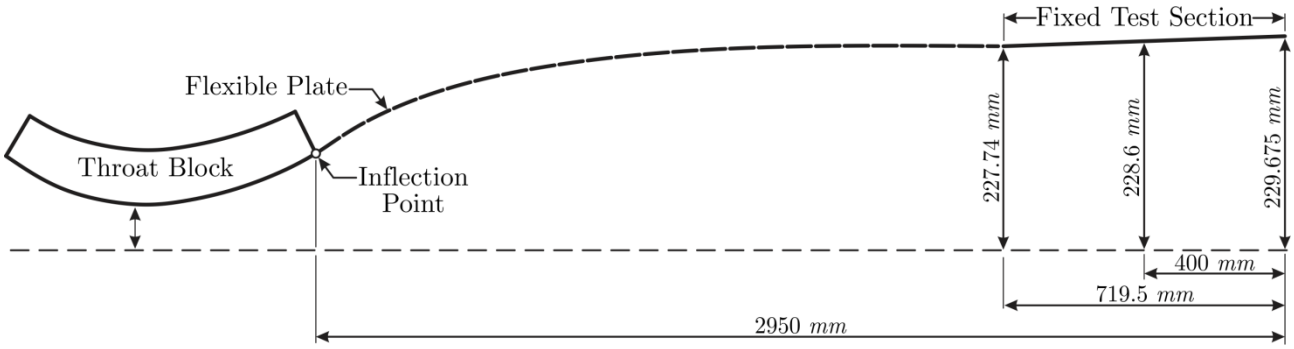

Figure 3.6: Geometric constraints of the flexible plate highlighting the fixed test section dimensions

3.2 Analytical Technique Adapted from Sivells' Nozzle Design Method

Sivells' nozzle design method allows for a variety of specified initial conditions, which need to be optimised such that the resulting nozzle profiles produce the best possible flow conditions within the operational region of the HSWT facility. Thus, Sivells' nozzle design method was adapted to incorporate optimised initial conditions that are within the geometric capabilities of the HSWT. The method followed can be divided into three broad segments, namely:

- A throat rotation procedure to optimise and match the inflection point angle and the constant K term which defines the rate of change of curvature of the nozzle profile.
- A source flow calculation, coupled with defining the characteristic mesh resolution.
- A traditional method of characteristics computation aided diagrammatically with a characteristic mesh.

For a specified test section Mach number, M the throat block orientation is to be determined by utilizing the throat geometry and rotating the throat block position until a suitable inflection point angle (θ_A) is met. The process commences with a one degree of freedom rotation, determined by the x and y throat geometry coordinates and the rotational angle, α as highlighted by Equation 3.1 and Equation 3.2.

$$X = x.\cos\alpha - y.\sin\alpha \tag{3.1}$$

$$Y = x.\sin\alpha + y.\cos\alpha \tag{3.2}$$

The gradient between two adjacent coordinates is then calculated, where only the coordinates for the positive gradients are applied to enable modelling of the throat block from the throat only. This implies that no translations are required in the initial computations, since the coordinate system used in the computations is defined relative to the throat. Since the geometry of the wetted region of the throat block can be approximated (with high confidence) by a sixth order polynomial, the Cartesian coordinates for the inflection point (x_A and y_A) can be determined relative to the defined coordinate system. Due to the relatively complex geometry of the throat block, an iterative process to attain the required throat block rotational angle (α) for the optimised inflection point angle (θ_A) is incorporated into the solution process.

The ratio between the constant, K and the inflection point angle, θ_A, referred to as K_{target} henceforth, is manipulated to adjust the curvature of the profile thereby modifying the contour to the required length. This parameter was incorporated into the procedure from the outset so that length adjustments of the profile can be made, in order to meet the geometric boundary conditions of the HSWT. This implies that the length of the profile is indirectly set as an initial condition by specifying K_{target}, rather than directly entering the length value into the procedure. It is worth recalling that practical values of the rate of change of curvature lie between $2\theta_A < K < 4\theta_A$ i.e. $2 < K_{target} < 4$ [12]. In the limit that $K_{target} = 4$, a maximum profile length for a specified test section Mach number is achieved. Since the physical throat block profile is used to determine θ_A, this maximum computed length is also the maximum possible length geometrically possible in the facility, for the specified Mach number. For a given inflection point angle, the K value is calculated by rearranging Equation 2.24 to Equation 3.3 where the Prandtl-Meyer angle at the nozzle exit is known from the desired Mach number. The ratio of K to θ_A is then computed, tested against the length parameter (K_{target}) and if it is not met, the throat block is further rotated. This forms part of the iterative process used to find the optimised inflection point angle (θ_A) by rotating the throat block, as discussed previously.

$$K = 4(\nu_T - \nu_A - \theta_A) \tag{3.3}$$

Once the optimised throat block position is determined for a specific test section Mach number, which meets all the physical constraints of the HSWT, the Sivells' nozzle design method proceeds from the inflection point downstream, based on the assumption that flow at the inflection point, A originates from a source flow point, S along the axis of the nozzle, as displayed in Figure 3.7. The

fixed throat block of the HSWT has discrete x and y coordinates with the inflection point located relative to the $x = 0$ position, i.e. the throat location. The source flow point must be determined relative to this throat location such that the coordinates of the inflection point remains unchanged with respect to the throat location, as this has become the reference point for all computations.

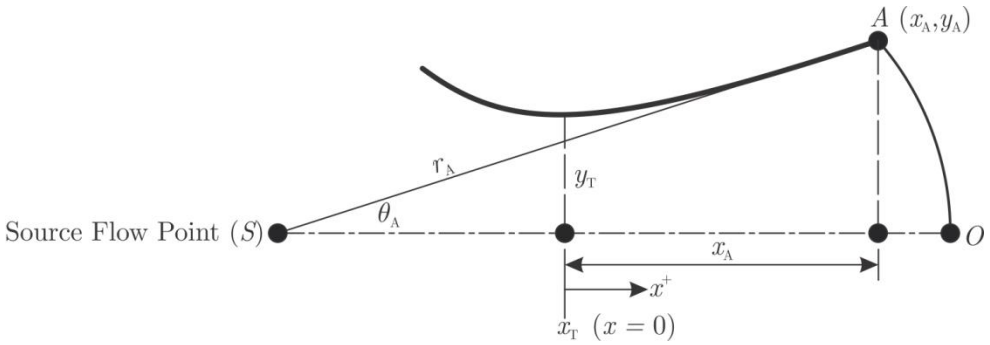

Figure 3.7: Schematic of the source flow transformation required for Sivells' nozzle design method

The location of the source flow point and hence the radius of the arc, AO, denoted as r_A, must be referenced from the $x = 0$ (at the throat) position, in order to develop a nozzle profile that is compatible at the optimised inflection point. We know that the line SA intersects the nozzle axis at the initial inflection point angle, θ_A, such that the gradient, m_A, of line SA is:

$$m_A = \tan \theta_A \tag{3.4}$$

As a result, the equation of the line SA is:

$$y = m_A x + c_A \tag{3.5}$$

If we substitute the known coordinates of the inflection point, A (x_A and y_A) into Equation 3.5, we can solve for the constant c_A. However, since the source flow point is located on the nozzle axis, $y_s = 0$ and $x_s = -x'$ such that $x' = c_A/m_A$. The arc of the radius, r_A is hence:

$$r_A = \sqrt{(x_A + x')^2 + (y_A)^2} \tag{3.6}$$

Furthermore, the characteristic mesh resolution (number of segments on the arc), r on arc AO is specified by dividing θ_A into segments such that $\Delta\theta = \theta_A/r$ as portrayed in Figure 3.8 when $r = 3$. Each characteristic point, however, lies in the centre of each segment making the angle of the first characteristic point subsequent to the nozzle axis equivalent to $\theta_1 = \Delta\theta/2$. The succeeding points will be calculated as $\theta = \Delta\theta/2 + \Delta\theta$. Consequently, the last characteristic point will have an angle of $\theta_3 = \theta_A - \Delta\theta/2$. The x and y coordinates of these characteristic points are computed using

traditional polar to Cartesian coordinate transformations, since the arc AO has a constant radius of r_A.

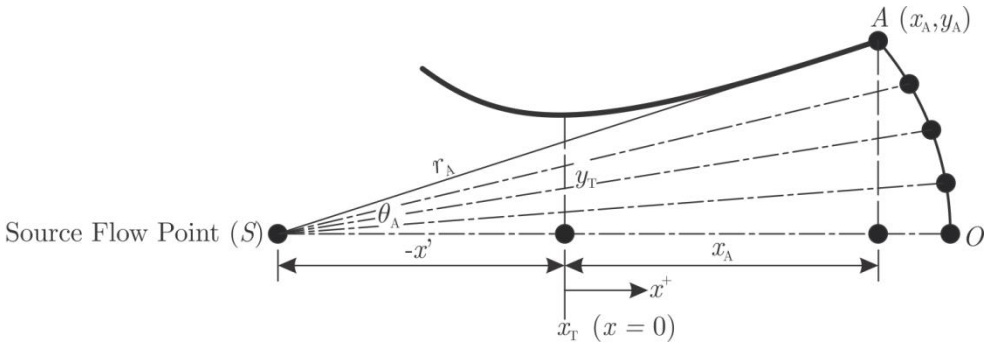

Figure 3.8: Characteristic mesh resolution for $r = 3$ and $k = 4$

These points are then used to initiate the characteristic network, labelled vertically between A and O as 1, 2 and 3, in Figure 3.9. The bold numbers at the top of Figure 3.9 correspond to the wall points defined by Sivells' in Equations 2.28 to 2.30, and the points A, P, Q and U have also been included to correspond to the definitions outlined in Section 2.4, Figure 2.15. The characteristic network is shown in a rectangular manner in this image for clarity. Subsequent to the diagrammatic aid, the steps listed below are followed sequentially to design the nozzle profile by means of the method of characteristics.

- Determine the Prandtl-Meyer angle at the inflection point, ν_A.
- Calculate the wall angles (θ_w) using Equation 2.28 to Equation 2.30.
- Set the centreline angles to zero, $\theta_{centrelines} = 0$.
- Knowing the wall angle at the test section is $\theta_{TS} = 0$, and the Prandtl-Meyer angles at the test section, ν_{TS}, determine the corresponding K^+ and K^- values.
- Calculate the remaining K^+ values for all the remaining nodes by assuming that all terms have a constant K^+ value along C^+ characteristic lines.
- Compute the Prandtl-Meyer angles at the centrelines by rearranging Equation 2.5.
- Evaluate the K^- values for the centreline terms.
- Determine the Prandtl-Meyer angles and the K^- values for the nodes lying on the arc AO.
- Calculate all K^- for the remaining internal characteristic nodes.
- Compute the flow and Prandtl-Meyer angles for the remaining internal characteristic nodes using Equation 2.6 and Equation 2.7.
- Evaluate the Mach number (M) and hence Mach angle (μ) at each nodal point.
- Determine the gradients, m^+ and m^- for each nodal point in the characteristic mesh using Equation 2.13 to Equation 2.16.
- Calculate the x and y coordinates using Equation 2.17 and Equation 2.18.

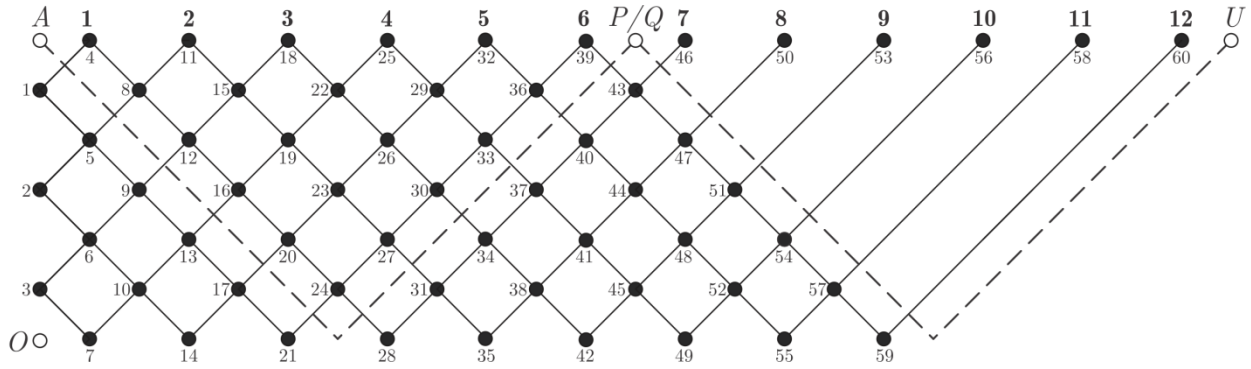

Figure 3.9: Schematic of characteristic mesh for a resolution, $r = 3$ utilizing Sivells' nozzle design method

A simple excel spreadsheet with a coarse mesh was initially used to understand the method to be followed. Thereafter, an automatic algorithm was scripted in MATLAB to assist with the method of characteristics computations with much higher characteristic network resolutions. The code also included the procedures to determine the optimised initial conditions by rotating the throat block, the source flow calculations, as well as post-processing functions for exporting the data in useable formats. Specific details of the code are documented in the section to follow.

In summary, the adaption of the Sivells' nozzle design method for the current study focused on incorporating the HSWT facility constraints into the design method as boundary conditions. This included an optimisation procedure where the physical throat block geometry was rotated to achieve a suitable inflection point angle for a given Mach number, such that the length criterion (defined by K_{target}) was satisfied. Thereafter, a source flow transformation was used to initiate the characteristic network for a specified resolution (r). Finally, the method of characteristics procedure was used to generate the nozzle contour for the desired test section Mach number.

3.3 MATLAB Code

For purposes of automatic optimisation and computation of the nozzle contours, a program was created in MATLAB. Figure 3.10 outlines the main MATLAB program (*Main_Program.m*) which calls on multiple functions used sequentially in the computations viz. *ProfileFileName.m*, *Throat_R.m*, *SourceFlow.m*, *WallFuntion.m*, and *ContourCalc.m*. Table 3.1 provides a brief description of each function in the sequence that they are executed. An example of the code, for a nozzle exit Mach number of $M_e = 3.0$, can be found in Appendix A.

```
% PROGRAM MAIN - SIVELLS NOZZLE DESIGN METHOD

clear all; clc; close all; format long;

%--INPUTS--%
%Nozzle Exit Mach number
Me = 3.0;

%Number of segments/equal parts on the arc AO
r  = 40;

%This is the ratio of K/Theta_A not the value of K
K_target = 4.0;

%Throat Rotation Increment Resolution
rot_res = 1/10000;

%Initial Throat Rotational Position
Initial_Alpha =  -8.05;
```

```
%--FILE NAME FOR EXCEL AND .MAT FILES--%
[FileName] = ProfileFileName(Me,r,K_target);
```

```
%--SIVELLS' VARIABLES FROM THROAT ROTATION--%
[theta_A,xA,yA,K,k,Xcalc,Ycalc,throat_halfheight] = Throat_R(Me,r,K_target,rot_res,Initial_Theta,FileName);
```

```
%--CONVERSION TO SOURCE FLOW--%
[arc_x,arc_y,theta_arc,xO,yO] = SourceFlow(xA,yA,theta_A,r,Xcalc,Ycalc,Me,FileName);
```

```
%--CALCULATION OF WALL ANGLES & PRANDLT-MEYER FUNCTIONS & MOC--%
[theta_w,nu_w,X_s_p,Y_s_p,X_c,Y_c] = WallFunction(Me,theta_A,r,k,K,arc_x,arc_y,theta_arc,xA,yA,xO,yO,FileName);
```

```
%--GENERATE WALL CONTOUR PROFILE AND WRITE TO EXCEL FILE--%
[Contour_X,Contour_Y] = ContourCalc(Xcalc,Ycalc,X_s_p,Y_s_p,X_c,Y_c,Me,xA,FileName);
```

Figure 3.10: Main program used to generate the nozzle contours by the method of characteristics

Table 3.1: Detailed explanations of the MATLAB functions

No.	File Name	Description
1.	*Main_Program.m*	Calls the functions required to compute the nozzle profiles and includes the inputs required to generate the profiles: • "M_e" is the required Mach number at the nozzle exit. • "r" is the resolution used to initiate the characteristic net on the arc AO. Increasing this value, increases the accuracy of the generated profile but results in longer computational times. • "K_target" is the ratio of the angle K to θ_A and is a profile length control parameter. This input variable can have a value of 0 to 4. Increasing this value, increases the length of the profile. • "rot_res" is the increment with which the throat block is rotated in degrees. A small value produces an increased

		resolution of the optimisation procedure by rotating the throat block in fine steps to a suitable value, but results in longer computational times. • "*Initial_Alpha*" is the initial throat block rotational position from where the optimisation process in initiated.
2.	*ProfileFileName.m*	Creates a unique name for each computation based on the inputs into the main program. This name is used when storing all the variables of the calculations in a .mat file and is also used to name the .xlsx file that contains the final computed profiles.
3.	*Throat_ R.m*	Imports the physical throat block geometry into MATLAB and executes the optimisation procedure. The function rotates the throat block until a suitable inflection point angle is reached, such that it satisfies the length target, as well as other geometric constraints of the HSWT facility.
4.	*SourceFlow.m*	Generates the source flow coordinates along the arc AO that is required to initiate the characteristic network.
5.	*WallFunction.m*	Completes all the method of characteristics calculations from the inflection point towards the test section region using the Sivells' nozzle design method for the wall angles and the Prandtl-Meyer functions at the wall. The function then works backwards to determine the flow angles at each point in the characteristic net thereby determining the wall coordinates of the profile.
6.	*ContourCalc.m*	Combines the throat points with the generated profile coordinates as well as the fixed test section dimensions to produce the final profile. It then writes the coordinates to an excel file. This function also produces graphical images of the profile for visual inspection.

3.4 Plate Stress

As is the case of a flexible nozzle, the plate is supported at a number of control points (seven jacks per plate for the HSWT) to position the contour to its required profile. The flexible plate can be modelled as a flexible beam with rectangular cross-section with a number of supports. In order to minimize the stress in the flexible plate, the profiles were generated aft of the inflection point to ensure that the plate has a smooth profile with continuous curvature. Additionally, the rate of change of curvature also adds stress to the plate whereby the plate stress is caused by the differential pressure across the plate which adds to the bending stress. The deflection of the plate, $v(x)$ is calculated using the profile coordinates as portrayed in Equation 3.7 [18].

$$v(x) = f(x) \tag{3.7}$$

Subsequently, the bending moment, M is calculated using the relationship found in Equation 3.8 [18] where $\frac{d^2v}{dx^2}$ refers to the second derivative of the deflection, E refers to the Youngs Modulus and I refers to the area moment of inertia of the plate. The shear stress induced onto the plate is negligible in comparison to the bending stresses. Therefore the maximum bending stress, σ is computed from the bending moment and the distance of the outer most material fibre from the neutral axis, y as represented in Equation 3.9 [18]. The maximum stresses induced by the shape of each profile was calculated and compared to the yield strength of the material of the plate, thereby ensuring that the plate does not deform plastically when the profiles are set in HSWT.

$$\frac{\frac{d^2v}{dx^2}}{1+\left(\frac{d^2v}{dx^2}\right)^2} = \frac{M}{EI} \tag{3.8}$$

$$\sigma = \frac{My}{I} \tag{3.9}$$

4. NUMERICAL FLOW INVESTIGATION

4.1 Computational Method

A computational study was exercised to evaluate the nozzle profiles in order to ascertain the Mach number distribution across the test section, determine whether the calculated profiles produce shock free flow in the test section, as well as use the computational results to correct the profiles for the viscous effects experienced in the tunnel. The Computational Fluid Dynamics (CFD) simulations (pre-processing, processing and post-processing) were completed in the commercial flow solver, STAR-CCM+ V9.06, where a coupled flow solver was employed and the air was modelled as an ideal gas.

All the points (expansion section, straightening section and fixed test section) were directly imported into SolidWorks V14 Computed Aided Design (CAD) software as a curve, in order to generate the geometry required for the CFD computations. Initially, Euler simulations of the profiles where completed to verify that the inviscid nozzle profiles generated by the method of characteristics computations produced acceptable flow in the test section of the HSWT. Thereafter, Reynolds-Averaged Navier-Stokes (RANS) computations were completed of the same profiles to assess the viscous effects in the wind tunnel.

After completing symmetry checks and analysing the field for transient effects, it was deemed that time-averaged (pseudo steady) computations, using a quarter three-dimensional model of the flow field would provide an adequate representation of the HSWT's actual flow field. The advantage of this approach is that computational time is minimized, which saves on the costs per simulation. The three-dimensional geometry employed in the simulations with the specified boundary conditions is depicted in Figure 4.1. It should be noted that although the MOC produces a two-dimensional nozzle profile, it was necessary to model the three-dimensional domain, since the boundary layer growth is not limited to the nozzle contour only, but develops along the side walls of the wind tunnel as well, consequently affecting the test section flow.

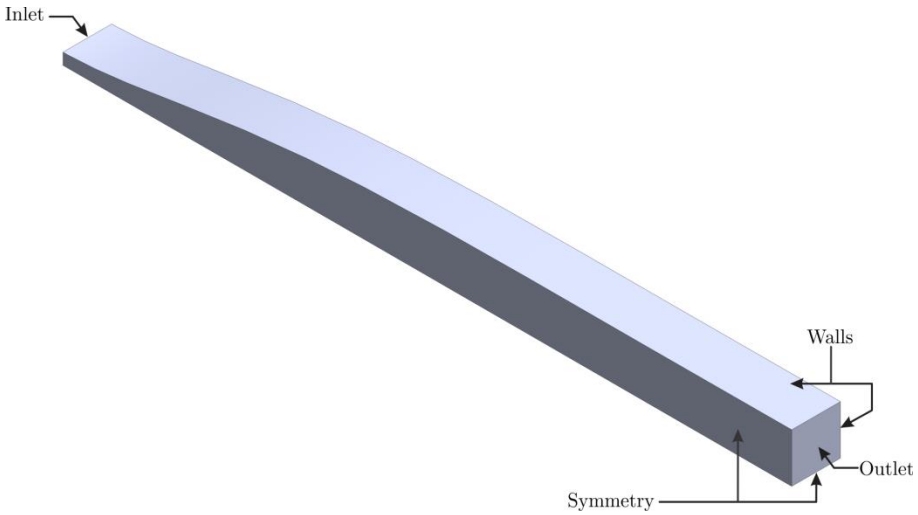

Figure 4.1: Three-dimensional quarter geometry required as an input for the CFD with specified boundary conditions

Since we are concerned with the air flow inside of the wind tunnel, an external fluid domain boundary was not required. The inlet to the fluid domain was specified as a stagnation inlet, and was set to sonic conditions, since the flow domain starts from the throat of the nozzle where choking conditions occur. The pressure settings at this boundary were calculated based on the required starting stagnation conditions for the Mach number of nozzle profile being simulated. The nozzle contour and side wall was specified as non-slip solid walls, while the pressure outlet was set to static conditions of the test section, for the Mach number of nozzle profile being simulated.

4.2 Discretisation Technique

An unstructured polyhedral cell based volumetric mesh was generated, as displayed in Figure 4.2, with a refined boundary layer mesh along the nozzle profile and side wall to adequately resolve the boundary layer region for the viscous simulations. The polyhedral mesher provides a balanced solution by reducing the cell count as opposed to a tetrahedral mesh, whilst the prism layer mesher extruded cells normal to the wall boundaries, which aids in improving the accuracy of the viscous flow solutions. Furthermore the surface remesher tool was utilised to re-tessellate the surfaces of the imported geometry in order to improve the quality of the surfaces, which optimises the mesh generation process [19].

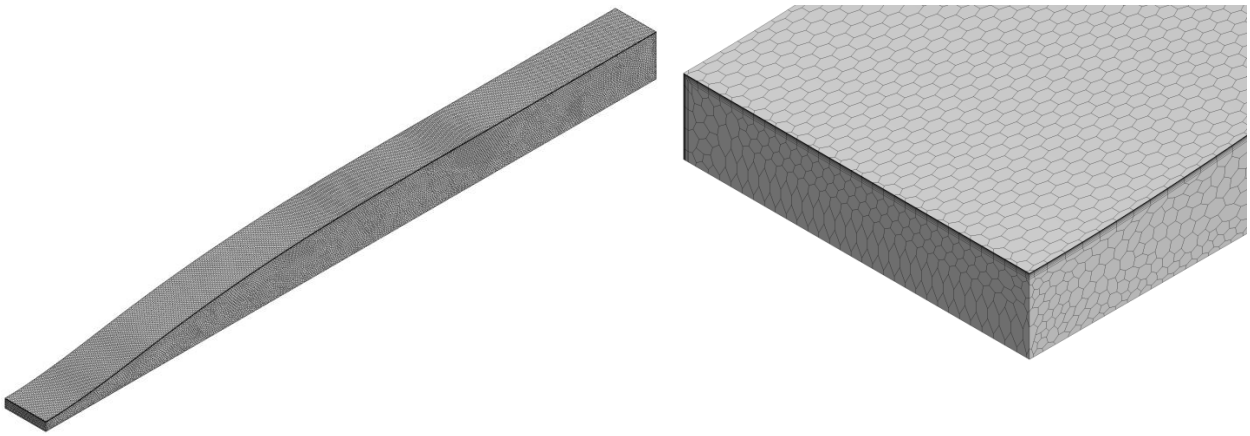

Figure 4.2: Unstructured volumetric mesh highlighting the boundary layer meshing technique implemented

Mesh independence studies were completed to ensure that the results were independent of the mesh resolution of the simulations. Figure 4.3 highlights the average Mach number variation in the test section with varying cell size, for a viscous simulation of a profile generated to produce a nozzle exit Mach number of $M_e = 3.0$. The error bars highlight the acceptable limits of the computed Mach number set point. It should be noted that the cell sizes have been normalised with the finest grids minimum element size. A curve fit was used to extrapolate the test section Mach number with an infinite number of grid points, i.e. when the minimum element size tends to zero. From Figure 4.3, it is evident that no appreciable gain in solution accuracy is achieved beyond a normalised base cell size of 4. For this reason, all solutions were computed at a base size of 0.01, with the total cell count lying between 350 000 to 1 000 000 depending on the profile shape.

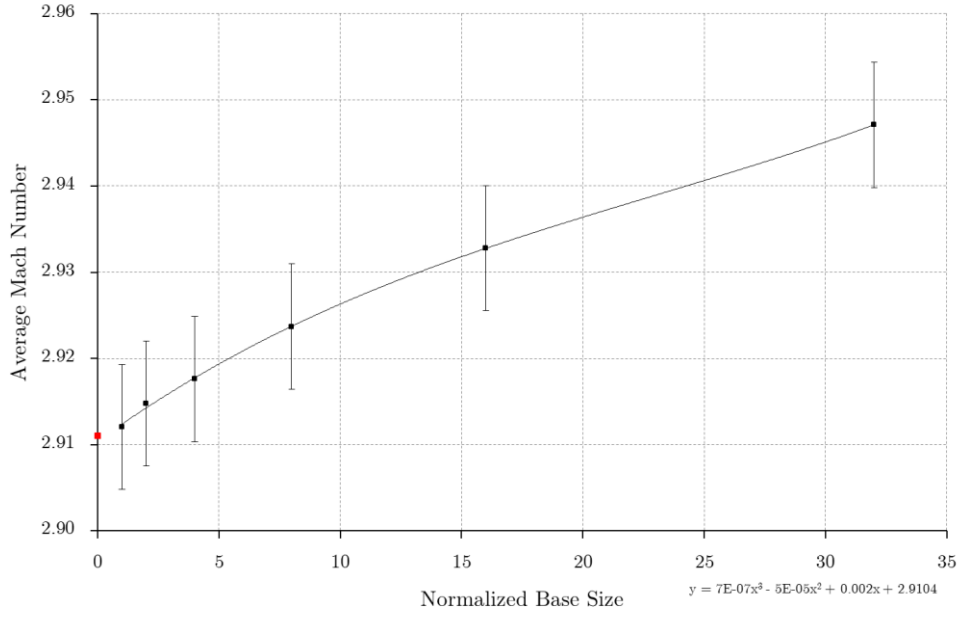

Figure 4.3: Results of the mesh independence study for a profile with a nozzle exit Mach number of $M_e = 3.0$

4.3 Turbulence Modelling

Inviscid solutions were computed as a verification of the test section Mach number predicted by the method of characteristics for each profile. For the viscous simulations, the viscous regime was set to model turbulent flow, since the flow in supersonic wind tunnels are generally turbulent as is the case with the "noisy" HSWT [20]. The Reynolds Averaged Navier Stokes (RANS) terms were approximated using the Spalart-Allmaras turbulence model, as this model yields the best results for flow with an attached boundary layer [21].

In addition to the mesh dependency checks, the wall y^+ (non-dimensional wall distance for a wall-bounded flow[22]) values were monitored, as displayed in Figure 4.4 (along the wall contour), to determine the accuracy and refinement of the mesh in the near wall layer of the turbulent flow. When using the Spalart-Allmaras model, the near-wall mesh spacing must be either $y^+ \leq 1$ or $y^+ \geq 30$ [23] so that the near wall cells lie within the logarithmic region of the boundary layer [24]. The value of $y^+ \geq 30$, as shown in Figure 4.4, at the resolution where the simulations were deemed acceptable was maintained for all nozzle configurations.

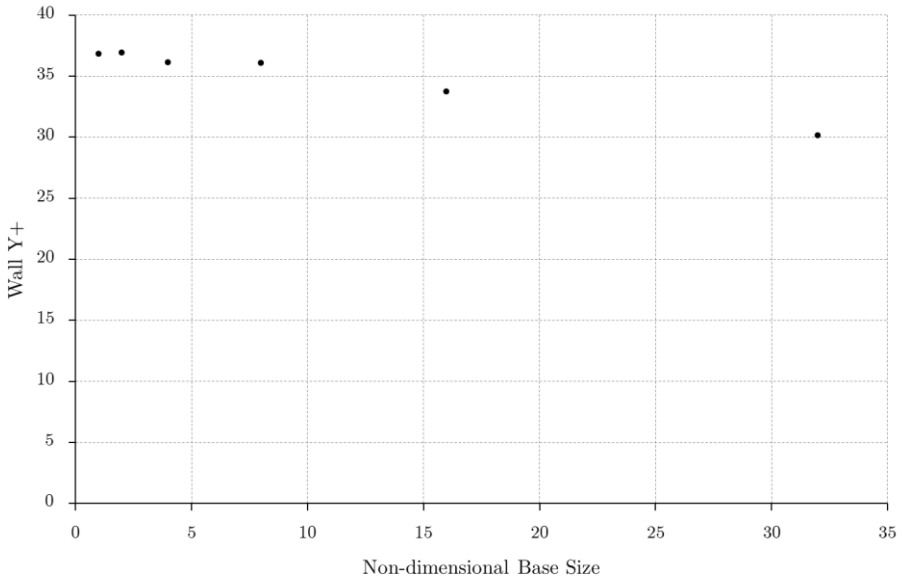

Figure 4.4: Average Wall y-plus values with varying cell size for a nozzle exit Mach number of $M_e = 3.0$

4.4 Boundary Layer Thickness Correction using CFD

The test section of the HSWT is fixed, with walls that are not perforated and sidewalls that are immovable and do not diverge to compensate for the displacement thickness of the boundary that develops over them. As mentioned previously, the test section walls do diverge, but this is insufficient to correct for the boundary layer effects. Hence, the sole technique to correct the nozzle exit Mach number for boundary layer development along the nozzle itself and along the side walls

(without substantial modifications to the HSWT facility) is to adjust the throat such that the effective area ratio is that of the desired freestream Mach number, in the presence of the boundary layer. The effective area ratio of the viscous CFD simulations ($\left({}^{A}/_{A^*}\right)_{viscous(CFD)}$) is calculated using Equation 4.1, where the Mach number extracted from the viscous CFD simulations ($M_{e-viscous(CFD)}$) is the average Mach number over the test volume in the HSWT.

$$\left({}^{A}/_{A^*}\right)_{viscous(CFD)} = \left(\frac{\gamma+1}{2}\right)^{-\frac{\gamma+1}{2(\gamma-1)}} \frac{\left(1+\frac{\gamma-1}{2}M^2_{e-viscous(CFD)}\right)^{\frac{\gamma+1}{2(\gamma-1)}}}{M_{e-viscous(CFD)}} \tag{4.1}$$

Since $M_{e-viscous(CFD)}$ is lower than the design exit Mach number of the nozzle, due to the boundary layer predicted by the CFD simulations, the computed area ratio will be lower than that of the ideal area ratio ($\left({}^{A}/_{A^*}\right)_{ideal}$) used in the method of characteristics calculations. It is convenient to work with the inverse of the area ratio, since we can then directly compute the corrected throat position by deriving the change in throat displacement required to increase the flow speed to the desired nozzle exit Mach number. Consider the change in area induced by the boundary layer in Equation 4.2.

$$\Delta\left({}^{A^*}/_{A}\right) = \left({}^{A^*}/_{A}\right)_{viscous(CFD)} - \left({}^{A^*}/_{A}\right)_{ideal} \tag{4.2}$$

It is known that $A = wy$, where w is the fixed wind tunnel width and y is the fixed nozzle exit height, so if Equation 4.2 is multiplied by ${}^{A}/_{w}$, then it becomes Equation 4.3. This equation gives the change in displacement necessary at the throat to correct the exit Mach number of a given profile to the desired Mach number in the presence of the boundary layer.

$$\Delta y^* = y^*_{viscous(CFD)} - y^*_{ideal} \tag{4.3}$$

The corrected throat position, and hence the corrected area ratio is given by Equations 4.4 and 4.5, respectively.

$$\Delta y^*_{corrected} = y^*_{ideal} - \Delta y^* \tag{4.4}$$

$$\left({}^{A^*}/_{A}\right)_{corrected} = \left({}^{A^*}/_{A}\right)_{ideal} - \Delta\left({}^{A^*}/_{A}\right) \tag{4.5}$$

The corrected input Mach number ($M_{e(corrected)}$) to the method of characteristics calculations is then computed from this corrected area ratio, as defined in Equation 4.6.

$$M_{e(corrected)} = f\left\{\left({}^{A}/_{A^*}\right)_{corrected}\right\} \tag{4.6}$$

For clarity, consider an ideal nozzle contour designed by the method of characteristics to produce a nozzle exit Mach number of $M_e = 3.0$. Subsequent to the completion of the viscous CFD simulations of this profile modelled in the HSWT, the actual average Mach number extracted over the test section region was determined to be substantially less than desired at $M_{e-viscous(CFD)} = 2.914$. After applying the boundary layer correction method described above, it was determined that a corrected nozzle profile with an exit Mach number of $M_{e(corrected)} = 3.093$ is required to produce a freestream Mach number of $M = 3.0$ in the test volume of the HSWT. The flow produced by this corrected design was simulated using viscous CFD computations and yielded a corrected test section Mach number of $M_{e(corrected)} = 3.003$, which lies within the acceptable wind tunnel limits.

It was initially anticipated that a few iterations of this method would be required to achieve the desired results, but since the boundary layer displacement thickness between the ideal profile and the first correction of the profile varies marginally, a single iteration through the correction procedure produced the desired test section Mach number. Although this is a first-order, crude correction method, it has the advantage that the profiles can be corrected from the initial phase of the nozzle contour design, without having to modify the HSWT. An algorithm to compute the corrected Mach number for the desired test section Mach number was scripted into MATLAB, which uses the initial viscous computations of the ideal profile as an input. The MATLAB code is detailed in Appendix B.

5. RESULTS AND DISCUSSION

5.1 Existing HSWT Nozzle Profiles

The theoretical nozzle profiles initially designed for the HSWT using the method of characteristics do not account for boundary layer effects. Moreover, the physical throat block geometry and the fixed test section region were not considered as constraints in the design of these nozzle profiles. Subsequently, these profiles were modified experimentally in the wind tunnel to essentially correct for the drop in test section Mach number, as well as improve the flow quality in the test section region, and are the profiles presently implemented in the HSWT. The initial phase of this research study evaluated these theoretical profiles to better understand the methodology followed and the problems encountered, and was completed by conducting a CFD analysis of these profiles. However, only the theoretical profiles initially designed for the HSWT were studied, since the Cartesian coordinates of the profiles that were experimentally modified and currently implemented in the wind tunnel have not been measured.

The analysis that follows is for an inviscid nozzle profile designed by the method characteristics to produce a nozzle exit Mach number of $M_e = 3.0$, as highlighted in Figure 5.1. It is believed that the existing profile models a generalised method of characteristics profile, such as the finite expansion method, which does not incorporate the physical constraints of the HSWT as boundary conditions. The profile shown in Figure 5.1 was calculated independent of the fixed test section region but has been modelled here with the test section region included, to enable realistic approximations of the flow in the wind tunnel. The overall profile takes a dip where the flexible plate meets the test section, and produces an abrupt change in curvature when merged to the fixed test section region. It is expected that this adds unnecessary stress onto the flexible plate, and it has been experimentally verified that it also induces Mach waves in the test section region, as highlighted previously in Figure 1.2. The results extracted from the CFD simulations, which were executed in the viscous regime described in Section 4.3, will be used to gain deeper insight into the effects that this “kink” in the profile has on the flow quality in the test section region of the HSWT.

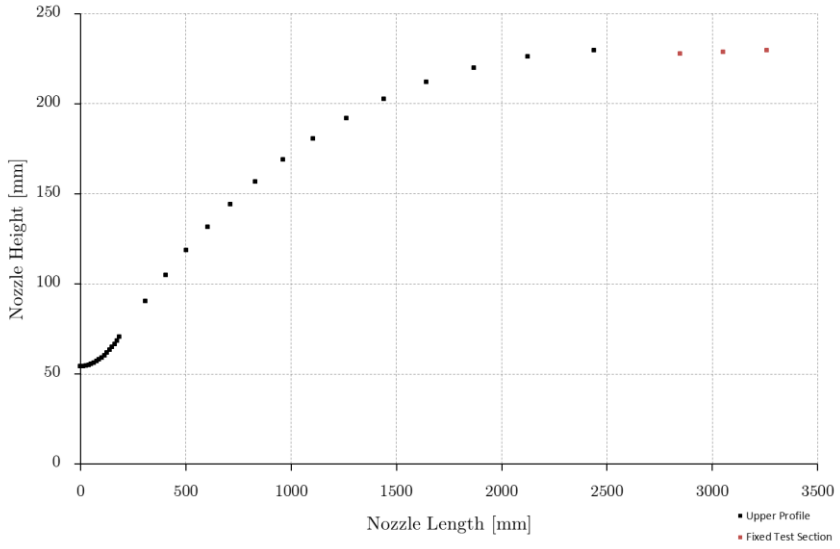

Figure 5.1: Existing inviscid, theoretical nozzle profile to produce an exit Mach number of $M_e = 3.0$

Figure 5.2 shows the Mach number variation along the centreline of the nozzle profile from the throat of the nozzle to the end of the test section, where the Mach number drop experienced due to the profile being calculated independent of a boundary layer correction is evident, as expected. It should be noted that although the profile was calculated using the inviscid method of characteristics theory, it was modelled using viscous CFD computations to simulate more realistic flow conditions of the HSWT. As a result, the average Mach number of 2.91 in the test section region is considerably less than the desired test section Mach number of $M_e = 3.0$, which accentuates the significance of the need for a boundary layer correction to be applied to the profiles during the initial design phase. In addition, the average test section Mach number produced by this existing theoretical profile is equivalent to the average Mach number for the uncorrected profiles designed in this study. This is due to the fact that the area ratios are the same, even though the actual profiles differ along the nozzle contour i.e. the test sections are the same and the throat heights are the same. This further implies that the boundary layer displacement thickness predicted by the CFD simulations is not very sensitive to the minor deviations on the nozzle contour and side walls. The accepted HSWT Mach number variation from the desired Mach number is $\pm 0.5\%$ of the set running condition. As one would expect, the minimum error occurs at the lowest Mach number and vice versa. Since this profile is not corrected for boundary layer effects, the test section Mach number produced by this profile falls out of the accuracy limits specified.

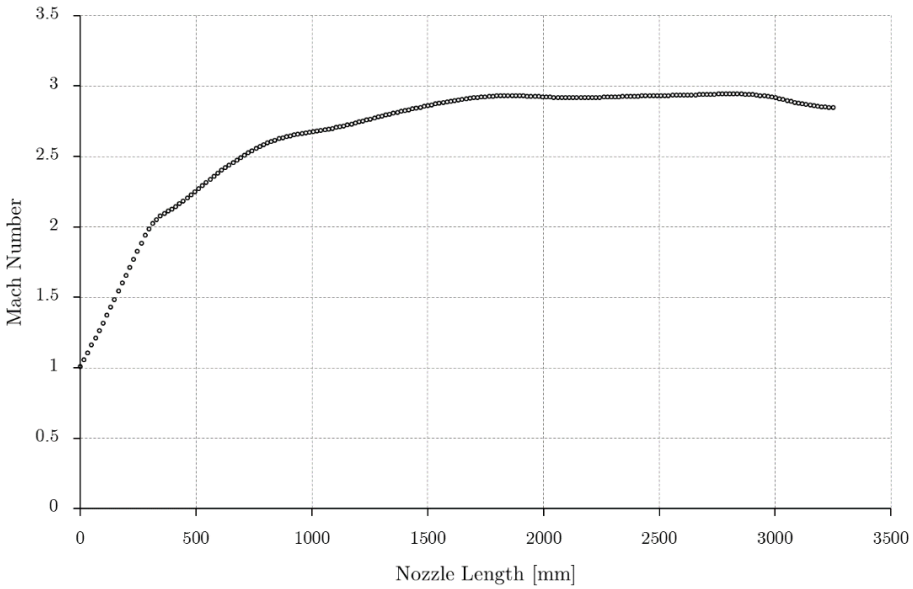

Figure 5.2: Predicted centreline Mach number distribution of the theoretical nozzle profile designed for $M_e = 3.0$

Figure 5.3 displays the Mach number distribution through a Mach number contour plot on the vertical symmetry plane of the same existing theoretical profile. In addition to the Mach number contours, verification of the irregular test section flow by the density gradient contour plot is highlighted in Figure 5.4, where the scale will be maintained henceforth with other density gradient images of the flow field. The flow irregularities, primarily induced by shocks and expansions that exist in the nozzle is highlighted considerably in this case though, mainly due to the nozzle profile not satisfying the geometric boundary condition at the fixed test section region, which causes a change in gradient of the profile i.e. a kink in the profile.

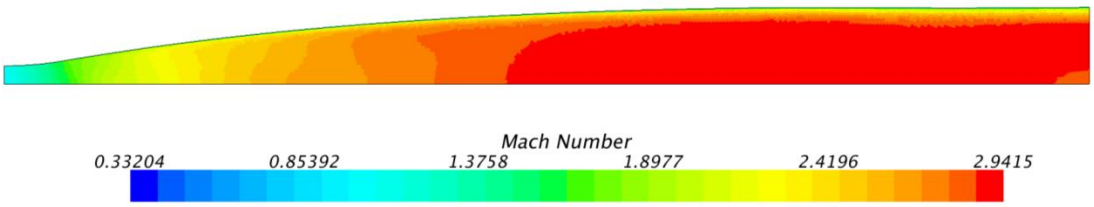

Figure 5.3: Mach number contours on the symmetry plane of the existing theoretical profile designed for $M_e = 3.0$

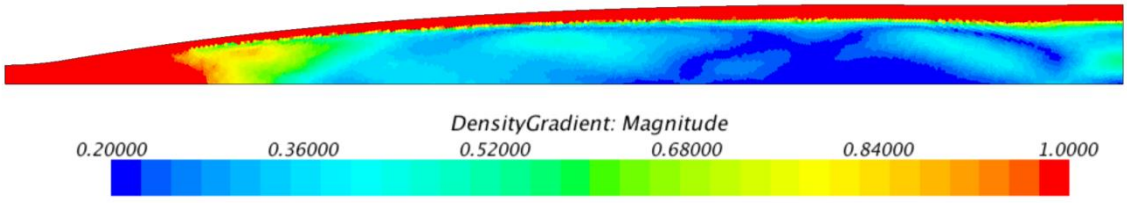

Figure 5.4: Density gradient $[(kg/m^3)/m]$ contours on the symmetry plane of the existing theoretical profile designed for $M_e = 3.0$

Flow angularity is a flow diagnostic used to determine the flow quality in aerodynamic testing of prototype airframes in wind tunnels. It is a measure of the flow direction or flow angle in relation to the test specimen's angle of attack. Experimentally, a five hole probe is usually used to quantify the flow angularity in the test section, but from CFD simulations the test section stream angle can be computed by taking the inverse tangent of the ratio of the normal velocity component (in the y direction) to the streamwise velocity component (in the x direction). The vertical flow angularity distribution in the test section at different x stages of the theoretical nozzle contour, as referenced from the throat, is shown in Figure 5.5. Accuracy criterion of the HSWT specifies that the flow angle should be within $\pm 0.2°$ for any Mach number setting in the facility. The simulation predicts that the exiting theoretical profile produces a maximum flow angularity greater than $0.8°$ at $x = 3.0\,m$ downstream of the throat, which is unfavourable as this causes offsets to the measured aerodynamic force and moment data, since the model is placed symmetrically in the wind tunnel and the flow is assumed to be uniform.

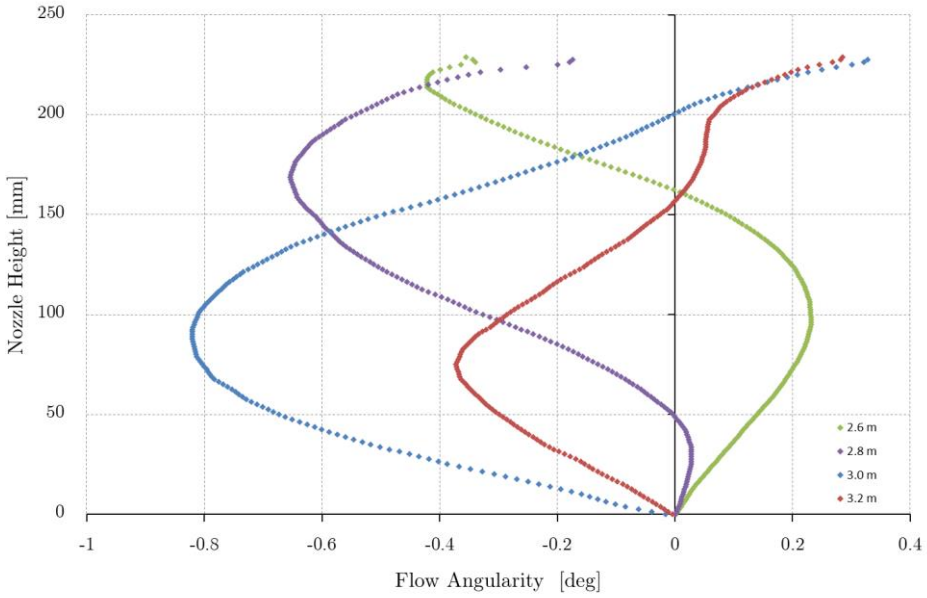

Figure 5.5: Predicted test section flow angularity distribution produced by the existing theoretical profile designed for $M_e = 3.0$

5.2 Initial Methods Considered for New Profiles

The various techniques of the method of characteristics for the design of supersonic nozzles have been documented in Section 2.3. It was deduced that the minimum length method and the traditional finite expansion methods would not be suitable for calculating the HSWT nozzle profiles, as it approximates the throat block as a point and a constant radius, respectively, which will result in the inability to set the profiles physically in the wind tunnel, due to the fixed throat block geometric limitation. Similarly, the constant gradient method could not be utilised as a straight section in the profile adds undesirable stress to the flexible steel plate.

Prior to applying Sivells' nozzle design method, the original idea was to model the throat block of the HSWT and subsequently apply the method of characteristics from the throat downstream to the test section. The aim of this was to use a modified version of the finite expansion technique, where instead of a constant radius in the expansion section, the exact throat block would be used. The profiles were hence calculated to meet the wind tunnels height constraint only, but no length constraint was explicitly applied. The throat block was rotated until the desired height was met, which prescribes the inflection point angle. However, a problem occurred when reflections in the expansion section developed, as highlighted in Figure 5.6. Typically characteristics originating from any point in the expansion section are always reflected in a way that it reaches the straightening portion of the nozzle [25]. The rare case does exist where multiple reflections of the characteristic lines can occur within the expansion portion of the nozzle, which increases the complexity of the problem. This occurs when the shape of the throat block and subsequently the throat height and the inflection point angle are positioned in a manner that forces the method of characteristics to produce reflections over the expansion region. Various attempts were made using this method in order to cancel the reflections in the expansion region but were not successful because of the limitation of the fixed throat block tunnel geometry. However, it is worth documenting that for a very small Mach number range and low characteristic network resolution, the method produced profiles that could potentially be used in the HSWT, but due to its limitations it was disregarded in this study.

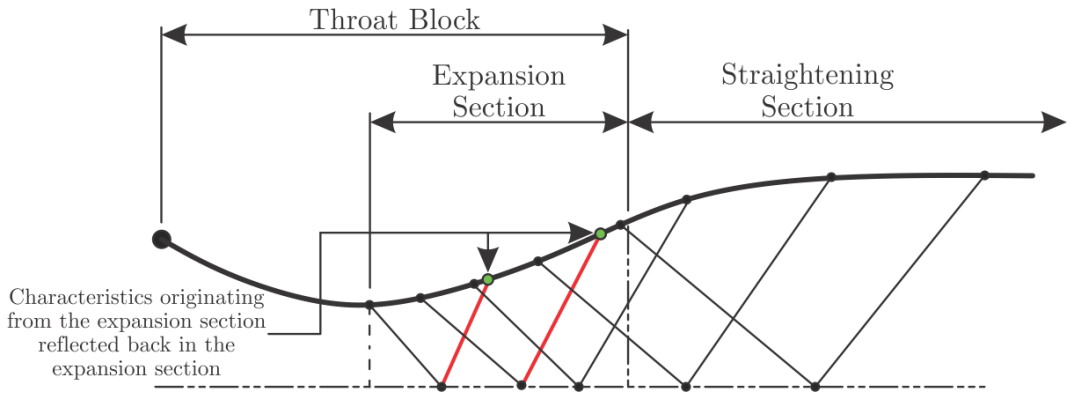

Figure 5.6: Incorporating the throat block into the finite expansion MOC induces reflections in the expansion section

5.3 Final Method for New Profiles

After an elaborate review of all the method of characteristics techniques used for nozzle designs of supersonic wind tunnels, the Sivells' method was determined to be the most suitable, as it initiates at the inflection point, which was described in detail in Sections 2.4 and 3.2. New theoretical inviscid (ideal) nozzle profiles were generated using the MATLAB code, which governed the input parameters to Sivells' technique by using the HSWT's geometric constraints as boundary conditions. A brief discussion of a nozzle profile to produce an uncorrected nozzle exit Mach number of

$M_e = 3.0$ will be outlined, followed by the contours at particular Mach number set points. The value of the non-dimensional length parameter was set to $K_{target} = 2.9$ and a value $r = 42$ was used to initiate the characteristic network on the source flow arc to compute the nozzle profile to a test section height of $y = 227.74\,mm$ using the characteristic method. The source points of the characteristic net and throat block geometry for the above configuration is demonstrated in Figure 5.7.

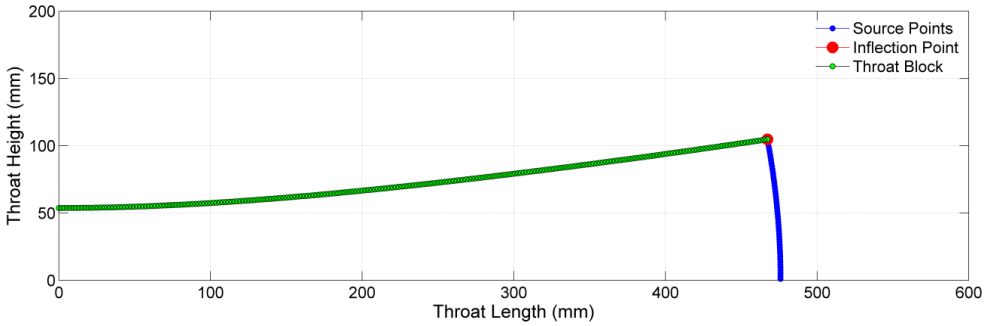

Figure 5.7: Source points for the characteristic net, inflection point and throat block profile for $M_e = 3.0$

The resultant wall contour as calculated using Sivells' nozzle design method coupled with the traditional method of characteristic calculations is displayed in Figure 5.8, where the straightening section has been inserted between the fixed throat block (expansion section) and the fixed test section regions of the HSWT. It is quite evident that the straightening section does not end precisely at the test section inlet. This was expected since the mechanical nozzle of the HSWT is designed such that the Mach number can be rapidly changed between runs in the facility. As a result, rather than having unique expansion sections for each Mach number setting, the HSWT incorporates a fixed throat block design that can be rotated and translated. The throat block or expansion section profile was designed for the mid-Mach number range of the facility rather than the maximum operating Mach number, which results in a higher flow accuracy over a greater range of operating Mach numbers in the HSWT [26]. For this reason, some of the calculated profiles do not terminate precisely at the test section inlet, even when the throat block rotational position optimisation procedure reaches the geometric limits of the HSWT facility, as is the case for the calculated profile being discussed. However, the nozzle has a finite number of control points that need to be moved to a suitable position when the profile is set in the facility, even when the calculated nozzle profiles fall short of the jacking positions.

The profiles were hence artificially lengthened, subsequent to the method of characteristics calculations, to meet the test section precisely. The lengthening was not done arbitrarily, but ensured that equal curvature and tangency of the profile was maintained at the nozzle exit and test section inlet, thereby following the elastic curve of the flexible plate. This was possible since the pin-jointed, diverging test section region is essentially a curve as well. The spline that joined these

positions was used to extrapolate the Cartesian coordinates of the lengthened section. Although K_{target} for this particular profile could be increased to lengthen the profile, increasing this value to $K_{target} = 4.0$ would lengthen the profile beyond the fixed test section, which is undesirable. Furthermore, in the lower Mach number ranges, even when the non-dimensional length parameter is set to a maximum value of $K_{target} = 4.0$, the profile does not meet the test section, so lengthening is necessary. The generated profile will be used as an example to validate the lengthening technique, and verify that the additional section does not perturb the flow through the HSWT using a CFD analysis, as documented in Sections 5.4 – 5.5. It should be duly noted that characteristic network resolution sensitivity studies were conducted to determine the numerical errors associated with the finite characteristic grid, where it was found that the error tends zero when $r > 40$.

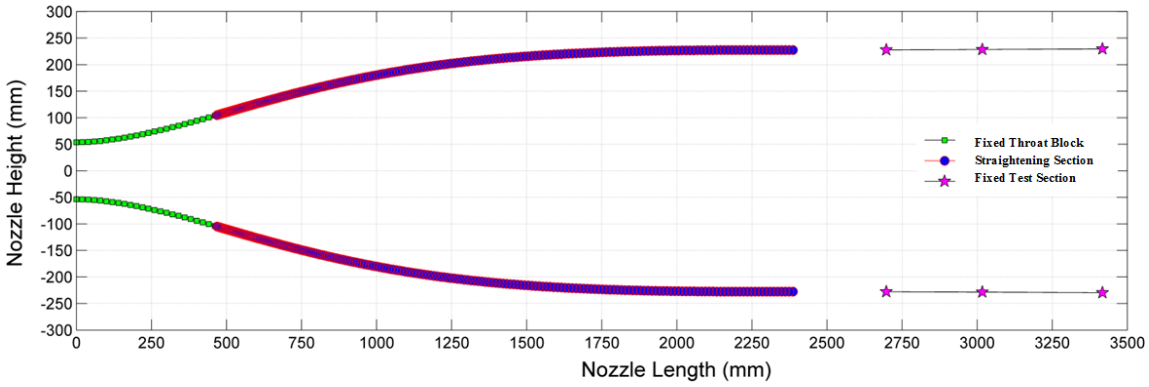

Figure 5.8: Expansion section (throat block), straightening section of wall contour and fixed test section region for $M_e = 3.0$

Continuing with the discussion of the generated profile for $M_e = 3.0$, it is inherent to Sivells' method that continuous curvature of the plate is ensured, by explicitly defining the wall angles for each point on the contour. Once the profile was generated, the continuous curvature criterion was verified by taking finite differences from the inflection point A, towards the nozzle exit. The resultant wall slope for each point of the straightening section is presented in Figure 5.9, which shows that the slope of the contour is a smooth curve, thereby ensuring continuous curvature. This is necessary to ensure that the plate's elastic curve can match the calculated aerodynamic curve.

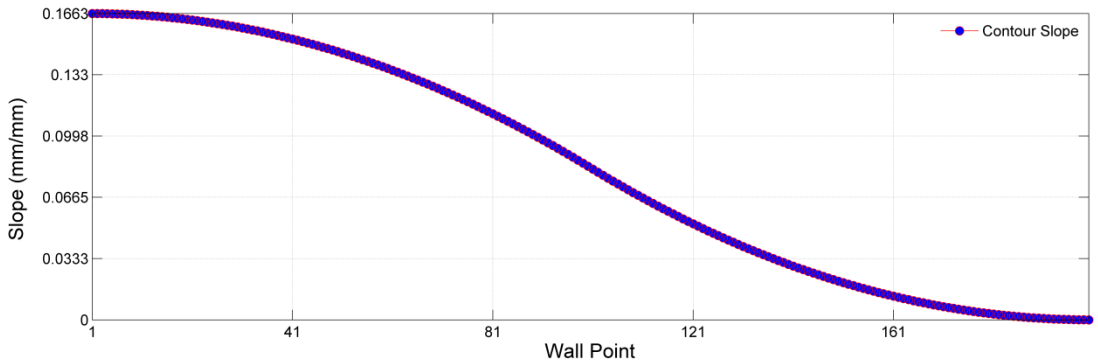

Figure 5.9: Wall slope of the straightening section curve generated for $M_e = 3.0$

Nozzle contour profiles were calculated for all HSWT supersonic Mach numbers in increments of $\Delta M_e = 0.1$ as these are the specified requirements of the HSWT. A comparison of the uncorrected contours, in $\Delta M_e = 0.5$ Mach number increments, is displayed in Figure 5.10 highlighting the various throat heights whilst maintaining the correct plate length and test section height.

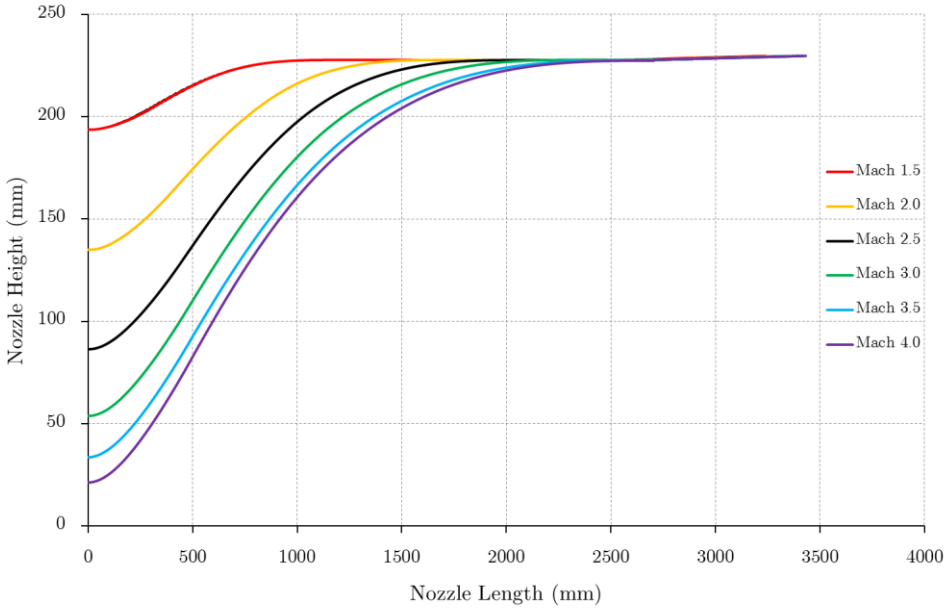

Figure 5.10: Nozzle contour profiles in increments of $\Delta M_e = 0.5$ with the fixed throat and test section regions

5.4 Computational Results of the Uncorrected Profiles

It is well known that the flow through the HSWT is viscous, but inviscid flow solutions were first completed to verify that the computed nozzle contours produce test section flow that is devoid of irregularities. Thereafter, viscous flow simulations were completed. Figure 5.11 to Figure 5.14 displays the final inviscid and viscous solutions, illustrating Mach number contours, followed by density gradient contours on the vertical symmetry plane. The density gradient visualisation technique is advantageous in verifying whether the test section is devoid of shock and expansion waves. The difference in the maximum Mach number on each scale should be noted where the elevated Mach number (i.e. greater than $M_e = 3.00$) for the inviscid solution is due to fact that the profile was generated for a terminal height of $y = 227.74\,mm$ (end of the flexible portion of the nozzle), which increases to $229.675\,mm$ along the fixed test section region (a feature built into the HSWT to potentially compensate for the wall boundary layer). The maximum Mach number decreases for the viscous solutions, in comparison to the inviscid case, since a finite boundary layer develops along the nozzle contour and the side walls of the tunnel. Close to the nozzle wall, the boundary layer thickness for the viscous approximations can be estimated by the high gradients detected in the near-surface flow, as shown in Figure 5.14. However, it does tend to exaggerate the boundary layer thickness in the test section, since the density gradient scale was finely set to expose

flow gradients in the test section. From a qualitative assessment of these contours, the generated nozzle profile appears to produce uniform test section flow, both in the inviscid and viscous regimes, when compared to that produced by the existing profiles shown in Figure 5.4.

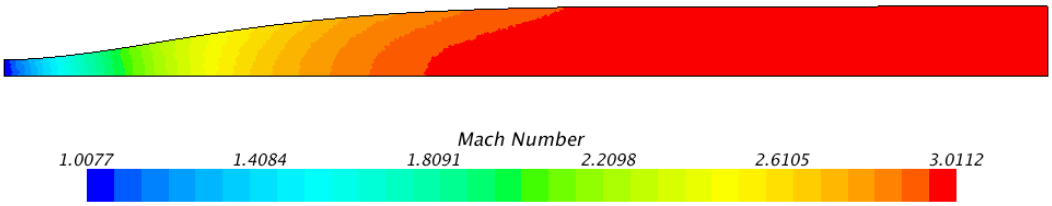

Figure 5.11: Uncorrected inviscid Mach number contours produced by the new nozzle design method for $M_e = 3.0$

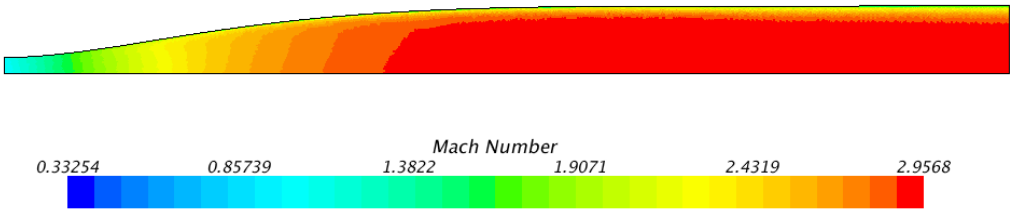

Figure 5.12: Uncorrected viscous Mach number contours produced by the new nozzle design method for $M_e = 3.0$

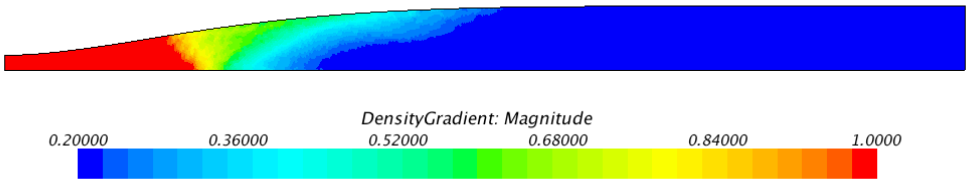

Figure 5.13: Uncorrected inviscid density gradient $[(kg/m^3)/m]$ contours produced by the new nozzle design method for $M_e = 3.0$

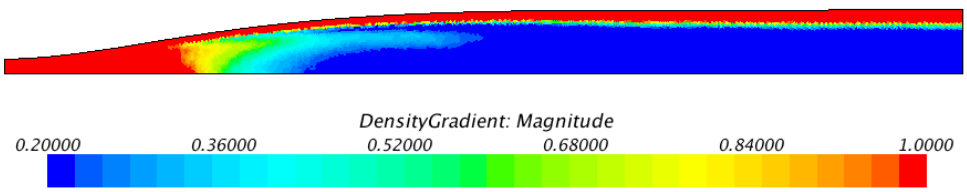

Figure 5.14: Uncorrected viscous density gradient $[(kg/m^3)/m]$ contours produced by the new nozzle design method for $M_e = 3.0$

Figure 5.15 demonstrates the variation in Mach number along the wind tunnel's centreline for the inviscid and viscous runs, which highlights the Mach number roll-off due to the viscous effects. It is quite evident that as the boundary layer thickens progressively along the walls, the flow Mach number decreases correspondingly. For this profile, which was designed to produce a test section Mach number of $M_e = 3.00$, the actual mean test section Mach number predicted by the viscous CFD simulation is $M_e = 2.914$, which is well below the target value, implying that a correction is required.

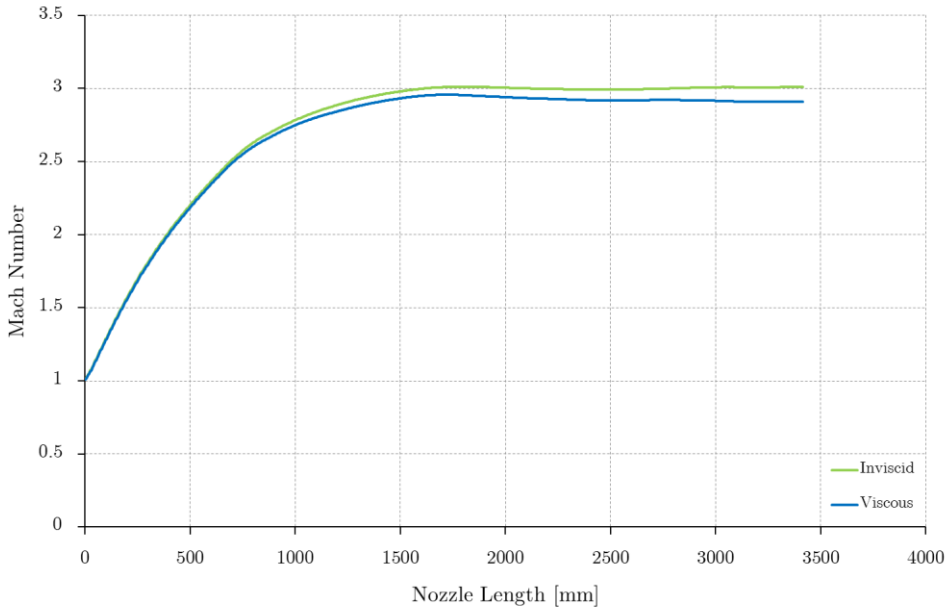

Figure 5.15: Inviscid and viscous centreline Mach distribution using the new nozzle design method for $M_e = 3.0$

Nonetheless, to quantify the flow quality in the test section, the flow angularity diagnostic parameter, extracted from the viscous CFD simulations, will be used. Figure 5.16 displays the flow angularity at various x stations along the test section, referenced from throat ($x = 0$). Flow angles reported above $y = 200\,mm$ are neglected since they lie in, or close to the viscous boundary layer along the contour walls. A maximum flow angle of approximately $0.13°$ is reported at $x = 2.6\,m$, which is considerably minute compared to the flow angularity of the existing profiles of $0.8°$ as highlighted in Figure 5.5. In addition the value of $0.13°$ is taken close to the test section walls where the flow angularity is affected by the boundary layer growth on the walls. The acceptable flow angularity in the HSWT is $\pm 0.2°$, which confirms that the newly designed profiles produce test section flow quality that falls within the acceptable tolerances of the HSWT facility. It should be noted that for a symmetrical nozzle profile (as modelled in this study), the flow angularity at the centreline is zero. Typically wind tunnels of this nature require the flow angularity accuracies of $\pm 0.2°$ along the centreline due to the inability to match the theoretical profiles both for the upper and lower contour exactly.

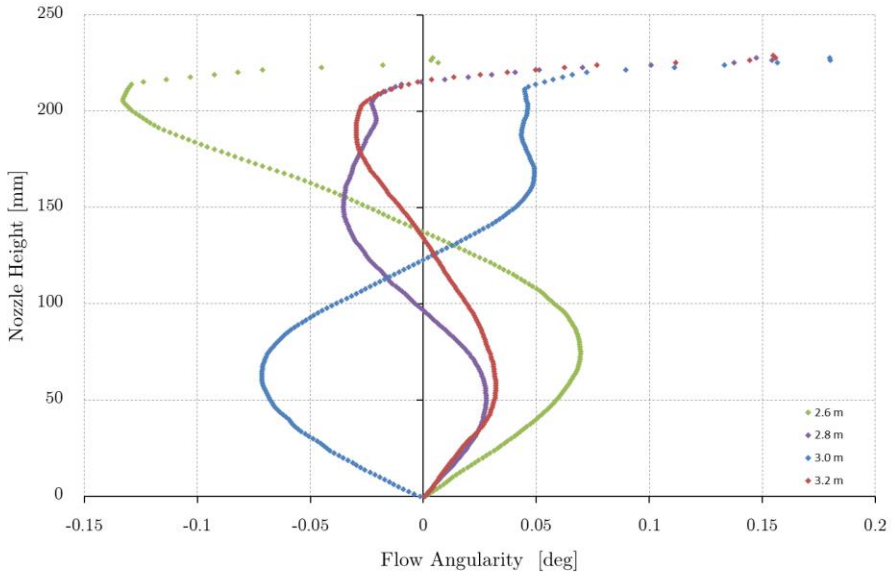

Figure 5.16: Viscous flow angularity in the test section region using the new nozzle design method for $M_e = 3.0$

5.5 Boundary Layer Thickness Correction

The test section is expanded slightly along its length to compensate for the boundary layer growth on the nozzle as well as the side walls of the facility, but it evident from the CFD analysis presented in the previous section that this small wall divergence does not make the HSWT self-correcting for viscous effects. The length of the contraction section (portion of the throat block upstream of the contour throat) has little effect on the boundary layer thickness at the nozzle throat and was excluded from the adjustment to correct the profiles for viscous effects. Based on the average test section Mach number produced by the uncorrected nozzle profile in the viscous CFD simulation ($M_e = 2.914$), the effective area ratio was calculated using Equation 4.1. After following the boundary layer thickness correction procedure documented in Section 4.4, the effective area ratio required to compensate for viscous effects was calculated, and the new design Mach number was determined to be $M_{e(corrected)} = 3.093$ i.e. a nozzle contour designed by the method of characteristics to produce an exit Mach number of 3.093 is required to get an average test section Mach number of $M_e = 3.00$ in the presence of the boundary layer that develops along the walls of the facility. It should be noted that it is inadequate to simply adjust the throat to achieve the corrected area ratio with rest of the profile remaining the same, because by moving the throat the entire expansion section shifts as well, and the uncorrected profile will not cancel all the expansion waves generated at the new throat block position. As a result, a complete new profile needs to be generated at the corrected design exit Mach number.

A comparison of the uncorrected and the corrected profiles is displayed in Figure 5.17, where the change in throat height is quite obvious, but it can also be seen that the entire profile has been altered along the nozzle contour. Both profiles were generated using the method of characteristics

MATLAB code as discussed in Section 3.3 and meet all the required conditions for compatibility with the test section, and satisfy the throat block's geometric constraints. So rather than displacing the nozzle contour outward by the boundary layer displacement thickness, which is the intuitive method to correct the area ratio but physically impossible in the HSWT facility due to the fixed test section, the current correction method speeds up the potential flow (outside the boundary layer) to the desired Mach number. The shortfall is that this method is computationally expensive because, firstly, the uncorrected profile needs to be generated. Thereafter, a viscous CFD analysis has be performed to determine the effective area ratio with the boundary layer present. Then the correction procedure is applied and the corrected profile is generated at the new design conditions. This is followed by a viscous CFD analysis of the corrected nozzle contour to verify that the corrected profile, in fact, produces the desired test section conditions, as documented subsequently.

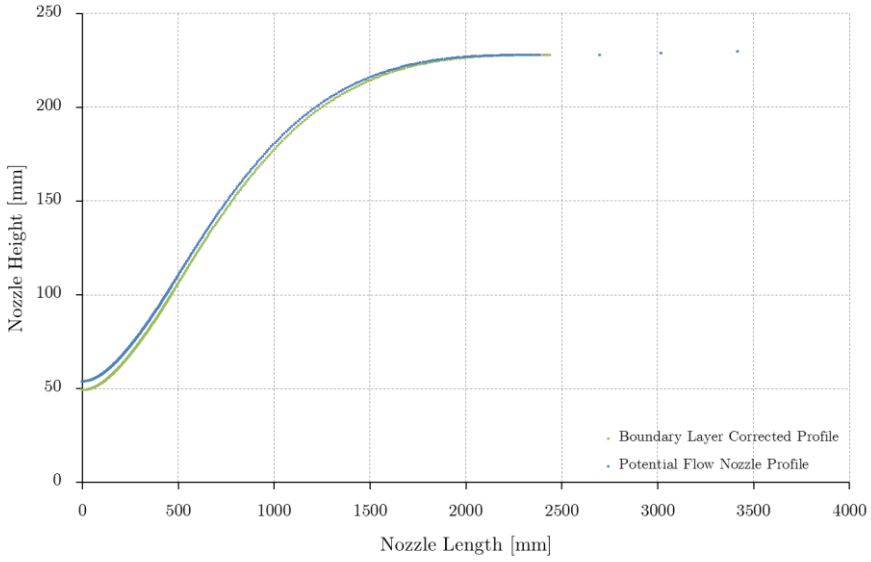

Figure 5.17: Comparison of uncorrected and corrected nozzle profiles for $M_e = 3.0$

Numerical flow simulations of the boundary layer corrected profiles were computed using the computational method described in Section 4, but inviscid solutions were also completed to qualitatively analyse the flow quality produced by the corrected profiles. Figure 5.18 shows Mach number contours and Figure 5.19 shows density gradient contours on the vertical symmetry plane, computed by the inviscid CFD simulation. Figure 5.18 highlights that the flow Mach number becomes uniform and Figure 5.19 portrays the density gradients becoming negligible as the flow expands towards the test section, implying straightening section is effectively cancelling expansion waves generated in the expansion section. The viscous solutions are presented in Figure 5.20, which shows Mach number contours, and Figure 5.21, which shows density gradient contours. Except for the distinct boundary layer, the flow trends are comparable to the inviscid solutions, in that the Mach number becomes uniform and the density gradients detect no irregularities in test section region. The Mach number distribution along the wind tunnel centreline is presented in Figure 5.22,

where the total Mach number deviation lies within $\Delta M = \pm 0.012$ over the entire test section region with an average Mach number of 3.003. These results are acceptable for testing in the HSWT.

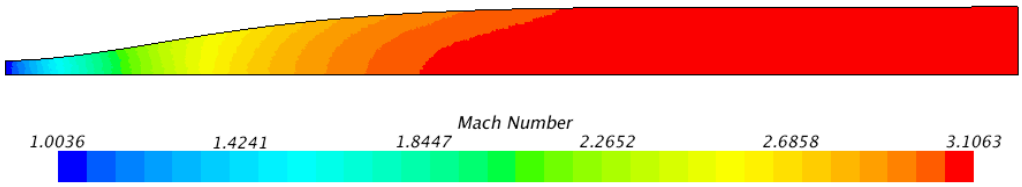

Figure 5.18: Corrected inviscid Mach number contours produced by the new nozzle design method for $M_{e(corrected)} = 3.0$

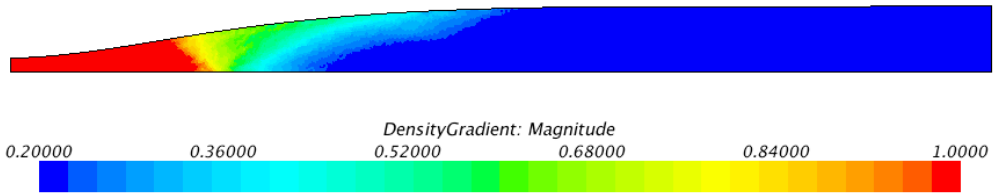

Figure 5.19: Corrected inviscid density gradient $[(kg/m^3)/m]$ contours produced by the new nozzle design method for $M_{e(corrected)} = 3.0$

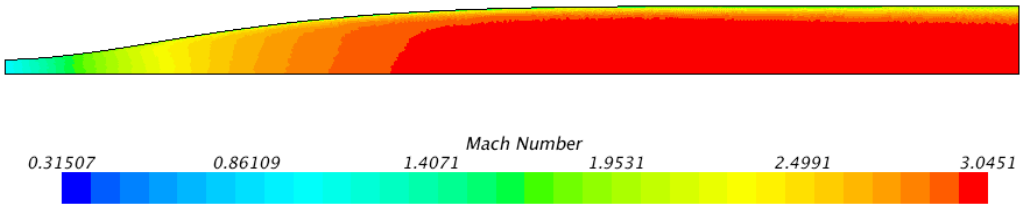

Figure 5.20: Corrected viscous Mach number contours produced by the new nozzle design method for $M_{e(corrected)} = 3.0$

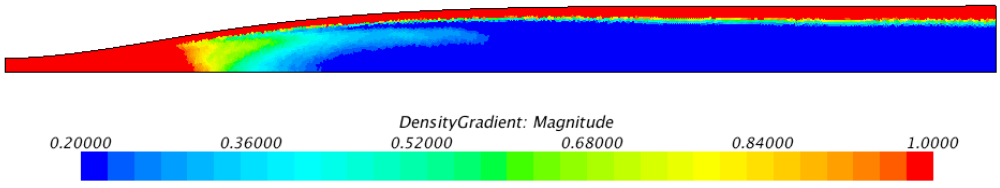

Figure 5.21: Corrected viscous density gradient $[(kg/m^3)/m]$contours produced by the new nozzle design method for $M_{e(corrected)} = 3.0$

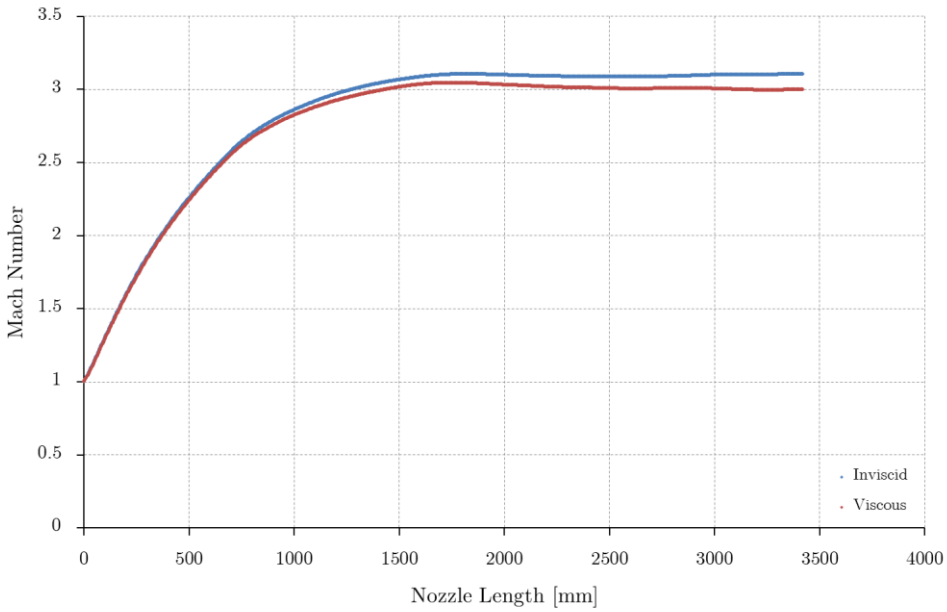

Figure 5.22: Inviscid and viscous centreline Mach distribution using the new nozzle design method for $M_{e(corrected)} = 3.0$

The flow quality, defined as the flow angularity in the test section region, is comparable to those of the uncorrected nozzle profile presented previously, as seen in Figure 5.23, and lies within facility specifications. Overall, the boundary layer correction technique developed in this study coupled to the characteristic method generates nozzle contours that produce the desired Mach number and flow quality in HSWT's test section, notwithstanding the thick, turbulent boundary layer developed along the walls.

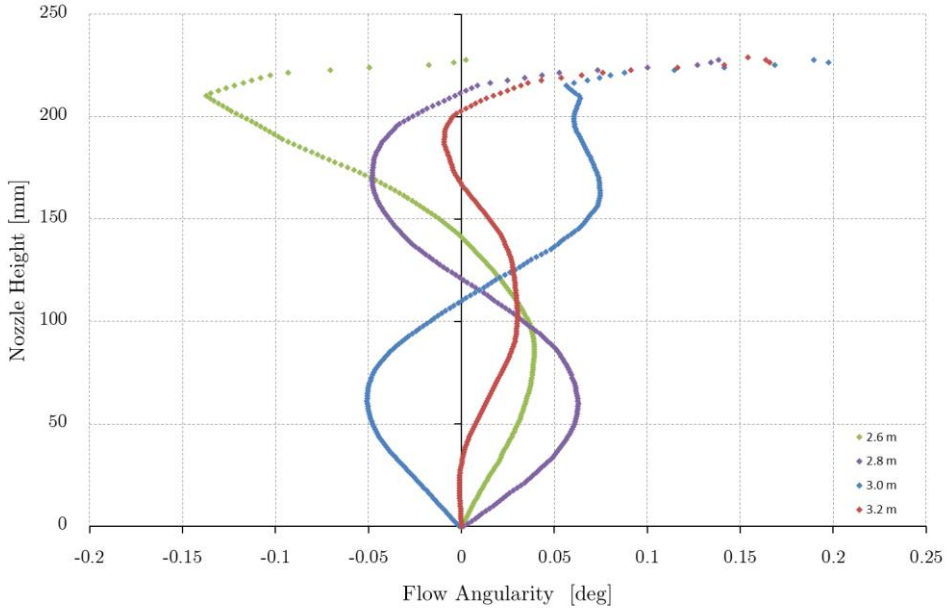

Figure 5.23: Viscous flow angularity in the test section region using the new nozzle design method for $M_{e(corrected)} = 3.0$

As mentioned previously, the boundary layer is over-exposed by the density gradient contours due to the fine scale of the density gradients necessary to highlight the formation of test section

irregularities. Figure 5.24 shows the velocity magnitude developed on the symmetry plane of a profile generated to produce an average test section Mach number of 3.00, where the contours have been truncated above the 99% of the freestream test section velocity. This then gives a better approximation of the actual boundary layer thickness developed along the nozzle contour, which appears to be marginally thinner than that exposed by the density gradient contours.

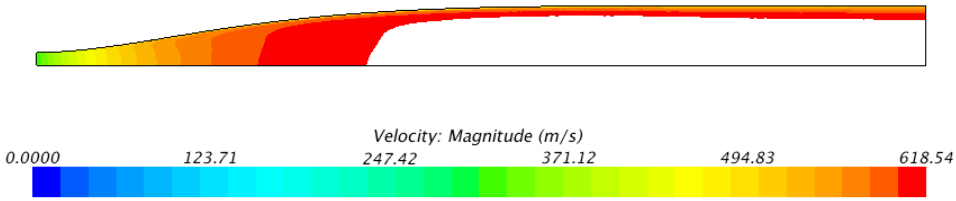

Figure 5.24: Velocity contours truncated above 99% of the freestream velocity

5.6 Plate Stress

A MATLAB code as represented in Appendix B, was utilised to transform the contour coordinates to respresent a beam fixed at the test section, where the first and second derivatives were then computed. The bending moment and bending plate stress were then calculated using the formulae documented in Section 3.4 i.e. Equation 3.8 and Equation 3.9, respectively. The yield strength of the plate is approximately $\sigma_{ys} = 500MPa$ with a Youngs' Modulus of $E = 250GPa$. The plate stress, is not uniform, since it is dependent on the curvature of the profiles with the highest curvature resulting in the largest plate stress. Figure 5.25 shows the maximum stresses developed in the plate at the various Mach number settings, where the calculated stress is lower than the yield stress in the plate, which implies that the profiles can be safely implemented in the HSWT.

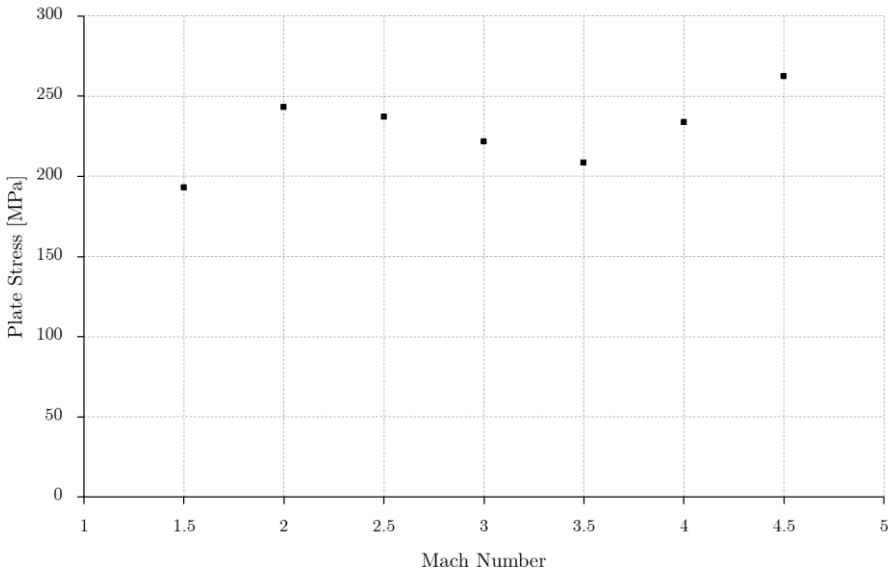

Figure 5.25: Maximum plate stress for various Mach numbers for corrected profiles calculated for the HSWT

5.7 Profile Uniqueness

For the very low Mach numbers, the angle of the inflection point becomes steep due the geometric constraints of the fixed throat block, and it becomes mathematically challenging to generate implementable profiles. Furthermore the profiles are fairly short since the nozzle itself was originally designed for the mid-Mach number range of the HSWT. A study was performed to investigate the difference between two profiles (referred to as "original" and "modified inflection point" profiles), as portrayed in Figure 5.26, which have the same output Mach number and throat height, but different inflection point angles (θ_A) i.e. different criteria were used in the throat block's rotational position optimisation procedure resulting in a modified inflection point angle that is lower than the original profile, which also shortens the profile in comparison to the original nozzle contour.

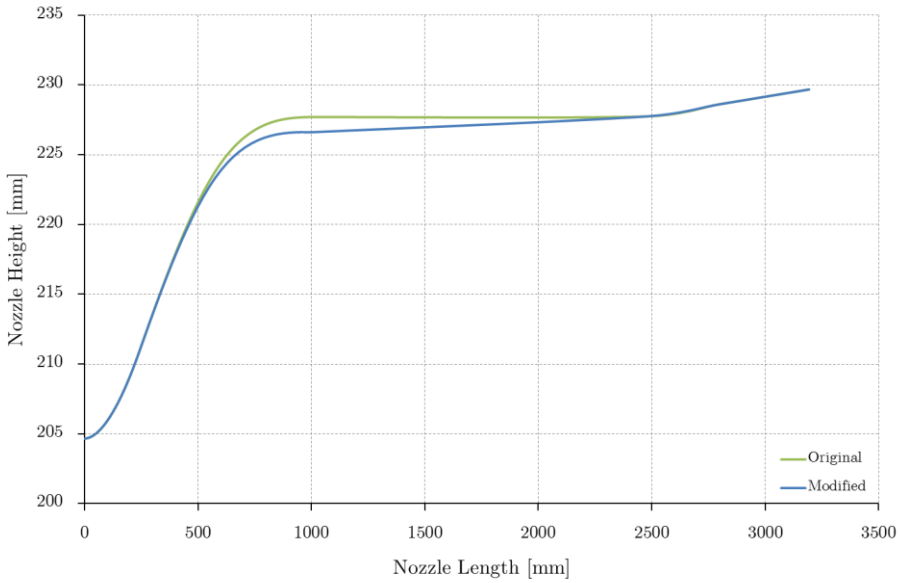

Figure 5.26: Nozzle profiles designed to produce a corrected test section Mach number of 1.3 at different inflection point angles

A summary of the computational results is presented in Figure 5.27 to Figure 5.30 where the original profile is presented first followed by the profile with the modified inflection point angle. Qualitatively, both calculated profiles produce uniform test section Mach numbers and negligible flow gradients in the test section. Moreover, Figure 5.31 presents the Mach number distribution along the centrelines of both, the original and modified profiles, which shows that the Mach number tends to the same value over the test section region, implying that profiles with differing inflection point angles are possible. It should be noted that the Mach number increases beyond the design Mach number initially, but tends to drop to the desired Mach number in test section region. This may be attributed to the boundary layer that develops along the walls of the facility, which increases in thickness along the nozzle thereby reducing the Mach number in the test section in comparison to the region upstream. Overall, the profiles are independent of the design Mach number, but are unique for a particular throat and inflection point combination.

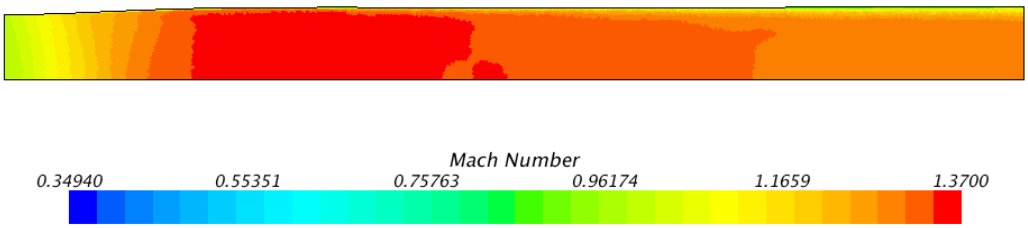

Figure 5.27: Corrected viscous Mach number contours produced by the "original" profile for $M_{e(corrected)} = 1.3$

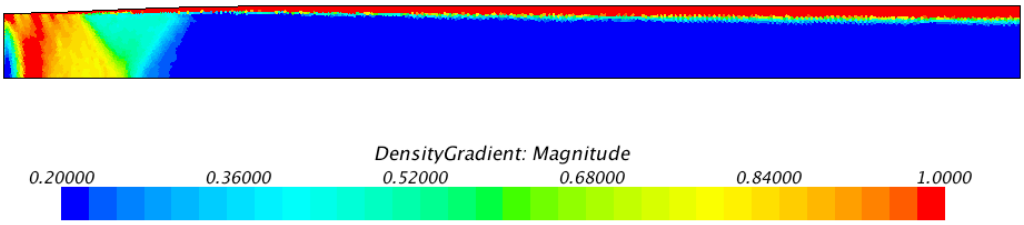

Figure 5.28: Corrected viscous density gradient $[(kg/m^3)/m]$contours produced by the "original" profile for $M_{e(corrected)} = 1.3$

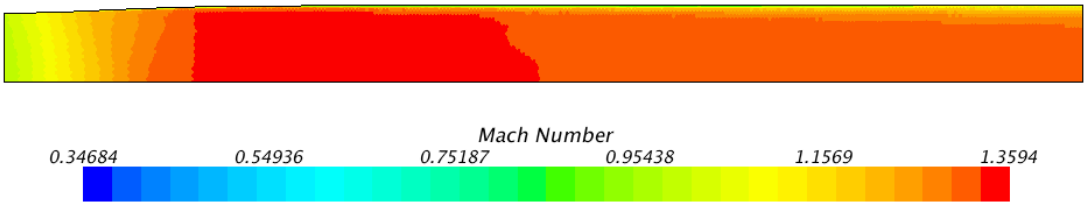

Figure 5.29: Corrected viscous Mach number contours produced by the "modified inflection point" profile for $M_{e(corrected)} = 1.3$

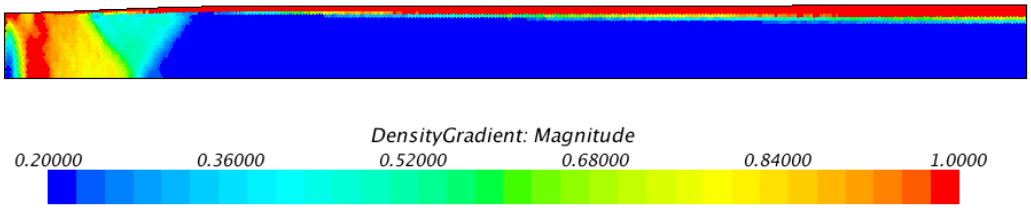

Figure 5.30: Corrected viscous density gradient $[(kg/m^3)/m]$contours produced by the "modified inflection point" profile for $M_{e(corrected)} = 1.3$

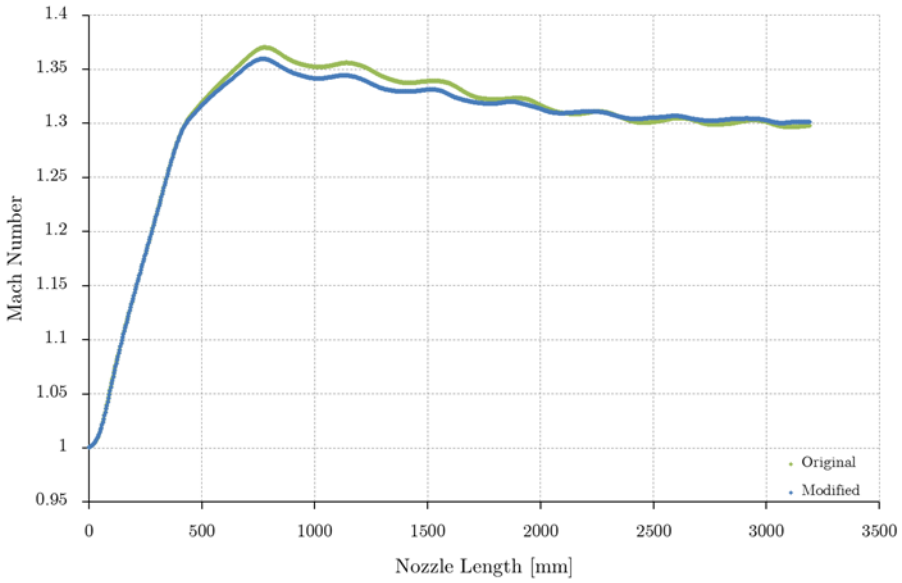

Figure 5.31: "Original" and "modified inflection point" centreline Mach distribution using the current nozzle design method for $M_{e(corrected)} = 1.3$

Further investigation of the flow angularity, as presented in Figure 5.32 for the original profile and Figure 5.33 for the modified profile, highlights that the flow angularity is marginally different near the test section region deducing that a slight decrease in the inflection point angle does not drastically modify the flow quality in the wind tunnel. The Mach number, which is dependent on the throat and the test section effective area ratios were maintained for both contours. The profiles are thus not unique for a set Mach number as multiple solutions are possible, however as the inflection point angle changes so too does the length of the profile. Therefore, in the throat rotation optimisation procedure, the throat was rotated to produce the maximum inflection point angle that is possible based on the throat's physical geometry. This allows the longest nozzle contours to be calculated for each Mach number setting, thereby enabling multiple physical control points to set the profile in the HSWT, which is desirable.

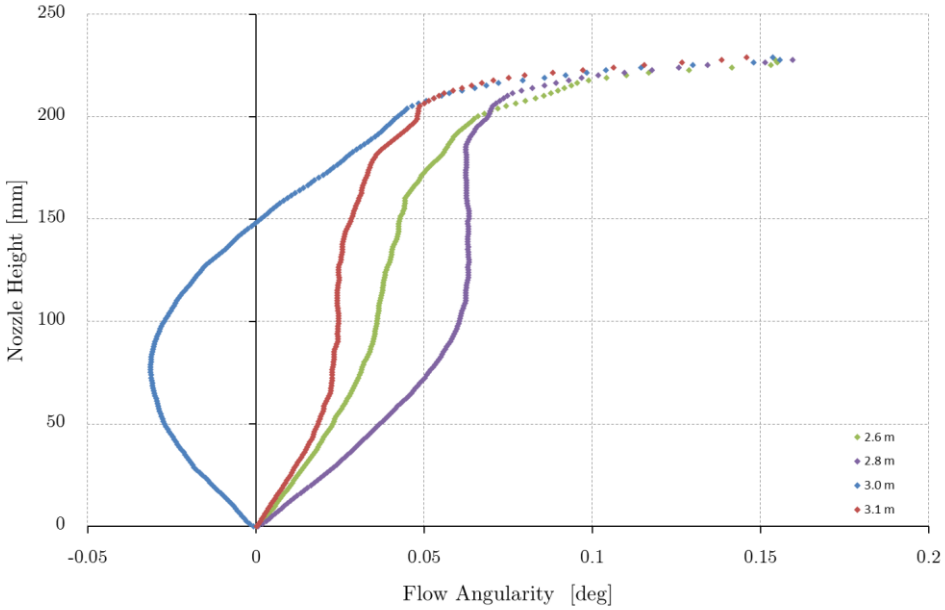

Figure 5.32: Viscous flow angularity in the test section region using the "original" profile for $M_{e(corrected)} = 1.3$

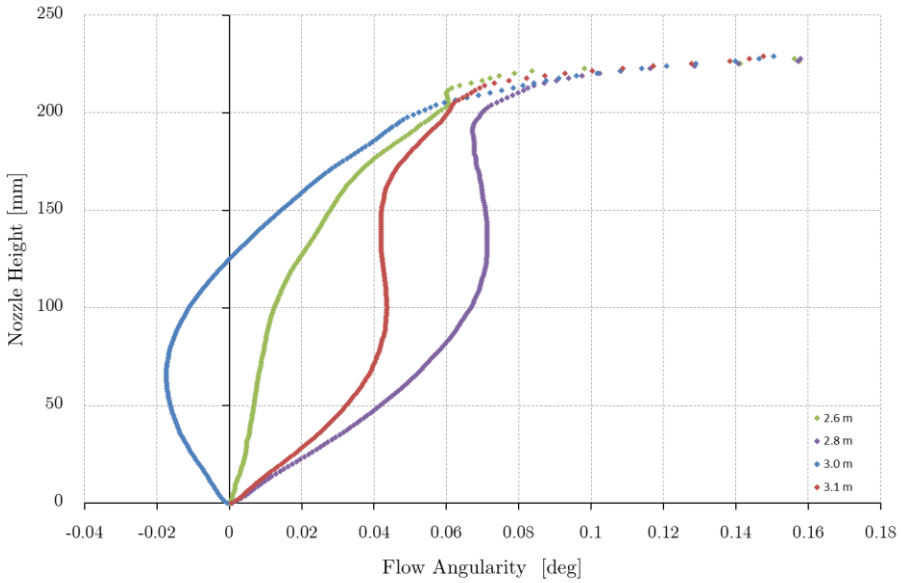

Figure 5.33: Viscous flow angularity in the test section region using the "modified inflection point" profile for $M_{e(corrected)} = 1.3$

5.8 Comparison of Profiles

To conclude the work completed in this study, the existing theoretical profiles currently implemented in the wind tunnel were compared with the newly designed, boundary layer corrected profiles generated in this study, as seen in Figure 5.34 with a centreline Mach number distribution plot shown in Figure 5.35. In general, the newly designed profiles tend to expand the flow from the throat much faster with respect to the streamwise position along the nozzle, but this expansion is done more smoothly than that achieved by the existing HSWT nozzle contours. This allows the straightening section of the newly designed nozzle contours to straighten the flow in the test section to acceptable levels of quality.

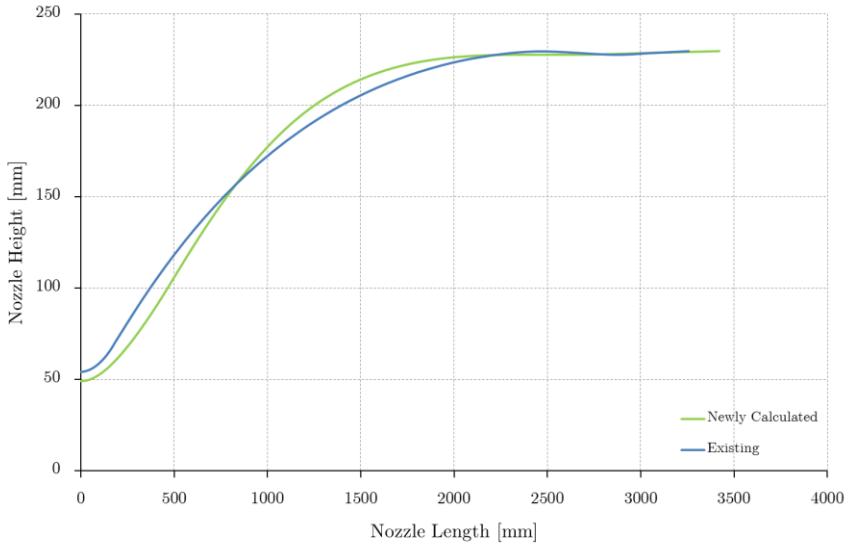

Figure 5.34: Profiles for the boundary layer corrected nozzle profiles existing and newly calculated for $M_e = 3.0$

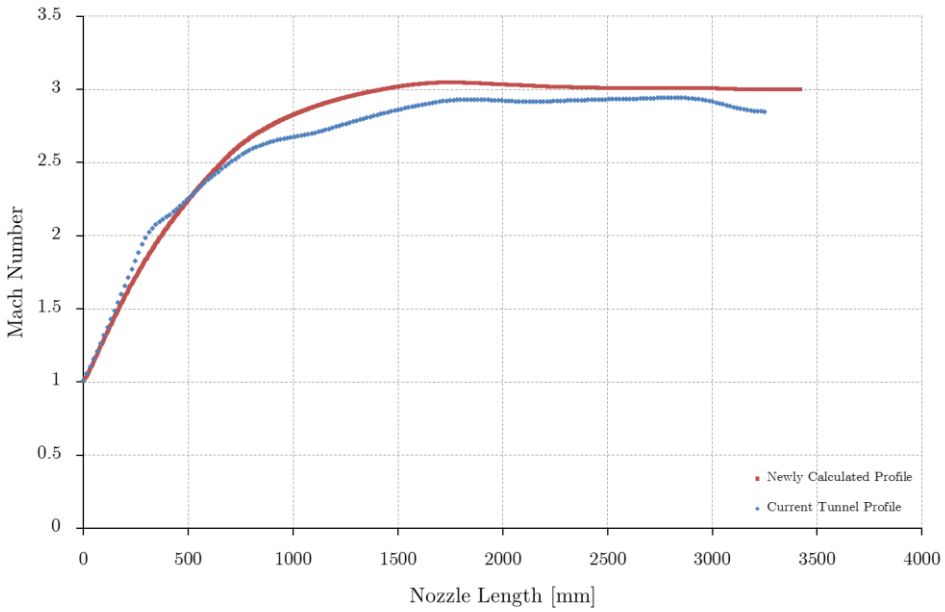

Figure 5.35: Viscous centreline Mach distribution for the boundary layer corrected nozzle profiles original and newly calculated for $M_e = 3.0$

As stated previously, for each nozzle contour calculation the contour minimum height or throat was used as the reference point ($x = 0$) for each profile. This allowed the translational motion of the profile to be neglected in the calculations, but in reality the throat region moves continuously upstream with increasing Mach number, in addition to the rotational motion modelled in the current calculations. As a result, the calculated contours places the test section at varying positions along the nozzle axis when referenced from the throat, as shown in Figure 5.36. However, if these contours are re-referenced such that the test section remains fixed, the throat position for each Mach number is changed and the required translation of the fixed throat block is derived, as demonstrated in Figure 5.37. This shows that by incorporating the geometric constraints imposed by the test section and throat block as boundary conditions to the characteristic method from the outset, the required rotational and translational movement of the throat block for each Mach number setting can be derived, thereby modelling the complex physical kinematics of the throat block in the HSWT. Moreover, the forward placement of the profiles generated in lower Mach number range, which were considerably shorter than those in the higher Mach number range, means that more hydraulic jack control points can be used to shape the flexible plate of the HSWT. Overall, the profiles generated in this study are not only boundary layer corrected to produce shock and expansion free, high quality test section flow, but these profiles are physically implementable within the geometric limits of the HSWT as well.

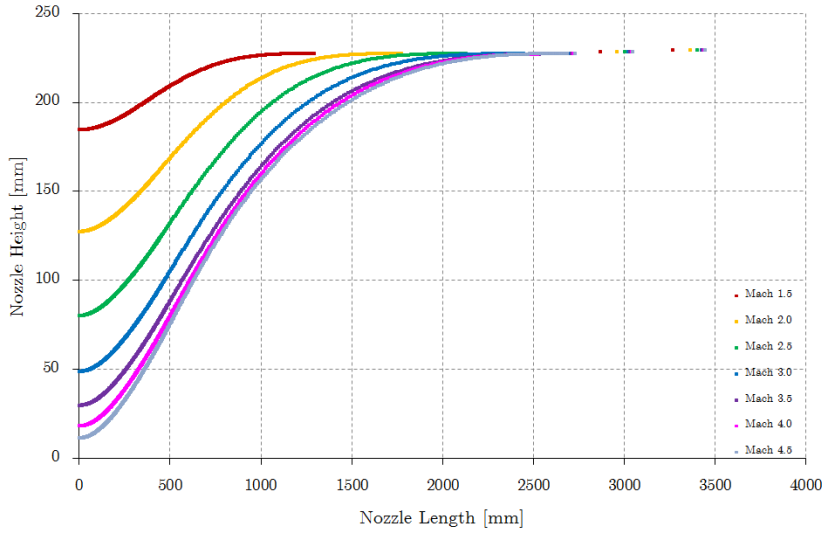

Figure 5.36: Nozzle profiles modelled with the throat at the origin

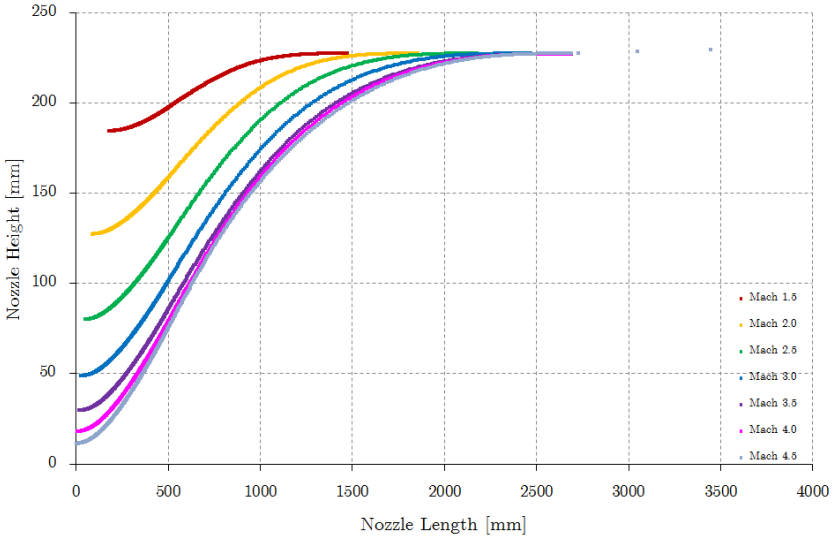

Figure 5.37: Nozzle profiles modelled with the test section fixed as is the case in the HSWT

6. CONCLUSIONS

The CSIR's High Speed Wind Tunnel (HSWT) currently has theoretical supersonic nozzle profiles implemented in the facility that produces irregular test section flow, even after the profiles were experimentally modified in an attempt to alleviate the problem. After a thorough investigation, it was deemed necessary to completely redesign the nozzle contours of the HSWT to produce high quality test section flow. Of the diverse methods available for supersonic nozzle designs, the Sivells' nozzle design technique was found be to be the most appropriate. Since this characteristic method allows profiles to be generated from the inflection downstream, it could be adapted to include the geometric constraints of the fixed throat block and test section as boundary conditions, which governed the input parameters to the nozzle design technique.

A MATLAB code was used to compute the Cartesian coordinates of the nozzle profiles, where the nozzle designs were optimised to produce suitable profiles for each Mach number that maintained physical compatibility with the throat block and test section of the HSWT. Based on the plate's deflection, the plate stresses were calculated to ensure that the newly designed profiles could be safely implemented in the wind tunnel facility. All nozzle profiles designed in this study were evaluated using computational fluid dynamics. The Mach number distribution, flow angularity and density gradients produced by the profiles in the test section of the wind tunnel were evaluated against stringent HSWT tolerances before being accepted. The viscous CFD simulations were also used to correct the profiles for boundary layer development along the wind tunnel's side walls and the calculated nozzle profiles itself, producing the desired Mach number in test section region of the facility. Overall, the newly designed nozzle profiles produces test section flow conditions that are devoid of shocks, expansions and other irregularities, have uniform flow and Mach number distribution, and the flow angularity falls within the acceptable quality limits of the facility.

7. RECOMMENDATIONS

The recommendations for this study are as follows:

- The nozzle profiles generated in this study should be implemented in the HSWT using the CSIR's Nozzle Contour Measurement System (NCMS).
- The mismatch between the implemented profile in the wind tunnel and the theoretical designed profile, caused by the limited number of jacks should be minimised during the implementation of the profiles for all Mach numbers.
- Experimentally verify that the test section flow is shock and expansion free using the colour schlieren system in the HSWT for the various Mach numbers.
- Experimentally verify the test section flow angularity and flow uniformity using probes installed in the test section of the wind tunnel.
- Experimentally verify that the final calculated profiles are adequately corrected for boundary layer formation along the walls, and that the average test section Mach number lies within the tolerances acceptable in the HSWT.

8. REFERENCES

[1] F. Dionisio, "KT470765, Task 29, Project HANDBOOG: *Contour Prediction Method for a Supersonic Nozzle*", Aerotek Report, AERO97/093, March 1997

[2] K. Naidoo, "*Dynamic Shock Wave Reflection Phenomena*", Ph.D, University of the Witwatersrand, Johannesburg, 2011.

[3] Council for Scientific and Industrial Research, "*Instruction Manual for Trisonic Wind Tunnel*", Mitsubishi Heavy Industries, LTD, November 1965.

[4] A. Pope and K. Goin, "*High-Speed Wind Tunnel Testing*". New York: Wiley, 1965.

[5] J. Anderson, "*Modern Compressible Flow with Historical Perspective*", 3rd ed. New York: McGraw-Hill, 2003, p. 377-430.

[6] P. Moore, "*Design of a Supersonic Wind Tunnel*", Undergraduate, Worcester Polytechnic Institute, 2009.

[7] J. Anderson, "*Modern Compressible Flow with Historical Perspective*", 3rd ed. New York: McGraw-Hill, 2003, p. Chapter 4.

[8] J. John and T. Keith, "*Gas Dynamics*". Upper Saddle River, N.J.: Pearson Prentice Hall, 2006.

[9] K. Butler, D. Cancel, B. Earley, S. Morin, E. Morrison and M. Sangenario, *"Design and Construction of a Supersonic Wind Tunnel"*, Undergraduate, Worcester Polytechnic Institute, 2010.

[10] J. Anderson, "*Fundamentals of Aerodynamics*", 4th ed. New York: McGraw-Hill, 2007, p. 559-596.

[11] J. Sivells, "*A Computer Program for the Aerodynamic Design of Axisymmetric and Planar Nozzles for Supersonic and Hypersonic Wind Tunnels*", AEDC-TR-78-63, Tennessee, 1978.

[12] James C. Sivells. "*Design of Two-Dimensional Continuous-Curvature Supersonic Nozzles*", Journal of the Aeronautical Sciences, Vol. 22, No. 10 (1955), p. 685-692.

[13] F. Kuno, "*A New Method of Designing Two-Dimensional Laval Nozzles for a Parallel and Uniform Jet*", North American Aviation, INC., 1946.

[14] H N Riise and Puckett, "*Flexible Plate Nozzle Design for Two-Dimensional Supersonic Wind Tunnels*", Jet Propulsion Laboratory Report, No. 20-74, California Institute of Technology, 1954.

[15] H. Schlichting, "*Boundary-layer theory*". New York: McGraw-Hill, 1979, p. Chapter 11.

[16] J. Kenney and L. Webb, "*A Summary of the Techniques of Variable Mach Number Supersonic Wind Tunnel Nozzle Design*", Sandberg-Serrell Corporation, Pasadena, California, USA, 1954.

[17] A. Ghosh, "*Supersonic Nozzle Design using 2D Method of Characteristics*", 1st ed. Department of Aerospace, University of Maryland, College Park.

[18] R. C. Hibbler, "*Mechanics of Materials*". Sixth Edition in SI Units, Prentice Hall, 2005, p. Chapter 6.

[19] CD-Adapco, STAR-CCM+ User's Guide, "*Generating the Mesh*", doc/en/online/index.html#page/STARCCMP/GUID-6EC4516D-8F53-41DF-95FD-C186E63EC69A=en=.html

[20] I.E. Beckwith, W.D. Harvey, J.E. Harris and B.B. Holley, "*Control of Supersonic Wind-Tunnel Noise by Laminarization of Nozzle-Wall Boundary Layers*" National Aeronautics and Space Administration, Washington, D.C, December 1973.

[21] CD-Adapco, STAR-CCM+ User's Guide, "*SpalartAllmaras Turbulent Model*", doc/en/online/index.html#page/STARCCMP/spalartAllmarasTurbulence.139.02.html

[22] CFD Online, "*Dimensionless Wall Distance*", http://www.cfd-online.com/Wiki/Dimensionless_wall_distance_(y_plus), last accessed 10 January 2016.

[23] CD-Adapco, STAR-CCM+ User's Guide, "*Wall Y Plus Treatment*",doc/en/online/index.html#page/STARCCMP/spalartAllmarasTurbulence.139.09.html

[24] CD-Adapco, STAR-CCM+ User's Guide, "*Wall Treatment Models*", doc/en/online/index.html#page/STARCCMP/usingWallTreatmentModels.138.02.html

[25] F.E. Goddard, "*High Speed Problems of Aircraft and Experimental Methods*", Volume VIII, Hogh Speed Aerodynamics and Jey Propulsion, Oxford University Press, London, 1961.

[26] A. Van Wyk, "*Design of Two-Dimensional Supersonic Wind Tunnel Nozzles having Continuous Curvature*", National Mechanical Engineering Research Institute, Council for Scientific and Industrial Research, Pretoria, Republic of South Africa, 1972.

APPENDIX A: HSWT NOZZLE DESIGN CODE

A.1 Main_Program.m

```
% PROGRAM MAIN - SIVELLS NOZZLE DESIGN METHOD
% USES NEWTHROAT.DAT
% USES 6TH ORDER POLYFIT TO FOR THROAT ROTATION

clear all; clc; close all; format long;

%--INPUTS--%
%Nozzle Exit Mach number
Me = 3.0;

%Number of segments/equal parts on the arc AO. Also, 1/r = rotation
resolution of throat block in Throat_R
r  = 42;

%This is the ratio of K/Theta_A not the value of K
K_target = 2.9;

%Throat Rotation Increment Resolution
rot_res = 1/10000;
%rot_res = 1/10;

%Initial Theta Rotation
Initial_Theta =  0.19;
%     -0.700000000000015
%plus make number smaller till second decimal
%minus make bigger by one (first) decimal

%--FILE NAME FOR EXCEL AND .MAT FILES--%
[FileName] = ProfileFileName_V5(Me,r,K_target);

%--SIVELLS' VARIABLES FROM THROAT ROTATION--%
[theta_A,xA,yA,K,k,Xcalc,Ycalc,throat_halfheight] =
Throat_R_V5(Me,r,K_target,rot_res,Initial_Theta,FileName);

%--CONVERSION TO SOURCE FLOW--%
[arc_x,arc_y,theta_arc,xO,yO] =
SourceFlow_V5(xA,yA,theta_A,r,Xcalc,Ycalc,Me,FileName);

%--CALCULATION OF WALL ANGLES & PRANDLT-MEYER FUNCTIONS & MOC--%
[theta_w,nu_w,X_s_p,Y_s_p,X_c,Y_c] =
WallFunction_V5(Me,theta_A,r,k,K,arc_x,arc_y,theta_arc,xA,yA,xO,yO,FileName);

%--GENERATE WALL CONTOUR PROFILE AND WRITE TO EXCEL FILE--%
[Contour_X,Contour_Y] =
ContourCalc_V5(Xcalc,Ycalc,X_s_p,Y_s_p,X_c,Y_c,Me,xA,FileName);
```

A.2 ProfileFilename.m

```
function [FileName] = ProfileFileName_V5(Me,r,K_target)


FileName1 = char('MPV2@Mach');
FileName2 = num2str(Me,5);
FileName3 = num2str(r,5);
FileName4 = num2str(K_target,5);
FileName5 = strcat(FileName1,FileName2,'-r=',FileName3,'-K_tar=',FileName4);
FileName = strrep(FileName5,'.','_');
save(FileName,'Me','r','K_target');

end
```

A.3 Throat _R.m

```
function [theta_A,xA,yA,K,k,Xcalc,Ycalc,throat_halfheight] =
Throat_R_V5(Me,r,K_target,rot_res,Initial_Theta,FileName)

message1 = char('INTERATIONS FOR THROAT')


h = 227.74;                          %(Test section Height)
w = 228.6;                           %(Test section Width)
Test_area = h*w;                     %(Test section area)
[mach,T,P,rho,area] = flowisentropic(1.4,Me,'mach');
A_ratio_Test = area;                 %(Test section area ratio)
y_star = (Test_area/A_ratio_Test)/w;%(Throat half height for Me)
throat_halfheight = y_star;

%rot_res = 1/(10);                  %(Throat rotation increment resolution)
theta = Initial_Theta-rot_res;      %(Initial Throat Position - -10.5 degrees
gives theta_A = 0)

Ratio_theta_A_K = 100;               %(K/Theta Wall at A - initial value high
to enter while loop) NB must be < 4 and > 2
Ratio_theta_A_theta_1P = -100;       %(K/Theta 1P/Theta Wall at A - initial
value high to enter while loop) NB must be > -1 < 0.5

while ((Ratio_theta_A_K > (K_target+rot_res)))%|(Ratio_theta_A_theta_1P < -
1)|(Ratio_theta_A_K < 2.0)|(Ratio_theta_A_theta_1P > -2))
    theta = theta + rot_res;          %(Throat rotation increments)
    clear alpha Xcalc Ycalc gradient x_curve y_curve c theta_A xA yA Xbar
Ybar;

    load NewThroat.dat;

    x=NewThroat(:,1);                        %(Throat x - co-ordinates)
    y=NewThroat(:,2);                        %(Throat y - co-ordinates)
    X = x*cosd(theta)-y*sind(theta);
    Y = x*sind(theta)+y*cosd(theta);
n=length(x)-1;
for i=1:n;
    gradient(i) = (X(i+1)-X(i))/(Y(i+1)-Y(i));
end

inc = 0;
for i=1:n
    if gradient(i)>0.0;
        inc = inc + 1;
            Xbar(inc)=X(i);
            Ybar(inc)=Y(i);
    end
end

cnt = 0;
for i=1:inc
    cnt = cnt + 1;
    Xcalc(cnt)=Xbar(i)-Xbar(1);
    Ycalc(cnt)=Ybar(i)-Ybar(1)+throat_halfheight;
end

format long
```

```
order = 6;
p = polyfit_MOC(Xcalc,Ycalc,order);
tanalpha(1) = (order-0)*p(1);
tanalpha(2) = (order-1)*p(2);
tanalpha(3) = (order-2)*p(3);
tanalpha(4) = (order-3)*p(4);
tanalpha(5) = (order-4)*p(5);
tanalpha(6) = (order-5)*p(6);
tanalpha(7) = (order-6)*p(7);

%--Generate Polyfit Curve--%
counter = 0;
for c=Xcalc(1):0.01:Xcalc(end)
    counter = counter+1;
    x_curve(counter) = c;
    y_curve(counter) =
p(1)*(c)^6+p(2)*(c)^5+p(3)*(c)^4+p(4)*(c)^3+p(5)*(c)^2+p(6)*(c)^1+p(7)*(c)^0;
end

%--Gradient of Polyfit Curve--%
cnt = 0;
i = 0;
for j=Xcalc(1):0.01:Xcalc(end)
    cnt = cnt + 1;
    i = i+1;
    c(cnt) = (tanalpha(1)*( x_curve(i)^5))+(tanalpha(2)*(
x_curve(i)^4))+(tanalpha(3)*( x_curve(i)^3))+(tanalpha(4)*(
x_curve(i)^2))+(tanalpha(5)*( x_curve(i)^1))+(tanalpha(6)*( x_curve(i)^0));
    alpha(cnt) = atand(c(i));
end


    theta_A = alpha(end);   %(this is theta_A)
    xA = Xcalc(end);        %(this is Inflection point (A) x)
    yA = Ycalc(end);        %(this is Inflection point (A) y)

%--Prandtl-Meyer Function at Exit based on Me--%
    [mach,nu,mu] = flowprandtlmeyer(1.4,Me,'mach');
    nu_T = nu;

%--Mach Number and Prandtl-Meyer Function at A from area ratio at A--%
    A_ratio_A = yA/y_star; %(this is the same as AA/A*)
    [mach,T,P,rho,area] = flowisentropic(1.4,A_ratio_A,'sup');
    MA = mach;
    [mach,nu,mu] = flowprandtlmeyer(1.4,MA,'mach');
    nu_A = nu;

%--Calculation of Sivells 'K'--%
    K = 4*(nu_T-theta_A-nu_A);                      %This is Eqn. 10 in
Sivells paper
    Ratio_theta_A_K = K/theta_A                     %This is K/Theta Wall at
A as in Sivells paper {2<Value<4}
    theta_1P = theta_A - (K/2);                     %This is Eqn. 7 in
Sivells paper
    Ratio_theta_A_theta_1P = theta_1P/theta_A;      %This is Theta 1P/Theta
Wall at A as in Sivells paper {-1<Value<0.5}
    k_actual = (r*(1-(Ratio_theta_A_theta_1P)));
    k = round(r*(1-(Ratio_theta_A_theta_1P)));   %This is Eqn. 56 in Sivells
paper
    Percentage_From_Target_Value = ((Ratio_theta_A_K-K_target))*100/K_target
end%(while)
```

```
clc;
Ratio_theta_A_K = K/theta_A
Ratio_theta_A_theta_1P = theta_1P/theta_A
theta_A
theta


save(FileName,'-append');

end
```

A.4 SourceFlow.m

```
function [arc_x,arc_y,theta_arc,xO,yO] =
SourceFlow_V5(xA,yA,theta_A,r,Xcalc,Ycalc,Me,FileName)

message2 = char('SOURCE FLOW CALC')

format long;

%--SOURCE POINT CALC--%
mA = tand(theta_A);
cA = yA-mA*xA;
x_prime = (-cA)/(mA);
rA = sqrt(((xA-x_prime)^2) + ((yA^2)));

%--CONSTRUCT ARC AO SEED POINTS--%--%--NB. IN THE MIDDLE OF THE r
SEGMENTS/PARTS--%
arc_x(1:r) = zeros;
arc_y(1:r) = zeros;
theta_arc(1:r) = zeros;
theta_delta = theta_A/r;    %Angle of each r part

theta_arc(1) = theta_A-(theta_delta/2);
arc_x(1) = rA*cosd(theta_arc(1))+x_prime;
arc_y(1) = rA*sind(theta_arc(1));

    for i = 2:1:r
        theta_arc(i) = theta_arc(i-1)-theta_delta;
        arc_x(i) = rA*cosd(theta_arc(i))+x_prime;
        arc_y(i) = rA*sind(theta_arc(i));
    end
    last_point_x = rA*cosd(0)+x_prime;
    last_point_y = rA*sind(0);

    xO = last_point_x;
    yO = last_point_y;

%--CONVERT ROW VECTORS INTO COLUMN VECTORS--%
    theta_arc = theta_arc';
    arc_x = arc_x';
    arc_y = arc_y';
    save(FileName,'-append');



    Heading = char('Source Points for Charateristic Net - Me=');
    Prof = num2str(Me,5);
    Title = strcat(Heading,' ',Prof);

    figure(2);
    hold on;
    plot(arc_x,arc_y,'-bo','MarkerFaceColor','b','MarkerSize',5);
    plot(xA,yA,'-ro','MarkerFaceColor','r','MarkerSize',10);
    plot(Xcalc,Ycalc,'-ko','MarkerFaceColor','g','MarkerSize',5);

    grid on
    box on;
    title(Title,'fontsize',20);
    xlim([0 600]);
```

```
    ylim([0 300]);
    set(gca,'XTick',0:100:600,'FontSize',20);
    set(gca,'YTick',0:50:300,'FontSize',20);
    xlabel(texlabel('Throat Length (mm)'),'fontsize',20);
    ylabel(texlabel('Throat Height (mm)'),'fontsize',20);
    legend(texlabel('Source Points'),texlabel('Inflection
Point'),texlabel('Throat Block'));
    legend('boxoff');
    hold off;

    save(FileName,'-append');
end%function
```

A.5 WallFunction.m

```
function [theta_w,nu_w,X_s_p,Y_s_p,X_c,Y_c] =
WallFunction_V5(Me,theta_A,r,k,K,arc_x,arc_y,theta_arc,xA,yA,xO,yO,FileName)

message3 = char('PROFILE CALCULATIONS')

%--AS PER SIVELLS' FIG. 2--%
P = k+0.5;       %Point P = (k + 1/2)
Q = 2*r+0.5;     %Point Q = (2r + 1/2)
U = 2*r+k+0.5;   %Point U = (2r +k + 1/2)

%--AS PER DISCRETISATION OF ARC AO--%
wall_points = 2*r+k;
m = 0;               %Point A - Inflection Point

%--CALCULATION OF WALL ANGLES - theta_w--%
    for m = 1:1:wall_points
        if (m < P)
            theta_w(m,1) = theta_A*(1-(((2*m-1)^2)/(16*r*k)));
        elseif (m > P)&&(m < Q)
            theta_w(m,1) = theta_A*(1-(((2*m-1-k))/(4*r)));
        elseif (m > Q)&&(m < U)
            theta_w(m,1) = theta_A*(((4*r+2*k+1-2*m)^2)/(16*r*k));
        end%if

        if m == wall_points
            theta_w(m,1) = 0;
        end%if
    end%loop


    inc1 =0;
for f = 1:1:wall_points
    if f<=k
        theta_ws(f,1) = theta_w(f,1);
    end
    if f>k
        inc1 = inc1 + 1;
        theta_wc(inc1,1) = theta_w(f,1);
    end
end

%--CALCULATION OF WALL PRANDTL-MEYER FUNCTIONS - nu_w--%
m = 0;          %Point A - Inflection Point
[mach,nu,mu] = flowprandtlmeyer(1.4,Me,'mach');
nu_T = nu;
    for m = 1:1:wall_points
        if (m < P)
            nu_w(m,1) = nu_T - theta_A - (K/4) - (theta_A-theta_w(m)) +
sqrt((theta_A-theta_w(m))*2*K);
        elseif (m > P)
            nu_w(m,1) = nu_T - theta_w(m);
        end
    end

    inc1 =0;
for f = 1:1:wall_points
```

```
    if f<=k
        nu_ws(f,1) = nu_w(f,1);
    end
    if f>k
        inc1 = inc1 + 1;
        nu_wc(inc1,1) = nu_w(f,1);
    end
end

%     figure(1);
%     plot(1:m,tand(theta_w),'-ko',0,tand(theta_A),'ro');

% inc1 =0;
% for f = 1:1:wall_points
%     if f<=k
%         Kplus_ws(f,1) = theta_ws(f,1)-(nu_ws(f,1));
%         Kminus_ws(f,1) = theta_ws(f,1)+(nu_ws(f,1));
%     end
%     if f>k
%         inc1 = inc1 + 1;
%         Kplus_wc(inc1,1) = theta_wc(inc1,1)-(nu_wc(inc1,1));
%         Kminus_wc(inc1,1) = theta_wc(inc1,1)+(nu_wc(inc1,1));
%     end
% end

q = k+1;
s = (2*k)+1;
n = r+1;
c = 2*r;

theta_s = zeros(s,n);
Mach_s = zeros(s,n);
nu_s = zeros(s,n);
Kminus_s = zeros(s,n);
Kplus_s = zeros(s,n);
mu_s = zeros(s,n);
x_s = zeros(s,n);
y_s = zeros(s,n);

theta_c = zeros(c,n);
Mach_c = zeros(c,n);
nu_c = zeros(c,n);
Kminus_c = zeros(c,n);
Kplus_c = zeros(c,n);
mu_c = zeros(c,n);

%--BUILD THETA MATRIX--%
message4 = char('BUILDING THETA S MATRIX...')
% theta_s (straightening)
for i=1:s
    for j=1:n
        if i==1 && j<n
            theta_s(i,j) = theta_arc(j,1);
        end
        if j==1 && (mod(i,2)==0) %(even)
            theta_s(i,j) = theta_ws(i/2,j);
            nu_s(i,j) = nu_ws(i/2,j);
            Kplus_s(i,j) = theta_s(i,j) - nu_s(i,j);
            Kminus_s(i,j) = theta_s(i,j) + nu_s(i,j);
        end
```

```
    end
end
message5 = char('BUILDING THETA C MATRIX...')
% theta_c (contour)
for i=1:c
    for j=1:n
        if j==1
            theta_c(i,j) = theta_wc(i,1);
            nu_c(i,j) = nu_wc(i,1);
            Kplus_c(i,j) = theta_c(i,j) - nu_c(i,j);
            Kminus_c(i,j) = theta_c(i,j) + nu_c(i,j);
        end
    end
end
message6 = char('BUILDING K+ MATRIX...')
% working backwards - all the Kplus' equal
for i=c:(-1):1
    for j=1:n-1
        if i>1
        Kplus_c(i-1,j+1) = Kplus_c(i,j);
        end
    end
end

for i=s:(-1):1
    for j=1:n
        if i==s
            Kplus_s(i,j) = Kplus_c(1,j);
        end
        if (mod(i,2)==1) && i>1 && j<n % odd
            Kplus_s(i-1,j+1) = Kplus_s(i,j);
        end
        if (mod(i,2)==0) % even
            Kplus_s(i-1,j) = Kplus_s(i,j);
        end
    end
end

message7 = char('BUILDING CENTRELINE K- MATRIX...')
% calculate theta_centreline nu and Kminus vvalues
for i=1:s
    for j=1:n
        if (mod(i,2)==0) && j==n
            nu_s(i,j) = theta_s(i,j) - Kplus_s(i,j);
            Kminus_s(i,j) = theta_s(i,j) + nu_s(i,j);
        end
    end
end

count = n;
for i=1:c
    for j=1:n
        if (mod(i,2)==1) && j==count
            count = count - 1;
            nu_c(i,j) = theta_c(i,j) - Kplus_c(i,j);
            Kminus_c(i,j) = theta_c(i,j) + nu_c(i,j);
        end
    end
end

message7 = char('BUILDING RESIDUAL K- MATRIX...')
% calculate the remainder Kminus
```

```
counter = c;
for i=1:1:c
    for j=1:1:n
        if Kminus_c(i,j) ~= 0
            for p = 1:i
                 Kminus_c(p,j) = Kminus_c(i,j);
            end
        end
    end
end

counter = s;
for i=s:(-1):1
    for j=1:n
        if (mod(i,2)==0) && j==n % even
            Kminus_s(i-1,j-1) = Kminus_s(i,j);
        end
        if i==s && j<n
            Kminus_s(i,j) = Kminus_c(1,j+1);
        end
        if (mod(i,2)==1) && i>1 && j==n-1 % odd
            Kminus_s(i-1,j) = Kminus_s(i,j);
        end
        if (mod(i,2)==0)  && j>1% even
            counter = counter - 1;
            Kminus_s(i-1,j-1) = Kminus_s(i,j);
        end
        if (mod(i,2)==1)  && i>1 && j>1 && j<n% odd
            counter = counter - 1;
            Kminus_s(i-1,j) = Kminus_s(i,j);
        end
     end
end
message8 = char('BUILDING RESIDUAL THETA AND NU MATRIX...')
% calculate the rest of the theta and nu values
for i=1:s
    for j=1:n
        if theta_s(i,j)==0 && j<n
            theta_s(i,j) = (Kplus_s(i,j)+Kminus_s(i,j))/2;
        end
        if nu_s(i,j)==0 && j<n
            nu_s(i,j) = (-Kplus_s(i,j)+Kminus_s(i,j))/2;
        end
    end
end

for i=1:c
    for j=1:n
        if theta_c(i,j)==0 && j>1
            theta_c(i,j) = (Kplus_c(i,j)+Kminus_c(i,j))/2;
        end
        if nu_c(i,j)==0
            nu_c(i,j) = (-Kplus_c(i,j)+Kminus_c(i,j))/2;
        end
    end
end

message9 = char('MACH NUMBER AND MU CALCS...')
% Mach number and mu calcs
for i=1:s
    for j=1:n
        Mach_s(i,j) = flowprandtlmeyer(1.4, nu_s(i,j), 'nu');
```

```
        mu_s(i,j) = (180/pi)*asin(1/Mach_s(i,j));
    end
end

for i=1:c
    for j=1:n
        Mach_c(i,j) = flowprandtlmeyer(1.4, nu_c(i,j), 'nu');
        mu_c(i,j) = (180/pi)*asin(1/Mach_c(i,j));
    end
end

message9 = char('NEGATIVE GRADIENT CALCS...')
% gradient minus calcs
for i=1:s
    for j=1:n
        if (mod(i,2)==0) && i==2 && j==1
            %gradientminus_s(i,j) =
tan((pi/180)*(.5*(theta_s(i,j)+theta_A)));
            gradientminus_s(i,j) = tan((pi/180)*((theta_s(i,j))));
        end
        if (mod(i,2)==0) && j==1 && i>2
           %gradientminus_s(i,j) = tan((pi/180)*(.5*(theta_s(i,j)+theta_s(i-
2,j))));
           gradientminus_s(i,j) = tan((pi/180)*((theta_s(i,j))));
        end
        if (mod(i,2)==0) && j>1
            gradientminus_s(i,j) = tan((pi/180)*(.5*(theta_s(i-1,j-1)-mu_s(i-
1,j-1))+.5*(theta_s(i,j)-mu_s(i,j))));
        end
        if (mod(i,2)==1) && i>1
            gradientminus_s(i,j) = tan((pi/180)*(.5*(theta_s(i-1,j)-mu_s(i-
1,j))+.5*(theta_s(i,j)-mu_s(i,j))));
        end
    end
end

for i=1:c
    for j=1:n
        if i==1 && j>1
            gradientminus_c(i,j) =  tan((pi/180)*(.5*(theta_s(s,j-1)-
mu_s(s,j-1))+.5*(theta_c(i,j)-mu_c(i,j))));
        end
        if i==1 && j==1
            %gradientminus_c(i,j) = tan((pi/180)*(.5*(theta_c(i,j)+theta_s(s-
1,j))));
             gradientminus_c(i,j) = tan((pi/180)*((theta_c(i,j))));
        end
        if j==1 && i>1
            %gradientminus_c(i,j) =  tan((pi/180)*(.5*(theta_c(i-
1,j)+theta_c(i,j))));
             gradientminus_c(i,j) =  tan((pi/180)*((theta_c(i,j))));
        end
        if i>1 && j>1
            gradientminus_c(i,j) =  tan((pi/180)*(.5*(theta_c(i-1,j)-mu_c(i-
1,j))+.5*(theta_c(i,j)-mu_c(i,j))));
        end
    end
end

message10 = char('POSITIVE GRADIENT CALCS...')
% gradient plus calcs
for i=1:s
```

```
    for j=1:n
        if (mod(i,2)==0) && j==n
            gradientplus_s(i,j) = 0;
        end
        if (mod(i,2)==0) && j<n
            gradientplus_s(i,j) =  tan((pi/180)*(.5*(theta_s(i-1,j)+mu_s(i-
1,j))+.5*(theta_s(i,j)+mu_s(i,j))));
        end
        if (mod(i,2)==1) && i>1 && j<n
            gradientplus_s(i,j) =  tan((pi/180)*(.5*(theta_s(i-1,j+1)+mu_s(i-
1,j+1))+.5*(theta_s(i,j)+mu_s(i,j))));
        end
    end
end

counter = n;
for i=1:c
    for j=1:n
        if i==1
            gradientplus_c(i,j) =
tan((pi/180)*(.5*(theta_s(s,j)+mu_s(s,j))+.5*(theta_c(i,j)+mu_c(i,j))));
        end
        if i>1 && j<n
            gradientplus_c(i,j) = tan((pi/180)*(.5*(theta_c(i-1,j+1)+mu_c(i-
1,j+1))+.5*(theta_c(i,j)+mu_c(i,j))));
        end
        if (mod(i,2)==1) && j==counter
            counter = counter - 1;
            gradientplus_c(i,j) = 0;
        end
    end
end
message11 = char('X AND Y CALCS...')
% x & y calcs
for i=1:s
    for j=1:n
        if i==1 && j<n
            x_s(i,j) = arc_x(j,i);
            y_s(i,j) = arc_y(j,i);
        end
        if i==2 && j==1
            x_s(i,j) = ((yA-arc_y(1,1))+(gradientplus_s(i,j)*arc_x(1,1))-
(gradientminus_s(i,j)*xA))/(gradientplus_s(i,j)-gradientminus_s(i,j));
            y_s(i,j) = y_s(i-1,j)+(gradientplus_s(i,j)*(x_s(i,j)-x_s(i-
1,j)));
        end
        if (mod(i,2)==0) && j>1
            x_s(i,j) = ((y_s(i-1,j-1)-y_s(i-1,j))+(gradientplus_s(i,j)*x_s(i-
1,j))-(gradientminus_s(i,j)*x_s(i-1,j-1)))/(gradientplus_s(i,j)-
gradientminus_s(i,j));
            y_s(i,j) = y_s(i-1,j)+(gradientplus_s(i,j)*(x_s(i,j)-x_s(i-
1,j)));
        end
        if (mod(i,2)==1) && i>1 && j<n
            x_s(i,j) = ((y_s(i-1,j)-y_s(i-1,j+1))+(gradientplus_s(i,j)*x_s(i-
1,j+1))-(gradientminus_s(i,j)*x_s(i-1,j)))/(gradientplus_s(i,j)-
gradientminus_s(i,j));
            y_s(i,j) = y_s(i-1,j+1)+(gradientplus_s(i,j)*(x_s(i,j)-x_s(i-
1,j+1)));
        end
        if (mod(i,2)==0) && j==1 && i>2
```

```
            x_s(i,j) = ((y_s(i-2,j)-y_s(i-1,j))+(gradientplus_s(i,j)*x_s(i-
1,j))-(gradientminus_s(i,j)*x_s(i-2,j)))/(gradientplus_s(i,j)-
gradientminus_s(i,j));
            y_s(i,j) = y_s(i-1,j)+(gradientplus_s(i,j)*(x_s(i,j)-x_s(i-
1,j)));
        end
        if (mod(i,2)==0) && j==n && i==2
            x_s(i,j) = ((y_s(i-1,j-1)-yO)+(gradientplus_s(i,j)*xO)-
(gradientminus_s(i,j)*x_s(i-1,j-1)))/(gradientplus_s(i,j)-
gradientminus_s(i,j));
            y_s(i,j) = 0;
        end
        if (mod(i,2)==0) && j==n && i>2
            x_s(i,j) = ((y_s(i-1,j-1)-y_s(i-2,j))+(gradientplus_s(i,j)*x_s(i-
2,j))-(gradientminus_s(i,j)*x_s(i-1,j-1)))/(gradientplus_s(i,j)-
gradientminus_s(i,j));
            y_s(i,j) = 0;
        end



    end
end

counter = n;
for i=1:c
    for j=1:n
        if i==1 && j>1
            x_c(i,j) = ((y_s(s,j-1)-y_s(s,j))+(gradientplus_c(i,j)*x_s(s,j))-
(gradientminus_c(i,j)*x_s(s,j-1)))/(gradientplus_c(i,j)-
gradientminus_c(i,j));
            y_c(i,j) = y_s(s,j)+(gradientplus_c(i,j)*(x_c(i,j)-x_s(s,j)));
        end
        if j==1 && i==1
            x_c(i,j) = ((y_s(s-1,j)-y_s(s,j))+(gradientplus_c(i,j)*x_s(s,j))-
(gradientminus_c(i,j)*x_s(s-1,j)))/(gradientplus_c(i,j)-
gradientminus_c(i,j));
            y_c(i,j) = y_s(s,j)+(gradientplus_c(i,j)*(x_c(i,j)-x_s(s,j)));
        end
        if j==n && i==1
            x_c(i,j) = ((y_s(s,j-1)-y_s(s-1,j))+(gradientplus_c(i,j)*x_s(s-
1,j))-(gradientminus_c(i,j)*x_s(s,j-1)))/(gradientplus_c(i,j)-
gradientminus_c(i,j));
            y_c(i,j) = 0;
        end
        if j==1 && i>1
            x_c(i,j) = ((y_c(i-1,j)-y_c(i-1,j+1))+(gradientplus_c(i,j)*x_c(i-
1,j+1))-(gradientminus_c(i,j)*x_c(i-1,j)))/(gradientplus_c(i,j)-
gradientminus_c(i,j));
            y_c(i,j) = y_c(i-1,j+1)+(gradientplus_c(i,j)*(x_c(i,j)-x_c(i-
1,j+1)));
        end
        if i>1 && j<n
            x_c(i,j) = ((y_c(i-1,j)-y_c(i-1,j+1))+(gradientplus_c(i,j)*x_c(i-
1,j+1))-(gradientminus_c(i,j)*x_c(i-1,j)))/(gradientplus_c(i,j)-
gradientminus_c(i,j));
            y_c(i,j) = y_c(i-1,j+1)+(gradientplus_c(i,j)*(x_c(i,j)-x_c(i-
1,j+1)));
        end
        if (mod(i,2)==1) && j==counter-1 && i>1 && j<n
            counter = counter - 1;
```

```
            x_c(i,j) = ((y_c(i-1,j)-y_c(i-2,j+1))+(gradientplus_c(i,j)*x_c(i-
2,j+1))-(gradientminus_c(i,j)*x_c(i-1,j)))/(gradientplus_c(i,j)-
gradientminus_c(i,j));
            y_c(i,j) = 0;
        end
    end
end



for i=1:s
    for j=1:n
        if j==1 && (mod(i,2)==0)
        X_s(i,j) = x_s(i,j);
        Y_s(i,j) = y_s(i,j);
        end
    end
end

y_count = 0;

for i = 1:length(Y_s(:,1))
    if Y_s(i,1) ~= 0
        y_count =  y_count + 1;
        Y_s_p(y_count,1) = Y_s(i,1);
        X_s_p(y_count,1) = X_s(i,1);
    end
end

for i=1:c
    for j=1:n
        if j==1
        X_c(i,j) = x_c(i,j);
        Y_c(i,j) = y_c(i,j);
        end
    end
end

save(FileName,'-append');


end%function
```

A.6 ContourCalc.m

```
function [Contour_X,Contour_Y] =
ContourCalc_V5(Xcalc,Ycalc,X_s_p,Y_s_p,X_c,Y_c,Me,xA,FileName)

message12 = char('WALL CONTOUR CALCULATIONS')

Test_X = [2230.5+xA;2550+xA;2950+xA];
Test_Y = [227.74;228.6;229.675];
%Test_X = [2230.5;2550;2950];
%Test_Y = [227.74;228.6;229.675];

Terminal_X = [X_s_p;X_c];
Terminal_Y = [Y_s_p;Y_c];

Contour_X =  [Xcalc';X_s_p;X_c;Test_X];
Contour_Y =  [Ycalc';Y_s_p;Y_c;Test_Y];

Contour = [Contour_X,Contour_Y];

[status,message] = xlswrite(FileName,Contour)



    Heading = char('HSWT Supersonic Nozzle Profile - Me=');
    Prof = num2str(Me,5);
    Title = strcat(Heading,' ',Prof);
    leg = strcat('Wall Contour - Me=',Prof);

    figure(3);
    hold on;

    plot(Xcalc(1:10:length(Xcalc)),Ycalc(1:10:length(Xcalc)),'-
ks','MarkerFaceColor','g','MarkerSize',5);
    plot(Terminal_X,Terminal_Y,'-ro','MarkerFaceColor','b','MarkerSize',7);
    plot(Test_X,Test_Y,'-kp','MarkerFaceColor','m','MarkerSize',10);
    grid on
    box on;
    title(Title,'fontsize',20);
    xlim([0 4000]);
    ylim([-300 300]);
    set(gca,'XTick',0:250:4000,'FontSize',20);
    set(gca,'YTick',-300:50:300,'FontSize',20);
    xlabel(texlabel('Nozzle Length (mm)'),'fontsize',20);
    ylabel(texlabel('Nozzle Height (mm)'),'fontsize',20);
    legend(texlabel('Fixed Throat Block'),texlabel('Terminal
Curve'),texlabel('Fixed Test section'),'Location','NorthWest');
    legend('boxoff');

    plot(Xcalc(1:10:length(Xcalc)),-1*Ycalc(1:10:length(Xcalc)),'-
ks','MarkerFaceColor','g','MarkerSize',5);
    plot(Terminal_X,-1*Terminal_Y,'-
ro','MarkerFaceColor','b','MarkerSize',7);
    plot(Test_X,-1*Test_Y,'-kp','MarkerFaceColor','m','MarkerSize',10);

    hold off;
```

```
    Term_X = [Xcalc(end);Terminal_X];
    Term_Y = [Ycalc(end);Terminal_Y];

    for i=1:1:(length(Term_X)-1)
        grad(i,1) = (Term_Y(i+1,1) - Term_Y(i,1))/(Term_X(i+1,1) -
Term_X(i,1));
    end

    figure(4)
    hold on;
    plot(1:1:length(grad),grad,'-ro','MarkerFaceColor','b','MarkerSize',7);
    grid on
    box on;
    title(Title,'fontsize',20);
    xlim([1 length(grad)]);
    ylim([0 grad(1,1)]);
    set(gca,'XTick',1:(length(grad)/5):length(grad),'FontSize',20);
    set(gca,'YTick',0:(grad(1,1)/5):grad(1,1),'FontSize',20);
    xlabel(texlabel('Wall Point'),'fontsize',20);
    ylabel(texlabel('Slope (mm/mm)'),'fontsize',20);
    legend(texlabel('Contour Slope'),texlabel('Terminal
Curve'),texlabel('Fixed Test section'),'Location','NorthEast');
    legend('boxoff');

    hold off;

    save(FileName,'-append');

end%function
```

APPENDIX B: BOUNDARY LAYER CORRECTION CODE

```
% THIS CODE IS TO USED AFTER CFD SIMULATIONS OF THE EXACT NOZZLE PROFILE
% FOR A SPECIFIC MACH NUMBER IS COMPLETED. THIS IS THE DESIGN MACH NUMBER
% OF THE PROFILE - THE VARIABLE Des_Mach. THE VISCOUS CALCULATION WILL
% PRODUCE AN ACTUAL MACH NUMBER THAT IS LOWER THAN THE DESIGN MACH NUMBER -
% THE VARIABLE Act_Mach. THESE ARE THE INPUTS FOR CORRECTION CALCULATION.
% IT WILL GIVE YOU A MACH NUMBER TO USE IN MAINPROGRAM - THE VARIABLE
% Required_Me_in_MainProgram

clear all; clc; close all; format long;

% INPUTS
Des_Mach = 3.0;
Act_Mach = 2.914;

% CALCULATIONS
h = 227.74;
w = 228.6;
Test_Area = h*w;

[mach,T,P,rho,area] = flowisentropic(1.4,Des_Mach,'mach');
Des_Area_star = Test_Area/area;
Des_y_star = Des_Area_star/w;

[mach,T,P,rho,area] = flowisentropic(1.4,Act_Mach,'mach');
Act_Area_star = Test_Area/area;

Delta_Area_star = Act_Area_star - Des_Area_star;

Delta_y_star = Delta_Area_star/w;

Req_y_star = Des_y_star - Delta_y_star;

Req_Area = h/Req_y_star;

[mach,T,P,rho,area] = flowisentropic(1.4,Req_Area,'sup');

Required_Me_in_MainProgram = mach
```

APPENDIX C: PLATE STRESS CODE

```
clc; clear all; close all;

[file,path] = uigetfile('*.csv','File Extention');
Data = csvread(strcat(path,'\',file),0,0);
n = length(Data(:,1));

X = Data(:,1)/1000; %(millimetres)
Y = Data(:,2)/1000; %(millimetres)

%First Derivative
dX = 0;
dY = 0;

for i = 2:n
    dX(i-1) = X(i) - X(i-1);
    dY(i-1) = Y(i) - Y(i-1);
    dXY(i-1) = dY(i-1)/dX(i-1);
    X1(i-1) = X(i);
end

dX2 = 0;
dY2= 0;
n1 = length(dXY);
i = 0;

%Second Derivative
for i = 2:n1
    dX2(i-1) = X1(i) - X1(i-1);
    dY2(i-1) = dXY(i) - dXY(i-1);
    dXY2(i-1) = dY2(i-1)/dX2(i-1);
    X2(i-1) = X1(i);
end

dXYmax = max(dXY);
dXYno = find(dXY==max(dXY));
counter = 0;
 for i = dXYno+10:n-3
     counter = counter + 1;
     dXYdash(counter) = dXY(i-1);
     dXY2dash(counter) = dXY2(i-1);
 end

n2 = length(dXY2dash);

%Moment From Elastica
I = (1/12)*(457.2e-3)*(12e-3)^3;
E = 249.6645e9;

for i = 1:n2-1
    LHS(i) = dXY2dash(i)/((1+(dXYdash(i+1)^2))^(3/2));
    M(i) = LHS(i)*I*E;
end

% Stress using Flexural Formula
```

```
for i = 1:n2-1
    S(i) = M(i)*(6e-3)/I;
    SM(i) = S(i)/1e6;
end

counter = 0;
 for i = dXYno+11:n-3
     counter = counter + 1;
     X3(counter) = X2(i);
end


figure;
hold on;
    plot(X,Y,'-ko','MarkerSize',10);
    grid on
    box on;
    %xlim([0 2.5]);
    %ylim([-0.25 0]);
    set(gca,'XTick',0:0.5:3,'FontSize',20);
    set(gca,'YTick',-0.5:0.1:0,'FontSize',20);
    xlabel('X Distance from Test Section','fontsize',24);
    ylabel(texlabel('Plate Deflection'),'fontsize',24);
    legend(texlabel('Plate Centreline'));
    legend('boxoff');
hold off;

figure;
hold on;
    plot(X3,M,'-ko','MarkerSize',10);
    grid on
    box on;
    %xlim([0 2.5]);
    set(gca,'XTick',0:0.5:3,'FontSize',20);
   xlabel('X Distance from Test Section','fontsize',24);
    ylabel(texlabel('Bending Moment (Nm)'),'fontsize',24);
    legend(texlabel('Plate Centreline Bending'));
    legend('boxoff');
hold off;

figure;
hold on;
    plot(X3,SM,'-ko','MarkerSize',10);
    grid on
    box on;
    %xlim([0 2.5]);
    set(gca,'XTick',0:0.5:3,'FontSize',20);
    xlabel('X Distance from Test Section','fontsize',24);
    ylabel(texlabel('Plate Stress (MPa)'),'fontsize',24);
    legend(texlabel('Plate Outer-fibre Stress'));
    legend('boxoff');
hold off;
```